

UNIVERSITA' DEGLI STUDI DI MILANO



PhD in Translational Medicine

XXXVII Cycle

Artificial intelligence available to the development of
a virtual reality software for an automated
cephalometric analysis of ultra-reduced CBCT FOV

Tutor: Prof. Chiarella SFORZA

Co-tutor: Prof. Gianluca Martino TARTAGLIA

PhD coordinator: Prof. Mario Salvatore CLERICI

PhD candidate:

Dr. Marco SERAFIN

Matr. R13593

A.A 2023-2024

Abstract

This thesis investigates the integration of artificial intelligence (AI), virtual reality (VR), and ultra-reduced cone-beam computed tomography (CBCT) fields of view (FOV) to develop a novel approach for automated cephalometric analysis in orthodontics. The study addresses key challenges such as enhancing diagnostic precision, ensuring radioprotection, and optimizing clinical workflows through innovative technological solutions.

Cephalometric analysis, a cornerstone of orthodontic diagnosis and treatment planning, has traditionally relied on manual or semi-automated methods using 2D radiographs. However, these methods face limitations, including superimposition of structures and the inability to assess depth. While 3D CBCT imaging offers significant advantages, its associated higher radiation exposure raises safety concerns, particularly for pediatric patients and cases requiring multiple imaging sessions. This research responds to the need for safer, more efficient imaging solutions by focusing on AI-driven automation and ultra-reduced FOVs in CBCT imaging.

The project developed an AI system based on the V-Net deep learning architecture to automate the detection of anatomical landmarks critical for cephalometric analysis. Using a robust training and validation process with expert-annotated CBCT datasets, the system achieved high accuracy, with a mean Euclidean distance error of less than 2 mm. Preprocessing techniques, such as intensity thresholding and data augmentation, enhanced the model's reliability and robustness. The introduction of ultra-reduced FOV CBCT scans further minimized radiation exposure by up to 70% compared to conventional protocols, without compromising diagnostic quality. The integration of intraoral scans with CBCT data provided a comprehensive and accurate anatomical representation, enhancing the precision of automated analyses.

The use of VR technology added a transformative dimension to the system, offering an immersive platform for clinicians to interact with 3D cephalometric data. Through dynamic manipulation and visualization of craniofacial structures, the VR interface enhanced diagnostic confidence and facilitated a more intuitive

understanding of patient anatomy. This approach streamlined the diagnostic workflow, reducing the time required for cephalometric measurements by over 50%, allowing clinicians to focus more on treatment planning and patient care.

Validation studies demonstrated the system's superior efficiency and reproducibility compared to traditional methods. Clinicians highlighted the VR platform's user-friendly interface and its potential to revolutionize diagnostic workflows. By combining AI automation, VR interactivity, and radioprotection-focused imaging, the research provides a comprehensive diagnostic tool tailored to modern orthodontic needs.

This thesis concludes that the integration of AI, VR, and ultra-reduced FOV CBCT imaging represents a significant advancement in orthodontic diagnostics. The proposed system offers a safer, faster, and more precise alternative to conventional methods, aligning with the principles of patient-centered care and radioprotection. Future research should aim to expand the dataset to ensure broader applicability and explore predictive modeling for personalized treatment strategies. The findings underscore the transformative potential of combining cutting-edge technologies to address the evolving challenges of orthodontics, setting a new standard for diagnostic excellence and patient safety.

Acknowledgements

I would like to express my deepest gratitude to Prof. Chiarella Sforza and Prof. Gianluca Martino Tartaglia, who not only guided me as tutor and cotutor but also gave me the opportunity to apply for the PhD program. Their invaluable support and encouragement have been pivotal throughout this journey.

I am immensely grateful to Prof. Caprioglio, not only for his assistance during this project but also for his role as a mentor, inspiring and motivating me to achieve my best in both academic and professional endeavors.

My heartfelt thanks go to Eng. Benedetta Baldini for her substantial contributions to the research, whose technical expertise and collaboration have significantly enriched this thesis.

Lastly, I extend my appreciation to the SynbrAIn development team for their innovative work and dedication to the software development aspects of this project. Their efforts have been crucial in achieving the technological milestones presented in this thesis.

Thank you all for your unwavering belief in this project and your dedication to its success.

Sofia, your patience and understanding have been extraordinary. You have stood by me through long nights of worries and moments of doubt, always ready with kind words and a warm smile.

As Paulo Coelho once wrote, *"When we love, we always strive to become better than we are. When we strive to become better than we are, everything around us becomes better too."* Your love has inspired me to become the best version of myself, and for that, I am forever grateful.

Acknowledgments

I would like to sincerely thank Prof. Andreu Puigdollers and Prof. Marco Ciccìu for their time and effort in reviewing the final draft of my thesis. Their valuable feedback and critical insights have helped refine the manuscript and enhance its clarity. I truly appreciate their willingness to contribute to this work and their support throughout this final stage.

Table of contents

<i>Radioprotection: what, where, when, and why</i>	8
<i>EURATOM directive</i>	14
<i>Italian Legislative Decree 101/2020</i>	22
<i>Branches in dentistry: the orthodontics</i>	31
<i>3D cephalometric analysis</i>	34
<i>PhD in Traslational medicine about green issues: the application of the project</i>	38
<i>Artificial intelligence and its application in the medical field</i>	42
<i>Introduction to virtual reality</i>	45
<i>Automated cephalometric analysis</i>	47
<i>Ultra-reduced field of view CBCT in dentistry and orthodontics</i>	51
<i>Project development</i>	54
<i>Automated landmark detection</i>	57
<i>Automated tooth segmentation from intraoral scans</i>	77
<i>Automated tooth segmentation from cbct data: monolabel and multilabel approaches</i>	85
<i>Automated cranial bone segmentation from CBCT data</i>	91
<i>Automated registration and fusion of IOS and CBCT segmented teeth</i>	97
<i>Automated face scan matching with CBCT data</i>	105
<i>Automated landmarking of facial reference points on facial scan</i>	109
<i>Scientific papers related to the purpose of new cephalometric measurements obtained by ultra-reduced FOV CBCT scans</i>	114
<i>AIOral – A Beta Software for Advanced Diagnostics and Radioprotection</i>	116
<i>Conclusions</i>	121
<i>References</i>	123

Radioprotection: what, where, when, and why

Radioprotection, also called as radiation protection, is a demanding scientific discipline committed to protecting people and their environment from the dangerous effects of ionizing radiation produced naturally or by the human activities. As the matter of fact, most of the ionizing radiation has enough proper energy to remove tightly bound electrons from atoms, thus creating subsequent ions. This mechanism can affect living tissues and organs producing molecular alterations, potentially causing cellular dysfunction and organic mutations such as cancer, and other health problems well known in medical disciplines.¹

The main purpose of radioprotection is based on three main fundamental and universal principles: justification, optimization, and dose limitation.² The justification principle guarantees that any procedure that produce radiation exposure should result in a clear benefit to the patient's health. The optimization one, often related to the known ALARA (As Low As Reasonably Achievable) principle, aims to minimize radiation exposure well beneath the mandated thresholds whenever feasible, taking into account factors related to the patient's real requisite of the exposure and the diagnostic process. Lastly, the principle of dose limitation guarantees that individual exposure remains within established safety boundaries to reduce the risk of radiation-related damage to delicate organs and bodily structures.³

Many regulatory agencies, world and European, establish severe guidelines and standards based on the extensive scientific research available to date.⁴ These regulations explain the permissible exposure limits to workers and patients, all the safety protocols adopted for the prevention of radiation contamination and exposure, and contingency plans for ionizing radiation emergencies involving not only operators but also the population; it is important to underline that radiation protection ranges along several aspects of our life and it is not limited to the medicine field only.

In medical applications, radioprotection is particularly vital due to the dual nature of radiation's role: diagnostic and therapeutic. In diagnostic radiology and nuclear medicine, radioprotection ensures that the benefits of the exam overpass the risks

to minimize unnecessary exposure, so there is a weighted balance between risks and benefits.⁵ In therapeutics, precise dose calculations and advanced shooting methods are used to target tumors while saving surrounding tissues;⁶ in this particular case the balance between risks and benefits must be pondered in favor of the curative aspects. Therefore, the differences among these two different usages of radiations are essential in distinguishing their utility: from a curative perspective to a dangerous one.

Therefore, continuous research and translational knowledges in radiation-related branches are crucial for improving radioprotection. Research into alternative types of radiations, improved diagnostics tools, and innovative shielding solutions, jointly to comprehensive education and training programs for operators in medicine, contribute to the ongoing knowledge to protect against the risks associated with ionizing radiation while increasing its benefits for patients. Not less important, innovative projects, like the present PhD one, should be considered as a part of the ongoing research focused on an alternative future characterized by radiation-free diagnostic techniques.

The history of radioprotection is deeply crossed with the discovery and subsequent utilization of ionizing radiation. The history of radiation began in the late 19th century with Röntgen's discovery of X-rays followed by Becquerel's discovery of natural radioactivity. In the first times, the potential hazards of these new discover was not well understood, and early pioneers, including Marie Curie, often managed radioactive materials without any protective measures, leading to significant health issues produced by intensive exposure to ionizing radiations.⁷

Fortunately, or unfortunately depending on the point of view, the first recorded sign of radiation injuries appeared shortly after their discoveries. Thomas Edison's assistant, Clarence Dally, suffered cutaneous burns by severe radiation and, ultimately, died from his exposure while working with X-rays, which revealed the risks associated with this kind of invisible rays. These early side effects on operators which studied the radiation's potential spurred initial efforts to understand and prevent the risks of radiation exposure; probably, in that exact moment the radiation protection was definitively born.

In the early 20th century, since X-rays in medicine and industry had expanded, so did awareness of the need for protective measures. The British X-ray and Radium Protection Committee, established in the year 1921, was one of the first organizations aimed to the study and regulation of radioprotection. At the same time, the International Commission on Radiological Protection was born in 1928, providing cornerstone guidance and recommendations on radiation safety that are still using to date.⁸

Next, in the mid-20th century, the development and deployment of nuclear technologies also for the army, particularly during and after the second World War, underscored the necessity for rigorous radioprotection standards out of the medical and technological fields.⁶ The subsequent atomic bombings of Hiroshima and Nagasaki in 1945 and the studies of their aftermath provided a huge amount of data on the tragic effects of radiations on human health, both immediate and long-term ones. High-impacting incidents such as the Windscale fire in the UK (1957), the Three Mile Island accident in the US (1979), and the Chernobyl disaster in the USSR (1986) suggested significant advancements in safety protocols and emergency preparedness. These events, jointly to the Japanese bombing, started the necessity for a universal legislation against the risks of radiations.

In the latter part of the 20th century and into the 21st century, the radioprotection continued to evolve and improve with advancements in medical imaging and nuclear energy available to diagnostics and therapeutics. Fortunately, the introduction of sophisticated regulations helped enhance safety standards.⁹

Nowadays, radioprotection is a well-known and well-established group of society supported by a robust body of scientific research background and international collaborations all over the world.¹⁰

As previously reported, radiation protection is founded on several key principles that have evolved and improved over years in response to advancing scientific understanding and technological developments. These principles are designed to prevent risks on human health first and the environment from the potential harmful effects of ionizing radiation scattered from a radiation source too.¹¹

The first principle of justification declares that any decision that alters the radiation exposure situation should have more benefits than risks.¹² This principle ensures

that unnecessary exposure to radiation is strictly avoided, and it is fundamental to the responsible use of radiation by medical operators.

Then, the optimization principle is often recognized by the acronym already cited ALARA. Moreover, ALARA principle has evolved passing from the ALADA (As Low As Diagnostically Acceptable) principle to the ALADAIP (As Low as Diagnostically Acceptable being Indication-oriented and Patient-specific) principle, ensuring a proper exposure related to a proper optimization of the radiodiagnostic exam.¹³

Finally, dose limitation involves setting upper bounds on the amount of radiation an individual can receive.¹⁴ These limits are designed to prevent deterministic effects and reduce the risk of stochastic effects.

Moreover, other principle should be respected: time, distance, and shielding. Time consists in reducing the total time spent close to a radiation source lowers the total exposure. The distance refers to the linear distance from a radiation source since it follows the inverse square law, which states that radiation intensity decreases with the square of the distance from the source. Therefore, more distant so less risky. Finally, shielding is promoted by using materials capable to absorb partially or block entirely the radiation, thus reducing exposure.

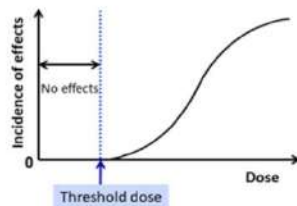
All these principles provide a comprehensive framework for managing radiation risks. They together ensure that the use of radiation in medicine is conducted safely, responsibly, and with minimal impact on health and the environment.

The health risks associated with ionizing radiation are significant and multifaceted, ranging from its capacity to ionize atoms and molecules within biological tissues to leading to genetic mutations. The effects related to radiation exposure on human tissues are easily categorized into deterministic and stochastic effects, each with distinct characteristics, mechanisms, and dose-response relationships.¹⁵

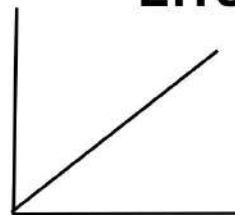
Deterministic effects, also known as non-stochastic effects or tissue reactions, appear above a specific threshold dose and increase linearly in severity with the dose. These effects result from the capability of radiation to direct kill cells and are typically observed immediately or shortly after exposure.

Stochastic effects occur without a threshold and the probability of occurrence increases with dose and time, while the severity is independent of the dose. Between the stochastic effects are mentioned carcinogenesis and hereditary effects.

Deterministic Effect



Stochastic Effect



Difference between determinist and stochastic effects, comparing the ratio of dose crossed with incidence.

Ionizing radiation produced its biological effects primarily through the production of DNA's chains damage. This alteration can occur directly by ionizing DNA molecules or indirectly through the generation of reactive oxygen species from the radiolysis of water. Cells can respond through a variety of repair mechanisms, including non-homologous end joining and homologous recombination. Despite that, these processes are not always error-free, and uncomplete reparations can lead to genetic mutations and cancer development.

Ag. ¹⁶

Radiation protection standards and regulations are designed to minimize health risks by setting dose limits, implementing safety protocols, and monitoring exposure. Several key international groups have been formed during the last century; between the main regulation bodies with can mention:

- International Commission on Radiological Protection (ICRP);⁸
- International Atomic Energy Agency (IAEA);¹⁷
- European Union (EU) and EURATOM.¹⁸

So, stochastic effects during radiological exams, particularly medical imaging procedures that use ionizing radiation, are a significant concern in radiation

protection. Many procedures are known to be related to stochastic risk. Among the radiological exams that use ionizing radiation can be includes:¹⁹

- X-rays. This type of ionizing rays is commonly used for diagnostic purposes such as dental X-rays;
- Computed Tomography (CT) or Cone Beam Computed Tomography (CBCT). These technologies provide detailed cross-sectional images and expose to patient to higher doses compared to standard radiation, since they return a 3D view of the irradiated structures;
- Fluoroscopy. This specific procedure allows real-time imaging for interventional procedures, and it involves continuous or pulsed radiation exposure, increasing the exposure to ionizing radiation;
- Nuclear Medicine. It involves the administration of radiopharmaceuticals to diagnose or treat pathologies, so exposure is indirectly beneficial.

The primary stochastic risk is the increased prevalence of cancer. But that risk is related to three basic factors:²⁰

- Dose. Higher radiation doses are associated with a higher probability of cancer induction;
- Age. Younger patients are more sensitive to radiation and have a longer post-exposure lifespan during which can develop pathologies;
- Cumulative Exposure. Repeated imaging studies over time can lead to significant cumulative doses, increasing the stochastic risk.

Based on these several factors and knowledges, each country transposes international guidelines into national legislation, enforced by regulatory authorities. Not least, Italy legislation was recently modified in the year 2020 to comply with European legislation about protection to ionizing radiation exposure.

EURATOM directive

The EURATOM Directive, formally known as the Council Directive 2013/59/EURATOM, lays down the basic safety standards for protection against the dangers arising from exposure to ionizing radiation.²¹ This directive, adopted in the year 2013, consolidates and updates the previous EU legislation on radiological protection and reflects the latest scientific findings. It aims to provide a high level of protection for workers, the public, and patients against the risks associated with ionizing radiation.

The primary objective of the EURATOM Directive is to ensure the protection of human health. The directive encompasses all exposure situations, including planned, existing, and emergency exposure situations, and applies to occupational, medical, and public exposures. The directive is also based on the same three main principles that founded the radiation protection: justification (Article 19), optimization (Article 5), and dose limits (Articles 9-14). In particular, the new directive sets stringent dose limits for various categories of exposure:

- occupational exposure. The annual dose limit for workers is 20mSv, averaged over five years, with no single year exceeding 50mSv. Additional limits are set for specific tissues, such as the lens of the eye (20 mSv/year) and the skin (500 mSv/year).
- Public exposure. The dose limit for the public is 1mSv per year, with specific limits for the lens of the eye (15 mSv/year) and the skin (50 mSv/year).
- Medical exposure. For patients, there are no explicit dose limits due to the variability in medical procedures. However, the directive emphasizes justification and optimization to minimize patient exposure.

Member states of EU were required to transpose the provisions of the EURATOM Directive into their national legislation by the year 2018.

The European Society of Radiology (ESR) has provided a summary of the EURATOM Directive 2013/59/EURATOM, highlighting the key elements and implications for radiological practice in EU.²¹ This directive, also known as the

Basic Safety Standards Directive, establishes comprehensive safety standards to protect individuals from the risks associated with ionizing radiation. Next, the original paper from the ESR is reported.

Insights Imaging (2015) 6:411–417
DOI 10.1007/s13244-015-0410-4

REPORT

Summary of the European Directive 2013/59/Euratom: essentials for health professionals in radiology

European Society of Radiology (ESR)

Received: 16 April 2015 / Accepted: 20 April 2015 / Published online: 27 May 2015
© The Author(s) 2015. This article is published with open access at Springerlink.com

Abstract The aspects of the new European Directive 2013/59/Euratom most relevant to diagnostic imaging and intervention are summarised. The Directive, laying down basic safety standards for protection against the dangers from exposure to ionising radiation, emphasises the need for justification of medical exposure (including asymptomatic individuals), introduces requirements concerning patient information and strengthens those for recording and reporting doses from radiological procedures, the use of diagnostic reference levels, the availability of dose-indicating devices and the improved role and support of the Medical Physics Experts in imaging. Relevant changes include new definitions, a new dose limit for the eye lens, non-medical imaging exposures, procedures in asymptomatic individuals, the use and regular review of diagnostic reference levels (including interventional procedures), dosimetric information in imaging systems and its transfer to the examination report, new requirements on responsibilities, the registry and analysis of accidental or unintended exposure and population dose evaluation (based on age and gender distribution). These changes will require Member States, the radiology community and the industry to adapt regulations, practices and equipment for a high standard of radiation safety. By 6 February 2018, the Directive has to be transposed into the national legislation of the Member States of the European Union.

Main messages

- *The new European Basic Safety Standards Directive impacts radiology departments*
- *Changes in justification, patient information, responsibilities and dose reporting are most significant*

- *Diagnostic reference levels and the role of medical physics experts are clarified*
- *Dose limits to the eye lens are lower than in the previous directive*
- *Responsibilities in radiation safety have been defined*

Keywords Protection · Radiation · Legislation · Medical · European Union · Government regulations

Introduction

The new European Directive 2013/59/Euratom [1], laying down basic safety standards (BSS) for protection against the dangers arising from exposure to ionising radiation and repealing Directives 89/618/Euratom, 90/641/Euratom, 96/29/Euratom, 97/43/Euratom and 2003/122/Euratom, is expected to have a relevant and positive impact on European radiology.

The basic safety standards take into account the new recommendations of the International Commission on Radiological Protection (ICRP) [2, 3] and are revised in the light of new scientific evidence and operational experience.

The Directive was unanimously adopted by the Council of the European Union (EU) on 5 December 2013 after 4 years of work by different European scientific and technical committees.¹ The press release after the Council meeting held in Brussels on 5 December 2013 highlighted that the new Directive, under which the Member States will establish legal requirements and an appropriate regime of regulatory control,

¹ The Council of the EU is the institution representing the member states' governments. Also informally known as the EU Council, it is where national ministers from each EU country meet to adopt laws and coordinate policies.

✉ European Society of Radiology (ESR)
communications@myESR.org

¹ Neutorgasse 9/2, 1010 Vienna, Austria

reflects a system of radiation protection based on the principles of justification, optimisation and dose limitation for all exposure situations. Dose limits shall not apply to medical exposures.

According to the new Directive, a high level of competence and a clear definition of responsibilities and tasks among all professionals involved in medical exposure are fundamental to ensure adequate protection of patients undergoing medical radiodiagnostic and radiotherapeutic procedures. This applies to medical doctors, dentists and other health professionals entitled to take clinical responsibility for individual medical exposures, to medical physics experts and to other professionals carrying out practical aspects of medical radiological procedures, such as radiographers and technicians in radiodiagnostic medicine, nuclear medicine and radiotherapy.

Furthermore, the Directive provides radiation protection education, training and provision of information. The Member States will have 4 years to transpose this Directive into national legislation.

The most relevant changes in the new Directive in comparison to the existing ones—96/29/Euratom [4] on the protection of workers and the general public and 97/43/Euratom [5] on medical exposures—are summarised in Tables 1 and 2.

The Directive distinguishes between existing, planned and emergency exposure situations. Taking into account this new framework, the Directive covers all exposure situations and all categories of exposure, namely occupational, public and medical.

Table 1 Most relevant changes for radiology imaging in Directive 2013/59/Euratom

1. New set of definitions
2. New dose limit for the lens of the eyes
3. Consideration of occupational doses in justification and optimisation
4. Regulation for radiological procedures in asymptomatic individuals
5. Use and regular review of diagnostic reference levels (including interventional)
6. Education and training (out of the chapter on medical exposures)
7. Responsibilities (the full Art. 57 should be analysed)
8. Role of medical physics experts in diagnostic and interventional procedures
9. New requirements for equipment in use
10. Procedures: optimisation process, clinical protocols and clinical audit
11. Registry and analysis of accidental or unintended exposures
12. Population dose evaluation taking into account age distribution and gender
13. Old “medico-legal” and new “non-medical imaging exposures”

Chapter VII in the new Directive deals with medical exposures but other chapters contain articles relevant to radiology imaging (see Table 2).

Table 2 Other requirements of Directive 2013/59/Euratom with high relevance to imaging

- Dose constraints for occupational, public and medical exposure (Art. 6)
- Dose limits for occupational exposure including the new limit for the lens of the eyes of 20 mSv in a single year (Art. 9)
- Pregnant worker protection (Art. 10)
- Education, information and training in the field of medical exposure (Art. 18)
- Chapter VI on occupational exposures, in particular:
 - Operational protection of exposed workers (Art. 32)
 - Operational protection of apprentices and students (Art. 33)
 - Consultations with radiation protection experts (Art. 34)
 - Controlled and supervised areas (Arts. 37–38)
 - Radiological surveillance of the workplace (Art. 39)
 - Categorisation of exposed workers (Art. 40)
 - Individual monitoring and access to the results (Arts. 41 and 44)
 - Medical surveillance of exposed workers (Art. 45)

The new Directive provides minimum rules, and Member States should be free to adopt or maintain more stringent measures in the subject matter covered by the Directive, without prejudice to the free movement of goods and services in the internal European Union market.

New set of definitions

The definition of “medical exposure” in the new Directive is similar to the previous one, but excludes the “medico-legal”, now called “non-medical imaging exposure”. The relevant definitions (with some changes in comparison to the previous Directives) are included in the Annex.

Occupational dose limits and new limit for the lens of the eye

New scientific information on tissue reactions calls for better protection of the eye lens and, following the ICRP guidance, the new Directive modifies the occupational dose limit for the eye lens to 20 mSv/year from the previous value of 150 mSv/year.

Articles 9 and 11 on dose limits for occupational exposure and dose limits for apprentices and students indicate that:

- Dose limits for occupational exposure apply to the sum of annual occupational exposures of a worker from all authorised practices.
- The limit on the effective dose shall be 20 mSv in any single year (in special circumstances 50 mSv if the

average annual dose over any 5 consecutive years does not exceed 20 mSv).

- The limit on the equivalent dose for the lens of the eye shall be 20 mSv in a single year or 100 mSv in any 5 consecutive years subject to a maximum dose of 50 mSv in a single year.
- The limit on the equivalent dose for the skin and extremities shall be 500 mSv in a year.
- Apprentices and students (aged 16–18 years) have more restrictive dose limits: an effective dose of 6 mSv in a year and equivalent doses of 15 mSv in a year to the lens of the eye as well as of 150 mSv in a year to the skin and the extremities.
- In addition, Art. 40 establishes the categorisation of exposed workers. Workers are required to be classified as 'category A' (i.e., subject to individual monitoring and medical surveillance) if (a) an effective dose greater than 6 mSv per year or (b) an equivalent dose greater than 15 mSv per year for the lens of the eye or (c) greater than 150 mSv per year for the skin and extremities might be expected.

Article 10 deals with pregnant and breastfeeding workers:

- As soon as a pregnant worker informs the employer of the pregnancy the employment conditions shall assure that the equivalent dose to the unborn child is as low as reasonably achievable and unlikely to exceed 1 mSv during at least the remainder of the pregnancy.
- As soon as workers inform the employer that they are breastfeeding an infant, they shall not be employed in work involving a significant risk of intake of radionuclides or of bodily contamination.

Consideration of occupational doses in justification and optimisation

Articles 55 and 56 in Chap. VII on Medical Exposures maintain most of the requirements of the previous 97/43/Euratom Directive, but the explicit consideration of occupational doses in justification and optimisation (as made by ICRP) in some previous articles should be noted.

Article 19.4. Practices involving medical exposure shall be justified both as a class or type of practice, taking into account medical and, where relevant, associated occupational and public exposures, and at the level of each individual medical exposure.

Article 32.b. Member States shall ensure that the operational protection of exposed workers is based on optimisation of radiation protection in all working conditions, including occupational exposures as a consequence of practices involving medical exposures.

Regulation for radiological procedures in asymptomatic individuals

A new article (55.2.h) on justification has been added, concerning medical radiological procedures on asymptomatic individuals, to be performed for early disease detection. Such procedures should either be part of a health screening programme or require specific documented justification for that individual by the practitioner, in consultation with the referrer, following guidelines from relevant medical scientific societies and the competent authority. Special attention shall be given to the provision of information to the individual subject to medical exposure.

Use and regular review of diagnostic reference levels (including interventional)

The new Directive strengthens and expands the previous requirements regarding diagnostic reference levels.

Article 56.2. Member States shall ensure the establishment, regular review and use of diagnostic reference levels for radiodiagnostic examinations, having regard to the recommended European diagnostic reference levels where available, and where appropriate, for interventional radiology procedures and the availability of guidance for this purpose.

Article 58.f. underlines the need for appropriate local reviews whenever diagnostic reference levels are consistently exceeded and requires that the corresponding corrective action is taken without undue delay.

Education, information and training in the field of medical exposure

Article 18 of the new Directive deals with education, information and training in the field of medical exposure. This article is now part of Chap. VII (Medical Exposures) and its content is the same as in the previous 97/43/Euratom Directive. Article 59 on "training and recognition" in the new Directive refers to this Art. 18.

- Member States shall ensure that practitioners and the individuals involved in the practical aspects of medical radiological procedures have adequate education, information and theoretical and practical training for the purpose of medical radiological practices, as well as relevant competence in radiation protection.
- For this purpose Member States shall ensure that appropriate curricula are established and shall recognise the corresponding diplomas, certificates or formal qualifications.

- Individuals undergoing relevant training programmes may participate in practical aspects of medical radiological procedures.
- Member States shall ensure that continuing education and training after qualification are provided and, in the special case of the clinical use of new techniques, training is provided on these techniques and the relevant radiation protection requirements.
- Member States shall encourage the introduction of a course on radiation protection in the basic curriculum of medical and dental schools.

Responsibilities

Article 57 deals with responsibilities and contains new requirements regarding the optimisation process and the provision of information to patients.

1. Member States shall ensure that:
 - (a) Any medical exposure takes place under the clinical responsibility of a practitioner;
 - (b) The practitioner, the medical physics expert and those entitled to carry out practical aspects of medical radiological procedures are involved, as specified by Member States, in the optimisation process;
 - (c) The referrer and the practitioner are involved, as specified by Member States, in the justification process of individual medical exposures;
 - (d) Wherever practicable, prior to the exposure taking place, the practitioner or the referrer, as specified by Member States, ensures that the patient or his/her representative is provided with adequate information relating to the benefits and risks associated with the radiation dose from the medical exposure. Similar information as well as relevant guidance shall be given to carers and comforters, in accordance with point (b) of Art. 56(5).
2. Practical aspects of medical radiological procedures may be delegated by the undertaking or the practitioner, as appropriate, to one or more individuals entitled to act in this respect in a recognised field of specialisation.

Role of the medical physics expert in imaging

Article 58 (procedures), part d, indicates that a medical physics expert shall be involved in radiodiagnostic and interventional radiology practices involving high doses as referred to in point (c) of Art. 61(1) (i.e. interventional radiology and

computed tomography). For other medical radiological practices, a medical physics expert shall be involved as appropriate, depending on the radiological risk posed by the practice, for consultation and advice.

Article 83 defines the responsibilities of the medical physics expert:

Member States shall require the medical physics expert to act or give specialist advice as appropriate on matters relating to radiation physics for implementing the requirements set out in Chap. VII and in point (c) of Art. 22(4) of the Directive (i.e. “Practices involving the deliberate exposure of humans for non-medical imaging purposes”).

Member States shall ensure that depending on the medical radiological practice, the medical physics expert takes responsibility for dosimetry, including physical measurements for evaluation of the dose delivered to the patient and other individuals subject to medical exposure, give advice on medical radiological equipment and contribute in particular to the following:

- (a) Optimisation of the radiation protection of patients and other individuals subject to medical exposure, including the application and use of diagnostic reference levels;
- (b) The definition and performance of quality assurance of the medical radiological equipment;
- (c) Acceptance testing of medical radiological equipment;
- (d) The preparation of technical specifications for medical radiological equipment and installation design;
- (e) The surveillance of the medical radiological installations;
- (f) The analysis of events involving, or potentially involving, accidental or unintended medical exposures;
- (g) The selection of equipment required to perform radiation protection measurements;
- (h) The training of practitioners and other staff in relevant aspects of radiation protection;

It is also required that the medical physics expert shall, where appropriate, liaise with the radiation protection expert.

New requirements for equipment in use

Article 60.3 (equipment) underlines the responsibility of Member States to ensure that:

- (a) The use of fluoroscopy equipment without a device to automatically control the dose rate, or without an image intensifier or equivalent device, is prohibited.
- (c) Any equipment used for interventional radiology has a device or a feature informing the practitioner and those carrying out practical aspects of the medical procedures of the quantity of radiation produced by the equipment

during the procedure. Equipment installed prior to 6 February 2018 may be exempted from this requirement.

- (d) Any equipment used for interventional radiology and computed tomography and any new equipment used for planning, guiding and verification purposes have a device or a feature informing the practitioner, at the end of the procedure, of relevant parameters for assessing the patient dose.
- (e) Equipment used for interventional radiology and computed tomography has the capacity to transfer the information required under 3(d) to the record of the examination. Equipment installed prior to 6 February 2018 may be exempted from this requirement.
- (f) Without prejudice to points (c), (d) and (e) of paragraph 3, new medical radiodiagnostic equipment producing ionising radiation has a device, or an equivalent means, informing the practitioner of relevant parameters for assessing the patient dose. Where appropriate, the equipment shall have the capacity to transfer this information to the record of the examination.

Procedures

Article 58.a now requires the establishment of written protocols for every type of standard medical radiological procedure and for each piece of equipment, but also “for relevant categories of patients”.

Article 58.b (procedures) indicates that Member States shall ensure that “Information relating to patient exposure forms part of the report of the medical radiological procedure”.

In Art. 58.c the previous term “recommendations concerning referral criteria” has been replaced with “referral guidelines for medical imaging” to better reflect the European practice.

Article 58.e maintains the requirements on clinical audits as in the previous Directive 97/43/Euratom [5], stating that “clinical audits are carried out in accordance with national procedures”.

Registry and analysis of the accidental or unintended irradiations

Article 63 introduces a new set of requirements for registration and analysis of accidental and unintended medical exposures.

Member states shall ensure that:

- (c) For all medical exposures the undertaking implements an appropriate system for the record keeping and analysis of events involving or potentially involving accidental or

unintended medical exposures, commensurate with the radiological risk posed by the practice;

- (d) Arrangements are made to inform the referrer and the practitioner, and the patient or their representative, about clinically significant unintended or accidental exposures and the results of the analysis;
- (e) (i) The undertaking declares as soon as possible to the competent authority the occurrence of significant events as defined by the competent authority;
(ii) The results of the investigation and the corrective measures to avoid such events are reported to the competent authority within the time period specified by the Member State;
- (f) Mechanisms are in place for the timely dissemination of information relevant to radiation protection in medical exposure regarding lessons learned from significant events.

Population dose evaluation taking into account the age distribution and the gender

Article 64 states that Member States shall ensure that the distribution of individual dose estimates from medical exposure for radiodiagnostic and interventional radiology purposes are determined, taking into consideration where appropriate the distribution by age and gender of the exposed.

Old medico-legal and new non-medical imaging exposures

The “medico-legal” exposures introduced in Directive 97/43/Euratom have been replaced in the new Directive by the “non-medical imaging exposures” defined as deliberate exposure of humans for imaging purposes where the primary intention of the exposure is not to bring a health benefit to the individual being exposed. The Directive adopts a different approach for procedures using medical radiological equipment and for procedures not using such equipment.

The practices using medical radiological equipment, as defined in Annex V, include:

1. Radiological health assessment for employment purposes;
2. Radiological health assessment for immigration purposes;
3. Radiological health assessment for insurance purposes;
4. Radiological evaluation of the physical development of children and adolescents with a view to a career in sports, dancing, etc.
5. Radiological age assessment;

6. Use of ionising radiation for the identification of objects concealed within the human body.

The Directive requires practices using medical radiological equipment to be placed under appropriate regulatory control and to be justified at three levels: before being generally adopted, for each particular application and for the particular exposed individual. The Directive also requires reviews of the general and particular justification of such practices.

Article 22.3 indicates that Member States may exempt justified practices involving non-medical imaging exposure using medical radiological equipment from the requirement for dose constraints according to point (b) of Art. 6(1) (i.e. dose constraint shall be set for the individual dose that members of the public receive from the planned operation of a radiation source) and from the dose limits set out in Art. 12 (i.e. dose limits for public exposure).

Article 22.4.c requires that for procedures using medical radiological equipment, the relevant requirements identified for medical exposure as set out in Chap. VII (Medical Exposures) are applied, including those for equipment, optimisation, responsibilities, training and special protection during pregnancy and the appropriate involvement of the medical physics expert.

Conclusion

The changes introduced with Council Directive 2013/59/Euratom will require Member States, the radiology community (including medical physics experts) and the industry to adapt their regulations, procedures and equipment to the new high standards of radiation safety.

Member States will have 4 years for the transposition of the Directive into national legislation (by 6 February 2018).

Acknowledgments This paper was prepared by Eliseo Vano (Madrid/ES), Reinhard Loose (Nuernberg/DE) and Peter Vock (Berne/CH) on behalf of the ESR Radiation Protection Subcommittee (chairperson: P. Vock; members: D. Akata, E.J. Adam, J. Damilakis, H. Ducou le Pointe, R. Loose, C. Owens, G. Frija, F. Kainberger, L. Oleaga, M. Prokop; advisers: E. Vano, A. Meghziène, G. Paulo, observers: D. Koff, W. Stiller, D. Sheppard). It was approved by the ESR Executive Council on 14 April 2015.

The authors thank Georgi Simxonov, Policy Officer, European Commission, Directorate-General for Energy, Unit D.3 Radiation Protection, for proof-reading and completing the final draft.

Appendix: Relevant definitions

Accidental exposure	An exposure of individuals, other than emergency workers, as a result of an accident.
Carers and comforters	Individuals knowingly and willingly incurring an exposure to ionising

Clinical audit	A systematic examination or review of medical radiological procedures that seeks to improve the quality and outcome of patient care through structured review, whereby medical radiological practices, procedures and results are examined against agreed standards for good medical radiological procedures, with modification of practices, where appropriate, and the application of new standards if necessary.
Clinical responsibility	Responsibility of a practitioner for individual medical exposures, in particular, justification; optimisation; clinical evaluation of the outcome; cooperation with other specialists and staff, as appropriate, regarding practical aspects of medical radiological procedures; obtaining information, if appropriate, on previous examinations; providing existing medical radiological information and/or records to other practitioners and/or the referrer, as required; and giving information on the risk of ionising radiation to patients and other individuals involved, as appropriate.
Diagnostic reference levels	Dose levels in medical radiodiagnostic or interventional radiology practices, or, in the case of radio-pharmaceuticals, levels of activity, for typical examinations for groups of standard-sized patients or standard phantoms for broadly defined types of equipment.
Dose constraint	A constraint set as a prospective upper bound of individual doses, used to define the range of options considered in the process of optimisation for a given radiation source in a planned exposure situation.
Interventional radiology	The use of X-ray imaging techniques to facilitate the introduction and guidance of devices in the body for diagnostic or treatment purposes.
Medical exposure	Exposure incurred by patients or asymptomatic individuals as part of their own medical or dental diagnosis

	or treatment, and intended to benefit their health, as well as exposure incurred by carers and comforters and by volunteers in medical or biomedical research.	Referrer	A medical doctor, dentist or other health professional who is entitled to refer individuals for medical radiological procedures to a practitioner, in accordance with national requirements
Medical physics expert	An individual or, if provided for in national legislation, a group of individuals, having the knowledge, training and experience to act or give advice on matters relating to radiation physics applied to medical exposure, whose competence in this respect is recognised by the competent authority.	Unintended exposure	Medical exposure that is significantly different from the medical exposure intended for a given purpose.
Medical radiological	Pertaining to radiodiagnostic and radiotherapeutic procedures and interventional radiology or other medical uses of ionising radiation for planning, guiding and verification purposes.		
Medical radiological installation	A facility where medical radiological procedures are performed.		
Medical radiological procedure	Any procedure giving rise to medical exposure.		
Non-medical imaging exposure	Any deliberate exposure of humans for imaging purposes where the primary intention of the exposure is not to bring a health benefit to the individual being exposed.		
Practitioner	A medical doctor, dentist or other health professional who is entitled to take clinical responsibility for an individual medical exposure in accordance with national requirements.		
Radiodiagnostic	Pertaining to in-vivo diagnostic nuclear medicine, medical diagnostic radiology using ionising radiation and dental radiology.		
Radiotherapeutic	Pertaining to radiotherapy, including nuclear medicine for therapeutic purposes.		

Open Access This article is distributed under the terms of the Creative Commons Attribution 4.0 International License (<http://creativecommons.org/licenses/by/4.0/>), which permits unrestricted use, distribution, and reproduction in any medium, provided you give appropriate credit to the original author(s) and the source, provide a link to the Creative Commons license, and indicate if changes were made.

References

1. European Council Directive 2013/59/Euratom on basic safety standards for protection against the dangers arising from exposure to ionising radiation and repealing Directives 89/618/Euratom, 90/641/Euratom, 96/29/Euratom, 97/43/Euratom and 2003/122/Euratom. *OJ of the EU. L13; 57: 1–73* (2014).
2. International Commission on Radiological Protection (2007) ICRP Publication 103. The 2007 Recommendations of the International Commission on Radiological Protection. *Ann. ICRP 37(2–4):1–332*
3. International Commission on Radiological Protection (2012) ICRP statement on tissue reactions and early and late effects of radiation in normal tissues and organs—threshold doses for tissue reactions in a radiation protection context. *ICRP publication 118. Ann ICRP 41(1–2):1–322*
4. European Council Directive 96/29/Euratom laying down basic safety standards for the protection of the health of workers and the general public against the dangers arising from ionizing radiation. *OJ of the EU. L 159; 1–114* (1996)
5. European Council Directive 97/43/Euratom on health protection of individuals against the dangers of ionizing radiation in relation to medical exposure and repealing Directive 84/466/Euratom. *OJ of the EU. L 180; 22–27* (1997)

Italian Legislative Decree 101/2020

In Italy, the implementation of radioprotection measures is guided by the European Union's EURATOM Directive 2013/59/EURATOM, which has been transposed into a national law to ensure compliance with its comprehensive radiological protection standards. Italy's regulatory framework for radiation protection is overseen by various national agencies and ministries, ensuring that both the legislative requirements and practical measures align with the directive's principles. Italy transposed the EURATOM Directive into national legislation through Legislative Decree No. 101 of August 31, 2020. This decree integrates and updates previous radioprotection laws, consolidating them into a comprehensive framework that addresses the protection of workers, the public, and the environment from ionizing radiation. In general, the key aspects of Legislative Decree 101/2020 include, similarly to the original EUROATOM directive that were already mentioned along and previously into the present text.

In Italy several national agencies and ministries are responsible for implementing and enforcing radioprotection regulations. Among them, the following ones were involved in the translation of the EURATOM directive to the Italian legislation:

- National Institute for Nuclear Physics (INFN).
- National Institute for Insurance against Accidents at Work (INAIL).
- Higher Institute of Health (ISS).
- Ministry of Health.
- National Inspectorate for Nuclear Safety and Radiation Protection (ISIN).

The Legislative Decree 101/2020 provides provisions and implementation to that was the original and older legislation about the radioprotection of patients and operators.²²

The Italian Society of Medical Radiology (Società Italiana di Radiologia Medica e Interventistica, SIRM) published a detailed PDF document discussing Legislative Decree No. 101/2020, which transposes the EURATOM Directive 2013/59/EURATOM into Italian law. This document provides a comprehensive overview of the legislative framework, practical applications, and implications for medical radiology practices in Italy. Below is an introduction and summary of the

key elements highlighted by SIRM. Like the document provided by the European Society of Radiology, the following pictured reported the summary of the decree.

DECRETO LEGISLATIVO 101/2020
Norme fondamentali di sicurezza relative alla protezione contro i pericoli derivanti dall'esposizione alle radiazioni ionizzanti
AGGIORNAMENTI PER IL RADIOLOGO

Con il Decreto Legislativo n.101 del 31 luglio 2020 (D.Lgs. 101/2020) (“Attuazione della direttiva 2013/59/Euratom, che stabilisce norme fondamentali di sicurezza relative alla protezione contro i pericoli derivanti dall'esposizione alle radiazioni ionizzanti, ... e riordino della normativa di settore ...”) (Tab. 1), pubblicato nella Gazzetta Ufficiale del 12 agosto 2020, in vigore dal 27 agosto 2020, il Governo Italiano ha recepito la Direttiva Europea 59/2013 (del 5 dicembre 2013).

Tabella 1. Direttive Europee abrogate.

Direttiva 96/29/Euratom: sulle norme fondamentali di sicurezza (BSS) relative alla protezione sanitaria della popolazione e dei lavoratori ;
Direttiva 89/618/Euratom: sulle emergenze radiologiche;
Direttiva 90/641/Euratom: sui lavoratori esterni;
Direttiva 97/43/Euratom: sulle esposizioni mediche ;
Direttiva 2003/122/Euratom: sulle sorgenti sigillate ad alta attività e orfane

Come è noto il recepimento è avvenuto in ritardo, di oltre 2 anni, rispetto al termine previsto del 6 febbraio 2018. La trasformazione della D.E. 59/13 in decreto legislativo è stata realizzata da più gruppi di lavoro composti da rappresentanti di vari ministeri, regioni e enti pubblici del nostro Paese, e in seguito a un’ampia discussione parlamentare anche con i soggetti professionali interessati in audizioni parlamentari.

Il D.Lgs. 101/2020 consta di 245 articoli in 337 pagine (la D.E. 59/13 è composta di 109 articoli) e raggruppa in un unico provvedimento quanto era contenuto in più norme legislative e riguarda le norme di radioprotezione relative all’ambiente, dei lavoratori e a scopo medico.

Le norme legislative abrogate e modificate sono indicate nella Tabella 2.

Tabella 2. Norme Italiane abrogate e modificate. Art. 243

<i>Abrogate alla data di entrata in vigore del D.Lgs. 101/2020 le seguenti disposizioni:</i> <i>a) art. 3, 4 e 5, della legge 31 dicembre 1962 n. 1860 (Impiego pacifico dell'energia nucleare);</i> <i>b) il decreto legislativo 17 marzo 1995, n. 230 così come modificato dal decreto legislativo n. 241 del 2000, dal decreto legislativo n. 23 del 2009, dal decreto legislativo n. 100 del 2011, dal decreto legislativo n. 185 del 2011, dall'articolo 3 del decreto legislativo n. 45 del 2014 e dall'articolo 2 del decreto legislativo n. 137 del 2017;</i> <i>c) il decreto legislativo 26 maggio 2000, n.187 (Attuazione della direttiva 97/43/Euratom in materia di protezione sanitaria delle persone contro i pericoli delle radiazioni ionizzanti connesse ad esposizioni mediche);</i> <i>d) il decreto legislativo 6 febbraio 2007, n.52 (Attuazione della direttiva 2003/122/CE Euratom sul controllo delle sorgenti radioattive sigillate ad alta attività e delle sorgenti orfane);</i> <i>e) il decreto del Ministro dello sviluppo economico 28 settembre 2011 (Detenzione e contabilità delle materie fissili speciali, materie grezze, minerali e combustibili nucleari).</i>

Modifiche

1. L’articolo 180, comma 3, del decreto legislativo 9 aprile 2008, n. 81 (*Testo unico sulla salute e sicurezza sul lavoro*) è sostituito dal seguente:

«3. La protezione dei lavoratori dalle radiazioni ionizzanti è disciplinata, nel rispetto dei principi di cui al titolo I, dalle disposizioni speciali in materia».

Molte delle disposizioni contenute nelle norme precedenti, riguardanti la radioprotezione in essere nel nostro Paese, sono state confermate a testimonianza della validità della normativa di recepimento delle direttive europee precedenti di oltre 20 anni fa.

Si ricorda che le direttive europee danno indicazioni minime a cui gli Stati membri l'U.E. si devono attenere e il cui recepimento deve essere modulato in relazione alle specificità di ogni Paese.

Il testo di recepimento è composto di diciassette titoli e trentacinque allegati che riguardano non solo la protezione delle persone e della popolazione esposte a qualsiasi titolo alle radiazioni ionizzanti, ma anche altri ambiti quali ad esempio:

- il mantenimento della sicurezza degli impianti nucleari,
- la gestione del materiale radioattivo, spedizione e trasporto, e dei rifiuti radioattivi,
- attività lavorative che implicano la presenza di sorgenti di radiazioni naturali con un incremento della esposizione dei lavoratori (funzionamento veicoli spaziali, personale navigante, con esclusione delle esposizioni alla radiazione cosmica durante attività di volo o di missioni nello spazio; lavorazione di materiali contenenti radionuclidi naturali),
- l'esposizione ambientale al radon con la istituzione del Piano di azione nazionale per la determinazione di nuovi livelli di riferimento per la individuazione prioritaria di aree da risanare;
- la preparazione e pianificazione delle risposte a situazioni di esposizione di emergenza.

Oltre le esposizioni mediche il D.Lgs. 101/2020 tratta in modo più completo le esposizioni con metodiche di immagini a scopo non medico ai fini assicurativi, medico legali ecc.¹

Lo scopo di questo documento è di indicare i capisaldi del D.Lgs. 101/2020 in ambito medico radiologico sia per quanto riguarda la radioprotezione dei pazienti (capo XIII) nell'impiego delle radiazioni ionizzanti ai fini medici e sia della radioprotezione degli operatori (capo XI). Si farà particolare cenno alle principali novità introdotte rispetto alla precedente normativa.

Nei primi articoli del D.Lgs. 101/2020 vengono indicati, come in precedenza, che i principi fondamentali su cui si basa la radioprotezione sono: la **giustificazione**, l'**ottimizzazione** e la **limitazione delle dosi**, con alcune novità.

Per la **giustificazione** si indica di porre particolare attenzione alle nuove pratiche medico-radiologiche e ai programmi di screening² e si ribadisce che tutte le esposizioni mediche devono essere giustificate preliminarmente, nell'ambito dell'attività e del ruolo professionale medico-specialistico, così come la revisione delle "pratiche" radiologiche (art.157 comma 2 l.c). Il D.Lgs. 101/2020 inserisce la novità che il processo di giustificazione deve tenere conto "*dei risultati della ricerca scientifica e delle linee guida riconosciute nell'ambito del Sistema Nazionale di cui alla legge 8 marzo 2017 n.24*" (c.d. Bianco Gelli) sulla sicurezza delle cure, buone pratiche e di responsabilità professionale (art.157 comma2 l.c). Il ruolo delle Società scientifiche è accresciuto, così come quello del Responsabile dell'impianto radiologico che deve garantire che gli esami su soggetti asintomatici rientrino nei programmi di screening o richiedano una specifica giustificazione, condivisa con il medico richiedente e rientrante nelle linee guida riconosciute (art.157 comma 11).

Ai fini della **ottimizzazione** si conferisce maggiore valore ai vincoli di dose e ai livelli diagnostici di riferimento (LDR), questi ultimi non più inseriti direttamente nel D.Lgs. ma predisposti dal Ministero della salute avvalendosi dall'Istituto Superiore di Sanità (ISS) con il concorso delle "*rilevanti società scientifiche*" allo scopo di avere LDR costantemente aggiornati (art.158 comma 4)

¹ Art.7, definizione 44. "esposizione a radiazioni ionizzanti con metodiche per immagini a scopo non medico: qualsiasi esposizione intenzionale di persone con metodiche per immagini quando l'intenzione primaria dell'esposizione non consiste nell'apportare un beneficio alla salute della persona esposta, comprese le procedure a fini assicurativi o legali senza indicazione clinica".

² Art.157 comma 10. "Le strutture sanitarie competenti, con il concorso delle istituzioni e società scientifiche, predispongono una giustificazione specifica per le procedure medico-radiologiche da svolgere nell'ambito dei programmi di screening sanitario".

secondo quanto previsto dall'Allegato XXVI del D.Lgs. 101/2020. L'Istituto Superiore di Sanità, avvalendosi delle Società Scientifiche tra cui SIRM, ha già realizzato nel 2017 il documento "Rapporti ISTISAN 17/33" "Livelli diagnostici di riferimento nazionali per la radiologia diagnostica e interventistica"³ in attuale fase di avanzata revisione e a cui fare riferimento. Come indicato dal D.Lgs. 101/2020 sono stati inseriti i LDR per la Radiologia Interventistica non presenti nella precedente normativa.

Vale la pena di ricordare che lo stesso ISS ha realizzato nel 2015, anche in questo caso con il concorso della SIRM, il "Rapporto ISTISAN 15/41" "Indicazioni operative per l'ottimizzazione della radioprotezione nelle procedure di radiologia interventistica"⁴, anch'esso in fase di aggiornamento.

In tale ambito il ruolo del fisico medico e del responsabile dell'impianto radiologico vengono rafforzati (art.158 comma 5 e allegato XXVI).

I vincoli di dose (art. 146):

- per le esposizioni mediche si applicano esclusivamente agli assistenti e accompagnatori⁵ dei pazienti non autosufficienti e ai volontari che partecipano a programmi di ricerca medica e biomedica (allegato XXV)⁶;
- per le esposizioni professionali vengono inseriti per la prima volta anche i lavoratori esterni. Il vincolo di dose è stabilito dall'esercente⁷ o dal datore di lavoro, con la supervisione dell'autorità autorizzativa o che ha ricevuto la notifica dell'attività.

Per le esposizioni sui luoghi di lavoro viene indicato che non possono essere adibiti a attività lavorative che prevedono l'impiego di radiazioni ionizzanti i minori di anni 18 (art.121), sono previste limitazioni in gravidanza (art. 166) e per gli apprendisti e studenti (art.120). Vengono indicati i limiti di dose per i lavoratori esposti e ridotto il limite di dose equivalente al cristallino per il personale professionalmente esposto in 20 mSv/anno rispetto ai 150 mSv/anno precedenti (art.146). Andrà individuato quale metodo di misura adottare e a quali operatori sanitari applicare il monitoraggio.

Per le esposizioni mediche, come già detto, il D.Lgs. 101/2020 riporta dettami coerenti con la precedente normativa.

L'art.156 indica quali sono le esposizioni mediche, differenziando, rispetto alla precedente normativa, in modo più chiaro alcune categorie come i soggetti che si sottopongono a programmi di screening, i soggetti asintomatici, coloro che effettuano procedure a scopo non medico e volontari che assistono persone sottoposte a esposizioni mediche.

Le **principali novità**, contenute nei vari articoli del **Titolo XIII (Esposizioni Mediche)**, riguardano:

- l'indicazione di dare specifiche e adeguate informazioni sui rischi e benefici dell'esposizione al paziente prima dell'esame da parte del medico specialista per alcune procedure ad alte dosi⁸.

³ <https://www.sirm.org/download/3367>

⁴ <http://old.iss.it/publ/index.php?lang=1&id=29238&tipo=5>

⁵ Art.7, definizione 5. "assistenti e accompagnatori: coloro che consapevolmente e volontariamente si espongono, al di fuori della loro occupazione, a radiazioni ionizzanti per assistere e confortare persone che sono, sono state o sono in procinto di essere sottoposte a esposizioni mediche".

⁶ Allegato XXV comma 3. I vincoli di dose efficace per l'esposizione delle persone di cui all'articolo 156, comma 3 sono i seguenti: a) soggetti di età compresa tra 18 anni e 60 anni: 3 mSv/trattamento; b) soggetti di età superiore a 60 anni: 15 mSv/trattamento

⁷ Art.7, definizione 38. "esercente: una persona fisica o giuridica che ha la responsabilità giuridica ai sensi della legislazione vigente ai fini dell'espletamento di una pratica o di una sorgente di radiazioni".

⁸ Art.164. Comma 8. Per le esposizioni di cui al comma 1, lettera c)*, punto 1, il medico specialista informa il paziente sui rischi radiologici connessi con la procedura e si assicura che il documento di consenso sia esplicito rispetto a tali rischi.

* c) esposti nell'ambito di pratiche radiologiche comportanti alte dosi per il paziente, come può avvenire nel caso delle seguenti procedure:

1) radiologia interventistica;
2) tomografia computerizzata;
3) medicina nucleare;

Sarà necessario individuare il modo migliore di comunicare e quale informazione dare. Saranno necessari aggiornamenti organizzativi per avere il tempo a disposizione per questa ulteriore attività da parte del medico radiologo. “*Ove praticabile*” tale indicazione viene riportata anche per le altre esposizioni mediche compresi gli “*assistenti e gli accompagnatori*” (art.159 comma 6). I medici devono esser preparati e avere il tempo per poter garantire una comunicazione efficace anche in questo caso. Maggiore attenzione deve essere posta alle richieste di esami radiologici non utili.

- Non è modificata l’attribuzione della figura del responsabile dell’impianto radiologico (RIR), ad eccezione delle attrezzature di radiodiagnostica endorale con tensione non superiore a 70 kV, per le quali il RIR può essere anche il medico odontoiatra non esercente nell’ambito della propria attività complementare (art.7 definizione 121).⁹ Il D.Lgs. 101/2020 fa inoltre specifico riferimento al documento del Ministero della Salute: “*Raccomandazioni per l’impiego corretto delle apparecchiature TC volumetriche Cone beam*” pubblicate nella Gazzetta Ufficiale n. 124 del 29 maggio 2010 (art. 161 comma 2).
- La giustificazione specifica per i programmi di screening, come già illustrato in precedenza.
- Si indica che l’attività di refertazione degli esami radiologici è responsabilità esclusiva del medico specialista in radiodiagnostica e che gli esami radiologici “*nell’ambito dei programmi di screening, la valutazione del risultato non include l’anamnesi individuale*” (art.159 comma 2). Tale punto chiarisce ulteriormente il contenuto di precedenti circolari ministeriali e di norme relative alla refertazione degli esami radiologici, esclusivo compito del medico radiologo o del medico nucleare, per quanto di competenza. Nell’ambito delle attività complementari il D.Lgs 101/2020 ribadisce quanto contenuto nella precedente normativa e indica che “*non possono essere effettuati esami per conto di altri soggetti o professionisti sanitari pubblici o privati, né essere redatti o rilasciati referti radiologici*” da parte di medici specialisti in altra branca in attività complementare (art. 159 comma 13). Anche in tale attività sarà necessario individuare analoghe modalità per la comunicazione della dose di esposizione delle procedure radiologiche e la registrazione dei dati di esposizione.
- Per gli aspetti pratici delle procedure medico-radiologiche il D.Lg. 101/2020 riporta quanto presente nella precedente normativa indicando che questi “*sono in capo al medico specialista o al tecnico sanitario di radiologia medica, oppure all’infermiere o all’infermiere pediatrico, ciascuno nell’ambito delle rispettive competenze professionali*” (art. 159 comma 3). Rispetto alla precedente norma il D.Lgs. 101/2020 indica la necessità da parte dell’esercente di garantire la graduale partecipazione dei professionisti sanitari coinvolti alle procedure medico-radiologiche “*secondo il livello di formazione e le cognizioni acquisite*” (art. 159 comma 14).
- La D.E. 59/13 prevede che “*l’informazione relativa all’esposizione faccia parte del referto della procedura medico-radiologica*”. Il D.Lgs. 101/2020 indica che sia l’esercente e il responsabile dell’impianto radiologico a garantire che “*il referto relativo alle procedure medico-radiologiche sia comprensivo dell’informazione relativa all’esposizione connessa alla prestazione in conformità alle linee guida in materia emanate dal Ministero della salute*” (art. 161 comma 5). Il comma successivo (art. 161 comma 6) indica che, nelle more della realizzazione di dette linee guida, “*l’informazione relativa all’esposizione da riportarsi sul referto. È costituita dall’indicazione della classe di dose (da I a IV) riconducibile all’esame in questione ... allegato sub B ... Linee guida per la diagnostica per immagini*” Gazzetta Ufficiale n.100 del 2 maggio 2005”¹⁰ di seguito riportato.

⁹ Art.7, definizione 121. “responsabile di impianto radiologico: il medico specialista in radiodiagnostica, radioterapia o medicina nucleare, individuato dall’esercente. Il responsabile di impianto radiologico può essere lo stesso esercente qualora questo sia abilitato quale medico chirurgo o odontoiatra a svolgere direttamente l’indagine clinica. Può assumere il ruolo di responsabile di impianto radiologico anche il medico odontoiatra che non sia esercente, limitatamente ad attrezzature di radiodiagnostica endorale con tensione non superiore a 70 kV, nell’ambito della propria attività complementare”.

¹⁰ [https://www.sirm.org/wp-content/uploads/2019/03/La diagnostica per immagini Linee guida nazionali di riferimento - Approvato CSR 2004.pdf](https://www.sirm.org/wp-content/uploads/2019/03/La_diagnostica_per_immagini_Linee_guida_nazionali_di_riferimento_-_Approvato_CSR_2004.pdf)

CLASSE	Dose efficace (mSv)	ESEMPI
0	0	US, RM
I	<1	RX torace, RX arti, RX bacino, Colonna cervicale
II	1-5	RX addome, Urografia, RX Colonna lombare TAC (capo e collo) MN (es. scintigrafia scheletrica)
III	5-10	TAC (torace ed addome) MN (es. cardiaca)
IV	>10	Alcuni studi MN
II-IV		Radiologia interventistica*

Tale disposizione entra in vigore con il D.Lgs 101/2020 il 27 agosto 2020 ed è del tutto evidente che il provvedimento non è immediatamente applicabile e che necessita almeno della individuazione di parametri e di una regolamentazione che possa essere diffusa a livello nazionale. Lo stesso comma 6 dell'art. 161 indica che *“la classe di dose dovrà essere individuata sulla base della tipologia e delle modalità di effettuazione degli esami radiologici e di medicina nucleare e delle indicazioni fornite dallo specialista in fisica medica”*. La SIRM insieme alle altre società scientifiche del settore ha emanato due documenti di consenso intersocietario nel 2017 *“Registrazione e informazione dei dati di esposizione radiologica alla luce della Direttiva 2013/59/EURATOM del 5 dicembre 2013”*¹¹ e 2018 *“Indicazioni e applicazioni pratiche in relazione al contenuto della Direttiva 2013/59/Euratom del 5 dicembre 2013 e al suo recepimento”*¹² che hanno affrontato il problema alla luce di quanto prevedeva la D.E. 59/13 non conoscendo cosa avrebbe indicato il legislatore nella norma di recepimento. Nei documenti intersocietari vengono indicati i parametri da considerare e viene indicato chiaramente che esistono livelli di incertezza nel rilevamento del dato che possono variare in percentuali dal 20 al 50 % in più o in meno. Inoltre, bisogna considerare come comportarsi in assenza di sistemi automatici di trasferimento del dato. È stato istituito un GdL intersocietario per la individuazione di criteri e modalità operative da inviare ai propri iscritti per la uniforme e corretta gestione del dato da inserire nel referto. Si pone, inoltre, la necessità di individuare analoghi criteri per le attività di radiologia complementare.

- Le apparecchiature per radiologia interventistica e tomografia computerizzata, installate dopo l'entrata in vigore del D.Lgs. 101/2020, *“devono essere munite di un dispositivo che informi il medico specialista, al termine della procedura, sui parametri utili alla valutazione della dose al paziente”* (art.163 comma 16), *“di sistemi di ottimizzazione della dose”* (art. 163 comma 17) e comprese le apparecchiature radiologiche utilizzate per la *“radiodiagnostica specialistica dovranno essere in grado di trasferire le informazioni i cui ai commi 15* (quantità di radiazioni

¹¹ https://www.sirm.org/wp-content/uploads/2019/06/Registrazione_dei_dati_di_esposizione_radiologica.pdf

¹² [file:///C:/Users/User/Downloads/Documento di Consenso Intersocietario Indicazioni e applicazioni pratiche in relazione al contenuto della Direttiva 2013_59_Euratom del 5 dicembre 2013 e al suo recepimento .pdf](file:///C:/Users/User/Downloads/Documento%20di%20Consenso%20Intersocietario%20Indicazioni%20e%20applicazioni%20pratiche%20in%20relazione%20al%20contenuto%20della%20Direttiva%202013_59_Euratom_del_5_dicembre_2013_e_al_suo_recepimento_.pdf)

durante la procedura) e 16 nella registrazione dell'esame" (art. 163 comma 18). Vengono indicati i parametri da archiviare per le specifiche tipologie di apparecchiature e esami radiologici, compresa le attività radiologiche complementari all'esercizio clinico (Allegato XXIX Registrazione dei dati).¹³

- Attenzione alla qualità e sicurezza delle apparecchiature viene ribadita nel D.Lgs 101/2020 con l'indicazione di tenere sotto stretta sorveglianza le attrezzature radiologiche da parte delle Regioni e Province autonome con programmi di ispezione (art. 163 comma 1). Il ruolo del RIR è centrale in questo processo, egli *"esprime il giudizio di idoneità all'impiego clinico delle attrezzature"* e per le apparecchiature di radiologia interventistica deve tenere *"conto anche delle valutazioni del medico specialista che svolge la pratica"* (art.163 comma 6).
- Particolare attenzione viene posta alle esposizioni accidentali e indebite con il coinvolgimento delle diverse figure professionali con elementi di novità rispetto alla precedente normativa. *"L'esercente e i RIR adottano tutte le procedure ragionevoli per ridurre al minimo la probabilità e l'entità delle esposizioni indebite alle persone soggette a esposizione medica"* (art 167 comma 1). L'esercente attua un sistema di registrazione e di analisi di eventi, anche solo potenziali, di esposizioni indebite, correlandole al rischio associato alla pratica radiologica (art. 167 comma 2). Il RIR ha il compito di informare *"il medico prescrivente, il medico specialista e il paziente o un suo rappresentante su eventuali esposizioni indebite o accidentali clinicamente significative e sulle conseguenze da esse derivanti"* (art. 167 comma 8 l.a) e di definire le modalità con cui i *"professionisti sanitari che svolgono aspetti pratici delle procedure comunicano tempestivamente ... ogni situazione, anche solo potenziale, di esposizione accidentale o indebita occorsa"* (art. 167 comma 3). Inoltre *"Il Ministero della salute provvede affinché nell'ambito del sistema SIMES sia prevista la definizione di uno specifico evento sentinella relativo a esposizioni accidentali o indebite a radiazioni ionizzanti"* (art 167 comma 9).
- Maggiore attenzione viene data alla valutazione delle dosi alla popolazione e viene inserita l'indicazione di effettuare audit clinici (art. 168). Si ribadisce l'obbligo affinché *"le indagini, i trattamenti con radiazioni ionizzanti e i principali parametri tecnici a essi attribuiti siano registrati singolarmente su supporto informatico"* (art. 168 comma 1) secondo le *"linee guida dell'Agenzia per l'Italia digitale"* (art. 167 comma 2). Il tutto ai fini del trasferimento dei dati entro tre anni dall'entrata in vigore del D.Lgs. 101/2020 e successivamente ogni quattro anni da parte dell'esercente alla Regione o provincia autonoma. I dati da trasmettere saranno definiti da apposito decreto del Ministero della salute, d'intesa con le Regioni, entro nove mesi dall'entrata in vigore del D.Lgs. 101/2020, con il concorso dell'ISS e delle società scientifiche (art. 168 comma 3). Nelle more si applicano le indicazioni dell'allegato XXIX del D.Lgs. 101/2020. Alle Regioni e le Province autonome è deputato il compito di valutare l'entità e la variabilità delle esposizioni a scopo medico tenendo conto delle indicazioni fornite dal documento della Commissione europea *"Radiation protection 154"* o documenti successivi e di promuovere la realizzazione di audit clinici *"finalizzati al miglioramento continuo della qualità e della sicurezza delle prestazioni radiologiche"* (art. 168 comma 5). I dati delle esposizioni mediche,

¹³ La registrazione dei dati di cui al comma 1 dell'articolo 168, relativa agli esami di diagnostica per immagini, alle procedure speciali e a quelle di medicina nucleare, dovrà prevedere almeno i seguenti elementi:

- a) esami TC: valore del Dose Length Product (DLP) associato all'intero esame; il valore dosimetrico dovrà essere espresso in mGy x cm;
- b) mammografia: valore della dose ghiandola media rilevata nell'ambito della verifica periodica dei LDR e calcolata secondo i protocolli di riferimento o le linee guida europee. Il valore dosimetrico dovrà essere espresso in mGy;
- c) altri esami di radiodiagnostica specialistica: valore del prodotto dose x area associato all'intero esame. Il valore dosimetrico dovrà essere espresso in Gy x cm²;
- d) esami di medicina nucleare: indicazione del radiofarmaco somministrato e valore dell'attività somministrata. Tutti i valori di radioattività riportati dovranno essere espressi in MBq;
- e) procedure interventistiche: indicazione del prodotto dose x area relativo all'intera procedura o la durata dell'esposizione, espressi rispettivamente in Gy x cm² e minuti e secondi;
- f) altre attività radiologiche complementari all'esercizio clinico: indicazione del prodotto dose x area relativo all'intera procedura o la durata dell'esposizione, espressi rispettivamente in Gy x cm² e minuti e secondi.

prima descritti, vanno inviati al Ministero della salute da parte delle Regioni e delle Province autonome ogni quattro anni avvalendosi dell'ISS (art. 168 comma 6) al fine di effettuare periodicamente una valutazione “del quadro nazionale di radioprotezione del paziente” al fine di raggiungere “elevati standard di sicurezza e qualità” anche richiedendo “una verifica inter pares internazionale” (art. 168 comma 7).

- Novità, rispetto alla precedente normativa, è l'inserimento di specifiche riguardanti le “pratiche implicanti l'esposizione intenzionale a scopo non medico con attrezzature medico-radiologiche” (art. 169); in particolare nell'ambito di “a) idoneità fisica al lavoro ... b) procedure medico-legali e assicurative ... c) determinazione della minore età eseguite presso strutture sanitarie pubbliche possibilmente dotate di reparti pediatrici ... d) ai fini dell'identificazione di oggetti occultati all'interno del corpo umano eseguite presso strutture sanitarie pubbliche (art. 169 comma 1 l.a,b,c,d) da effettuarsi su richiesta motivata rispettivamente del medico prescrivente (l.a,b) e dell'autorità giudiziaria (l. c,d). Per tali fini sono da ritenersi “generalmente accettate e giustificate le procedure che comportano basse dosi” (art. 169 comma 2 l.a). La tomografia computerizzata è da ritenersi non giustificata per tali scopi e il suo impiego richiede la giustificazione individuale da parte di “un medico specialista in radiodiagnostica” (art. 169 comma 2 l.c). È richiesto il consenso alla persona sottoposta all'esame salvo quanto disposto dall'autorità giudiziaria (art. 169 comma 2 l.e). Il Ministero della salute, sentite le istituzioni e le società scientifiche, elabora ulteriori criteri e prescrizione inclusi eventuali specifici livelli diagnostici di riferimento, ai fini dell'applicazione di tali attività (art. 169 comma 3).
- Particolare rilevanza viene data alla formazione e aggiornamento delle figure professionali coinvolte nelle attività radiologiche specificamente per quanto riguarda la radioprotezione (art. 162). Novità rilevante, non presente nella precedente normativa, è la indicazione del termine di un anno (dall'entrata in vigore del D.Lgs. 101/2020) alle università entro cui assicurare “l'inserimento di adeguate attività didattiche in materia di radioprotezione del paziente nell'esposizione medica all'interno degli ordinamenti didattici dei corsi di laurea di medicina e chirurgia, di odontoiatria, di tecniche di radiologia medica per immagini e radioterapia, dei diplomi di specializzazione in radiodiagnostica, radioterapia, medicina nucleare, e delle specializzazioni mediche che possono comportare attività radiodiagnostiche complementari all'esercizio clinico” (art. 162 comma 1). Inoltre l'aggiornamento periodico, anche in tema di radioprotezione, viene riportata nell'ambito dei programmi di educazione continua in medicina (ECM) con l'obbligo di acquisire “almeno il 10 per cento dei crediti complessivi previsti nel triennio per i medici specialisti, i medici di medicina generale, i pediatri di famiglia, i tecnici sanitari di radiologia medica, gli infermieri e gli infermieri pediatrici, e almeno il 15 per cento dei crediti complessivi previsti nel triennio per gli specialisti in fisica medica e per i medici specialisti e gli odontoiatri che svolgono attività complementare” (art. 162 comma 4). Viene eliminata la formazione quinquennale prevista in precedenza. Non sono state inserite nel D.Lgs. di recepimento della D.E: 59/13 la formazione di altre figure professionali quali ad esempio i veterinari per la valutazione del rischio nel caso di accompagnatori degli animali sottoposti ad accertamenti con radiazioni ionizzanti.
- L'apparato sanzionatorio (Titolo XVI) per le inosservanze delle disposizioni del D.Lgs. 101/2020, già previsto nella normativa precedente, viene suddiviso per i singoli Capi e separatamente per gli illeciti penali (Capo I) e amministrativi (Capo II). Rispetto alla precedente normativa sono aumentate significativamente la durata delle sanzioni penali e di quelle amministrative e sono stati introdotti delle novità come quella di sanzionare l'esercente se non provvede alla sostituzione delle apparecchiature considerate obsolete dal RIR ai sensi dell'art 163 comma 12¹⁴ e il RIR per la mancata esposizione dell'avviso indicante il potenziale pericolo per il nascituro (art. 166 comma 5) o della mancata informazione relativa alle esposizioni indebite accidentali al medico prescrivente o al paziente (art. 167 comma 8). La mancata indicazione nel referto della informazione relativa all'esposizione connessa alla prestazione è

¹⁴ L'esercente, su segnalazione del responsabile dell'impianto radiologico, adotta gli opportuni interventi correttivi sulle attrezzature medico-radiologiche e provvede, ove necessario, alla loro dismissione.

punita con la sanzione amministrativa (da 4.000,00 a 10.000,00 euro) (art.233 comma 1) a carico dell'esercente e del RIR.

Viene individuata la nuova figura professionale dell'Esperto di radioprotezione (art.128,129,130) per assicurare la sorveglianza fisica, nominato dal datore di lavoro che incorpora le funzioni dell'Esperto qualificato della precedente normativa.

Con il presente documento sono stati affrontati i principali aspetti del D.Lgs. 101/2020 ritenuti di interesse per il Radiologo. Non si ritiene pertanto di essere completamente esaustivi della ampia e complessa normativa a cui si rimanda il lettore per maggiori e più specifici approfondimenti.

Roma, 26 agosto 2020

Branches in dentistry: the orthodontics

Orthodontics represents a specialized discipline within dentistry dedicated to the diagnosis, prevention, and treatment of dental and facial irregularities. The primary objective of orthodontic intervention is to rectify misaligned teeth and jaws, thereby enhancing both functional efficacy and aesthetic appeal.

The history of orthodontics is a rich and complex narrative that traces the evolution of dental science dedicated to correcting teeth and jaw alignment. Orthodontics has really ancient roots and has undergone significant advancements over the centuries, evolving from rudimentary techniques to sophisticated treatments backed by rigorous scientific research.

First, a little history about the orthodontic practice along the centuries.²³ The evidence of orthodontic practices goes back to ancient civilizations. Archaeological findings suggest that Egyptians, Greeks, and Etruscans recognized the importance of dental health. During the Middle Ages, the progress of orthodontics, like many scientific fields, stopped. However, the Renaissance period saw a resurgence in scientific inquiry and medical advancements. Ambroise Paré, a French surgeon in the 16th century, is credited with significant contributions to dentistry, including a primordial orthodontics.

The 18th century marked the real beginning of orthodontic practice. Pierre Fauchard published "Le Chirurgien Dentiste" in 1728. This seminal work included descriptions of dental anomalies and proposed various corrective devices.

In the 19th century, orthodontics began to emerge as a distinct dental specialty. The American Norman William Kingsley made significant strides in orthodontic theory. His book, "A Treatise on Oral Deformities," published in 1880, showed several insights into the diagnosis and treatment of malocclusions. Another pivotal figure in the history of orthodontics is Edward Hartley Angle. Angle developed the first classification system for malocclusions, which also remains the main foundation of orthodontic diagnosis today. He also founded the first school of orthodontics in 1901, the Angle School of Orthodontia.

The 20th century witnessed remarkable advancements in orthodontic techniques and technologies. The introduction of stainless steel in the 1920s revolutionized orthodontic appliance design, providing greater flexibility and durability compared

to earlier materials. Cephalometric radiography was also invented in the 1930s, thanks to the advent and control of the x-rays, allowing for precise measurement and analysis of craniofacial structures.

The latter half of the century saw the implementation of various innovations that are still investigating nowadays. Today, orthodontics is a highly specialized and technologically advanced field in medicine. The latest digital technologies have transformed treatment planning and appliance fabrication.

Therefore, from ancient attempts to align teeth with rude materials to the sophisticated digital technologies of today, orthodontics has continually evolved to meet the changing needs of patients. The future of orthodontics is poised for further transformation with ongoing research and technological advancements.²⁴ The area of the most active investigation is artificial intelligence (AI) for predictive modeling and personalized treatment planning. This innovation hold promise for improving treatment efficiency, reducing duration, and minimizing adverse effects, i.e., stochastic effects produced during the cephalometric phase.

Cephalometry is a diagnostic tool used in orthodontics, maxillofacial surgery, and other medical fields to measure the dimensions of the head, particularly the bones of the skull, using radiographic imaging. It involves the analysis of specific radiographs, which are standardized lateral and sometimes posteroanterior. These images are used to assess the relationships between dental and skeletal components, providing essential data for diagnosing malocclusions, planning treatments, and evaluating growth and treatment outcomes.

Cephalometry relies on the identification of specific anatomical landmarks on the image that are used to provide the measurement of distances and angles between these landmarks. Several standardized analyses exist, each focusing on different aspects of craniofacial morphology.

Conventional bidimensional cephalometric analysis, that has been used over time, has several advantages but also limitations. Between the main advantages we can mention the standardization and reproducibility of the obtain images. Between the main limitations we can cite the two-dimensional representation and the radiation exposure.^{25,26}

Despite all those factors might confute its performance, the cephalometry is a cornerstone of orthodontic diagnosis, offering a detailed and standardized method for assessing craniofacial structures. Its ability to provide quantitative data on skeletal and dental relationships makes it an invaluable tool in both clinical practice and research. As technology advances, the integration of 3D imaging promises to enhance the precision and utility of cephalometric analysis, further improving patient outcomes in orthodontics and maxillofacial surgery.

From a radiological point of view, cephalometry has evolved significantly since its invention.²³ The bases of cephalometry were made in the early 20th century, with the introduction of cephalometric radiographs taken on standardized lateral position by Dr. Broadbent, who in 1931 developed the cephalostat. This innovation was extremely important for producing reproducible radiographs, allowing for precise longitudinal studies of cranial anatomy.

Then, the advent of computer technology in the late 20th century revolutionized cephalometry. Key developments include digital radiographs and informatic analysis, that changed from analog to digital radiography. This technological era improved image quality, reduced radiation exposure, and allowed for easier digital storage of data.

In latest years, the introduction of 3D imaging technologies represents a significant step forward. Cephalometry continued to evolve with the integration of advanced imaging techniques such as 3D cephalometric analysis to became more feasible than ever.²⁶

Lastly, the incorporation of AI represents a crucial development. AI-driven software can automatically identify reference point used in craniofacial analysis, analyze growth patterns, and predict treatment results with high accuracy.²⁷ These newest technologies can have the potential to reduce errors depending on the human expertise, enhance diagnostic precision, and individualize treatment strategies based on predictive modeling trained on previous results.²⁸

As technology continues to improve, cephalometry and face analyses will likely become even more intrinsic to orthodontics and craniofacial surgery, driving improvements for operators who work with them.

3D cephalometric analysis

3D cephalometry represents a significant advancement in the craniofacial radiology, overpass the traditional 2D cephalometry by providing a comprehensive volumetric analysis of craniofacial organs.²⁹ The advent of CBCT has facilitated the development and application of 3D cephalometry. As the matter of fact, unlike conventional CT, CBCT uses a cone-shaped X-ray beam and a reciprocating flat-panel detector to acquire a volumetric image in a single rotational scan. This results in a lower radiation dose compared to conventional CT.³⁰

CBCT specifications usually include:³¹

- Voxel Size, typically ranging from 0.075 to 0.4 mm, affecting the resolution and detail of the images.
- Field of View, adjustable depending on the region of interest, with options ranging from scans of specific teeth to full craniofacial scans.
- Radiation Dose, significantly lower than traditional CT due to the intrinsic technology of cone beam.

The data acquired by scanners are reconstructed using sophisticated informatic algorithms and then they can be manipulated by dedicated softwares; images can be segmented into different anatomical structures, analyzed for automated landmarking, and measured in linear, angular, and volumetric dimensions.

CBCT-based cephalometry, off course, represents probably the most important advent in the modern orthodontics but it still involves radiation exposure, necessitating judicious use during orthodontic practice, especially applied on pediatric patients.^{32, 33}

Cephalometry, derived from the Greek words "kephale" (head) and "metron" (measure). The pioneering work of Downs in the 1940s and the development of standardized cephalometric analysis methods, such as the Steiner, Ricketts and the McNamara analyses, laid the foundation for modern orthodontic diagnosis.

While 2D cephalometry has been extremely important in orthodontics, it has several limitations:

- Superimposition of structures. The 2D images result in overlapping of anatomical structures, which can obscure important details, and in errors in landmark identification and pointing.

- Lack of depth and transversality. 2D images do not provide information about the depth of structures, as well as the coronal dimension from one side to the other.
- Magnification and distortion. Variations in patient positioning can result in magnification and distortion, affecting the precision of linear measurements, especially between different cephalostats.

The introduction of CBCT marked a significant advancement in cephalometry by addressing many of the limitations associated with 2D imaging, well known since its development in the late 1990s.³⁴ Of course, the main objective of the present thesis in working on radioprotection-based techniques. For this reason, the main aspects in CBCT development have been represented by the pulsed X-ray emission and the interactive reconstruction techniques. The joint of these two features provided high resolution images but with a control of the exposure of the patients to the ionizing radiation. Moreover, the incorporation of AI and machine learning algorithms into CBCT analysis has transformed diagnostic capabilities compatibly with radioprotection.³⁵

One of the primary advantages of CBCT over traditional CT is the reduced radiation dose.³⁶ Typical radiation doses for CBCT scans range from 29 to 477 μSv , significantly lower than the doses associated with CT, which can range from 1000 to 3300 μSv . However, CBCT doses are higher than those from traditional dental X-rays, necessitating careful consideration of indications and patient selection. But, nowadays, these limits need to be overcome being more restrictive to the patient's safety against the stochastic risk pronounced by several institutions built to the prevention of uncontrolled radiation exposure. As the matter of fact, as already mentioned, orthodontics exams and procedures should be repeated more than one time, so irradiating the same patient more than the untreated people. It is clear that finding new less-invasive methods for cephalometric analysis must be addressed to provide better and safer diagnostic instruments, combining the most recent advents of digital orthodontics.

One of the challenges of 3D cephalometric analysis is the precise identification of cephalometric reference points also known as landmarks.³⁷ In fact unlike 2D analysis, where landmarks are identified on the sagittal or coronal plane for lateral

and posteroanterior cephalometries, respectively, 3D analysis requires the identification of landmarks in three orthogonal planes (axial, coronal, and sagittal) and, finally, onto a rendered volume. This requires a better knowledge of craniofacial anatomy and the spatial relationships between different structures.

3D cephalometric analysis allows for the measurement of linear distances, angular relationships, and volumetric assessments that are not possible with 2D imaging. Common measurements include linear distances, angular measurements, and surface and volumetric data; these last, represents an important finding provided by CBCT-based cranial analysis.

Numerous studies have investigated the accuracy and reliability of 3D cephalometric measurements derived from CBCT and annotated by human experts.³⁸ 3D measurements generally provide greater accuracy than their 2D counterparts, but several factors can influence measurement precision, including image resolution (slicing), landmark identification accuracy, and software algorithms (post-processing).

In the modern orthodontic era, AI algorithms can automate landmark identification. Also, emerging visualization techniques, such as virtual reality (VR) and augmented reality (AR), offer new ways to interact with 3D cephalometric data.³⁹ All these technologies that improve day by day have the potential to allow an holistic assessment of the patient's craniofacial anatomy, leading to customized treatment plans tailored to individual needs.⁴⁰ Furthermore, operator's ergonomic should be increased thank to the use of these supporting methods.

Teeth segmentation is another important tool in the use of CBCT technology, but it also be an extremely useful tool for all the human body.⁴¹ In dentistry, the process involves the isolation and delineation of individual teeth from the surrounding bones, enabling detailed analysis of dental morphology, occlusion, and spatial relationships within the craniofacial complex. As the other branches of informatic engineering, the development of robust teeth segmentation AI-tools has emerged as a key area of research. Moreover, teeth segmentation plays a crucial role in the design and fabrication of custom orthodontic appliances, such as clear aligners, where exact tooth contours and positions are essential for effective treatment.

Teeth segmentation can be performed manually, semi-automatically, or fully automatically, depending on the software used and the complexity of the clinical scenario. Manual segmentation, while extremely accurate, is time-consuming and requires significant expertise, making it less practical for routine clinical use. Semi-automatic segmentation tools offer a balance between user control and efficiency, allowing clinicians to guide the segmentation process while relying on the software to handle much of the computational workload.⁴² These tools typically involve the clinician marking key points or regions on the tooth surface, after which the software completes the isolation based on these inputs. Automated segmentation, on the other hand, can rapidly and accurately segment teeth with minimal user intervention thanks to AI-based algorithms. These systems analyze the grayscale values (Hounsfield units) and geometric features to distinguish between teeth, bone, and soft tissues, automatically generating detailed 3D models.

Despite the advancements in this segmentation tool, several challenges remain. One of the primary difficulties is dealing with the presence of artifacts in CBCT scans such as scattering caused by metallic restorations or braces. Additionally, variations in tooth morphology, such as those seen in cases of crowding, impaction, or developmental anomalies, can make it difficult for automated algorithms to accurately delineate individual teeth. Lastly, the proximity of teeth to dense structures further complicates segmentation, necessitating advanced algorithms capable of distinguishing subtle differences in grayscale values after a proper training on manually annotated databases.

The future of organ segmentation in general lies in the continued refinement of AI algorithms and the development of fully integrated digital workflows.⁴³ As machine learning models are trained on increasingly large and diverse datasets, the accuracy and reliability of automated segmentation are expected to improve significantly, reducing the need for manual help and making the technology accessible to a broader range of practitioners, from neophytes to expert ones.

PhD in Traslational medicine about green issues: the application of the project

Radioprotection is a critical consideration in the use of diagnostic imaging. The modern application of CBCT in orthodontics, while highly beneficial, introduces a level of radiation exposure that necessitates stringent adherence to radioprotection guidelines. The principles of justification, optimization, and dose limitation, as outlined by international regulatory bodies, must be meticulously followed to ensure that the benefits outweigh the risks, especially when it is used for pediatric patients.

This thesis aims to explore the application of CBCT in orthodontics within the framework of radioprotection principles, helped by AI algorithms that can ensure demonstrated advantages compared to convention 3D imaging.

By integrating the principles of radioprotection into the use of CBCT, especially the optimization and dose limitation, this thesis seeks to establish a balanced approach that maximizes the diagnostic benefits of advanced 3D imaging while safeguarding patient health. Through a combination of literature review, clinical studies, and practical recommendations, this work aims to contribute to the development of best practices in the use of CBCT in orthodontics, ensuring that this powerful diagnostic tool is utilized responsibly and effectively. The reduction of FOV, combined to AI-driven technologies, represent the focus of the present research.

The concept of being "green" in radiodiagnostics involves adopting practices and technologies that minimize environmental impact by ionizing radiations while maintaining high standards of patient care. Continuous research and collaboration within the healthcare industry and medicine are essential to further advance sustainability and promote a greener future in radiodiagnostics too.

The Programma Operativo Nazionale Ricerca e Innovazione 2014-2020 (PON RI) is an initiative launched by Italy to enhance higher education quality, bolster research, technological development, and foster innovation. Managed by the Ministry of University and Research (MIUR), this program aligns with the European Union's cohesion policy and strategic objectives outlined in Horizon 2020 and Cosme.

The primary goal of PON RI is to improve the competitive positioning of Italy's less advantaged regions by fostering high-quality research and innovation. It aims to facilitate intelligent, sustainable, and inclusive development through three main axes:

- Investment in human capital. This axis focuses on advanced education and research, supporting initiatives like innovative industrial doctorates and researcher mobility. A significant portion of the budget, approximately 317 million euros, is dedicated to these activities.

- Strengthening research and innovation systems. This includes enhancing research infrastructures, promoting business investment, and fostering collaboration between universities, research institutions, and enterprises. Around 74% of the total resources are allocated to this area.

- Technical assistance. A smaller portion of the funds is reserved for supporting the program's implementation, ensuring efficient and effective use of resources.

The program's total budget is 1.189 billion euros, with substantial funding from the European Regional Development Fund (ERDF) and the European Social Fund (ESF). These funds are intended to stimulate private investment in research and innovation, create new jobs, and modernize research infrastructures, among other objectives.

PON RI targets several strategic sectors, including aerospace, agrifood, blue growth (marine economy), green chemistry, energy, intelligent manufacturing, sustainable mobility, health, and cultural heritage technologies. These areas are chosen to create innovation hubs that nurture new knowledge, talents, and entrepreneurial opportunities.

By fostering public-private partnerships and enhancing research capacities, PON RI has significantly contributed to regional development. For instance, it has supported the creation of numerous doctoral and research positions, modernized research facilities, and encouraged the private sector to engage more actively in innovation.

In the context of radiodiagnostics and the use of CBCT technology, PON RI emphasizes the importance of radioprotection principles. Efforts to reduce radiation exposure include optimizing imaging protocols, adopting advanced low-dose

technologies, and educating healthcare professionals on best practices for radiation safety. Additionally, the program supports research into sustainable technologies and green innovations, aligning with broader goals of reducing environmental impact and promoting eco-friendly, in term of surround contamination, practices in medical imaging and other fields.

By integrating these principles into its initiatives, PON RI not only advances technological and scientific capabilities but also ensures that such progress is sustainable and responsible, minimizing risks to both patients and the environment.

Artificial intelligence available to the development of a virtual reality software for an automated cephalometric analysis of ultra-reduced CBCT FOV

The present PhD project title suggests a cutting-edge research focus that combines several advanced technologies: artificial intelligence (AI), virtual reality (VR), cephalometric analysis, and ultra-reduced cone-beam computed tomography (CBCT) fields of view (FOV). Here's a brief breakdown of what your project involves:

- Artificial Intelligence (AI). Developing or utilizing AI algorithms to automate aspects of cephalometric analysis. This could involve training models to recognize and measure anatomical landmarks within CBCT images, even with very small FOV.
- Virtual Reality (VR) software development. Work on a VR application that integrates with the AI to provide an immersive environment for analyzing CBCT data. This could allow for more interactive and intuitive cephalometric analyses, where users can manipulate and examine 3D reconstructions in real-time and shared face to face with patients.
- Automated cephalometric analysis. The project seems focused on automating this process using AI, which could make the analysis faster, more accurate, and less dependent on human input.
- Ultra-Reduced CBCT FOV. The mention of ultra-reduced FOVs suggests it works with CBCT scans that cover very small anatomical regions, perhaps to reduce radiation exposure or focus on specific areas. Analyzing these smaller datasets can be challenging, but it sounds like AI and VR tools are designed to handle this.

Artificial intelligence and its application in the medical field

Artificial Intelligence (AI) has emerged as a transformative force across various industries, with the healthcare sector being one of the most significantly impacted ones. AI encompasses a range of computational techniques that enable machines to mimic human cognitive functions such as learning, reasoning, problem-solving, perception, and language understanding. These techniques are transformed into algorithms and models that learn from data, adapt to new inputs, and improve extremely over time.

The evolution of AI can be traced back to the mid-20th century, but its practical applications in complex fields such as medicine have gained momentum only in the last few years, largely due to advancements in computational power, the proliferation of big data, and the development of sophisticated IT algorithms. AI in medicine is now at the forefront of innovation, offering new methodologies to enhance diagnostic accuracy, optimize treatment plans, and improve patient outcomes through personalized medicine.⁴⁴

The integration of AI into healthcare began with the development of early decision support systems in the 1970s, such as MYCIN, which was designed to diagnose bacterial infections and recommend antibiotics.⁴⁵ Although MYCIN was never widely adopted in clinical practice, it laid the groundwork for the future of AI in medicine.

As AI technology evolved, its applications in medicine expanded from rule-based systems to more complex learning algorithms. The 1990s and 2000s saw the emergence of machine learning (ML) techniques that could analyze large datasets to uncover patterns and make predictions.⁴⁶ These years are characterized by the increasing adoption of deep learning (DL) algorithms, which have transformed fields such as medical imaging and genomics by providing unprecedented levels of accuracy and insight.

AI in healthcare is underpinned by several core tools. These techniques include machine learning, deep learning, natural language processing, and computer vision.

- Machine Learning (ML) is a subset of AI that focuses on the development of algorithms that can learn from and make predictions based on data. ML models are

trained on large datasets, learning to recognize patterns and make decisions with minimal human intervention.⁴⁷

- Supervised Learning (SL). In this setting, the model is trained on labeled data, meaning that each training example is paired with an output label.⁴⁸ SL approach is widely used in healthcare for tasks such as disease prediction.

- Unsupervised Learning (UL): UL requires training the model on data without labeled outcomes.⁴⁹ This technique is used to identify patterns or clusters within the data such as patient clustering, where patients with similar characteristics are grouped together for more targeted characterization.

- Reinforcement Learning (RL). RL is a subarea of ML where an agent learns to make decisions by taking actions to maximize benefits.⁵⁰

- Deep Learning (DL). It is a subset of ML that uses neural networks with multiple layers to model complex patterns in data. Each layer in a deep learning model extracts progressively higher-level features from the input data, allowing the model to learn complex representations.⁵¹

- Convolutional Neural Networks (CNNs). CNNs are a type of DL model specifically designed for processing structured grid data, such as images.⁵² In medical imaging, CNNs have been instrumental in tasks such as image classification, object detection, and segmentation.

- Recurrent Neural Networks (RNNs). RNNs are designed for sequential data and are commonly used in natural language processing (NLP) tasks.⁵³ In healthcare, RNNs can be used to analyze time-series data, such as patient vital signs, to predict clinical outcomes.

- Generative Adversarial Networks (GANs). GANs consist of two CNN trained together in a competitive setting.⁵⁴ GANs have been used in healthcare for generating synthetic medical images for training purposes, improving the quality of imaging, and even in drug discovery.

Also, computer vision is a field of AI that enables computers to interpret and process visual data. In medicine, computer vision is primarily used in medical imaging to automatically analyze images and extract diagnostic information. Computer vision can be analyzed through different capabilities it can provide:

- Image Segmentation, dividing an image into meaningful regions or objects. In medical imaging, segmentation is used to isolate and analyze specific anatomical structures or pathological regions.⁵⁵
- Object Detection, to identify and locate objects within an image.⁵⁶ In healthcare, object detection can be used to detect and localize abnormalities.
- Image Classification. Image classification involves assigning a label to an entire image based on its content.⁵⁷ In healthcare, image classification can be used to identify disease states in medical images.

In computer vision, AI has demonstrated remarkable success in the automatic detection and classification of diseases in medical images. Dentistry also is undergoing a technological transformation, with AI playing a central role in its development. The integration of AI into dental practice is particularly evident in the areas of dental imaging and treatment planning.

Dental imaging is a cornerstone of diagnostics and treatment planning in dentistry. Traditional imaging modalities in dentistry include periapical and panoramic radiographs, while more advanced techniques such as CBCT in still increase in number. AI has been integrated into these imaging modalities to improve the accuracy and efficiency of diagnostics.⁵⁸

Not only, also orthodontics has been significantly impacted by AI nowadays. AI-driven tools in orthodontics are enhancing the accuracy of diagnostics, automating cephalometric analysis for example. Image analysis algorithms are based on DL models, particularly CNNs, trained on large datasets of annotated cephalometric images.⁵⁹

As AI technology continues to advance, the possibility of real-time diagnostics during dental procedures becomes more feasible. AI-driven tools could analyze intraoperative data, such as images from intraoral scanners or surgical videos, to provide immediate diagnostic support to dentists.

In conclusion, AI is transforming the field of medicine as well as the fields of dentistry and orthodontics. The integration of AI into dental practice is driven by advances in ML, DL, natural language processing, and computer vision, each of which contributes to the development of sophisticated AI-driven software.

Introduction to virtual reality

Virtual Reality (VR) is a technology that creates immersive environments, often simulating real-world scenarios and images, that users can interact with through specialized hardware and software.⁶⁰ The concept of VR is not new; it has its roots in the mid-20th century with the development of early simulation systems. However, the past few decades have seen significant advancements in VR technology, making it a powerful tool in various fields, including entertainment, education, military training, and, most notably, healthcare.

In the medical field, VR is increasingly being used for a range of applications, from surgical training and simulation to pain management and therapeutic interventions.⁶¹ The immersive nature of VR allows for highly controlled environments where users can engage in realistic simulations that closely mimic real-world scenarios.

VR systems are composed of several key components that work together to create immersive experiences. These include hardware, software, and content.

The creation of content for VR, particularly in medical field, requires a combination of technical expertise and domain-specific knowledge. The following sections explore some of the key areas where VR is being applied in medicine, with a particular focus on dentistry and orthodontics.

Dentistry, like many other medical fields, is experiencing a technological revolution with the integration of VR. VR is being used in dental education, treatment planning, and patient care, offering new ways to enhance the precision and effectiveness of dental procedures.⁶²

Among the steps in which VR can be useful there are:

- 3D visualization of patient-specific data, such as CBCT scans, intraoral scans, and digital impressions, in a 3D virtual environment.⁶³ This visualization allows dentists and surgeons to examine the patient's anatomy in detail, identify areas of concern, and plan interventions with greater accuracy.
- Surgical planning for complex surgical procedures, such as implant placement or orthognathic surgery, VR allows for detailed preoperative planning.⁶⁴ Surgeons can

simulate the procedure in the virtual environment, testing different approaches and predicting potential challenges.

- Patient communication and education: to enhance the patient communication and education by allowing patients to visualize their own dental anatomy and the proposed treatment plan.⁶⁵

Orthodontics, the branch of dentistry that focuses on the diagnosis, prevention, and correction of malocclusions and dentofacial deformities, has seen significant advancements with the integration of VR too. By importing 3D imaging data, such as CBCT and facial scans, into the VR environment, orthodontists can perform a more detailed and accurate analysis of the patient's skeletal and dental structures. VR also allows for dynamic analysis, where the orthodontist can simulate jaw movements and assess the functional relationships between different anatomical components.

Despite the numerous advantages, the integration of VR into medical practice requires overcoming several technical challenges, including real-time execution, high-resolution imaging, and system integration. The ongoing advancements in VR, coupled with innovations in AI, and telemedicine also, promise to change the future of medicine.

Automated cephalometric analysis

Cephalometric analysis is a cornerstone of orthodontic diagnosis and treatment planning. It involves the study of craniofacial morphology through the precise measurement of anatomical landmarks on cephalometric radiographs. Traditionally, this process has been manual, requiring significant expertise and time to ensure accurate and consistent results. However, with the advent of advanced computational techniques and artificial intelligence (AI), cephalometric analysis has become increasingly automated, offering the potential for greater precision, efficiency, and consistency in orthodontic care.⁶⁶

This chapter will explore the technical foundations of automated cephalometric analysis, review current advancements, and discuss the integration of these systems into clinical practice. While some aspects of this topic have been introduced in previous sections, here we will delve deeper into the specific methodologies, algorithms, and clinical applications that make automated cephalometric analysis a transformative tool in orthodontics.

Cephalometric analysis was first introduced by Broadbent in 1931, and since then, it has become an essential tool in orthodontics. The technique involves the use of standardized lateral and frontal cephalometric radiographs to measure craniofacial dimensions and relationships. These measurements are crucial for diagnosing malocclusions, planning orthodontic treatment, and evaluating the outcomes of surgical interventions.

The traditional approach to cephalometric analysis involves the manual identification of anatomical landmarks on radiographs. These landmarks include points such as Sella (S), Nasion (N), Anterior Nasal Spine (ANS), and Pogonion (Pg), among others. Once identified, these landmarks are used to construct reference lines and planes, such as the Frankfort Horizontal Plane and the Occlusal Plane, which serve as the basis for various angular and linear measurements.

Automated cephalometric analysis leverages advanced computational techniques to address the limitations of manual methods. By automating the identification of landmarks and the calculation of measurements, these systems offer the potential for greater accuracy, consistency, and efficiency in orthodontic practice.

The foundation of automated cephalometric analysis lies in image processing—a branch of computer science that focuses on the manipulation and analysis of images to extract meaningful information. Several image processing techniques are employed in automated systems to enhance the quality of cephalometric radiographs and facilitate the accurate identification of landmarks. Among them:

- Preprocessing: Before landmark identification can occur, cephalometric images often undergo preprocessing steps to improve image quality. These steps may include noise reduction, contrast enhancement, and edge detection. Techniques such as Gaussian filtering, histogram equalization, and Sobel operators are commonly used to enhance the visibility of anatomical structures.

- Segmentation: Image segmentation is the process of partitioning an image into distinct regions or objects. In the context of cephalometric analysis, segmentation algorithms are used to isolate the craniofacial structures of interest, such as the skull, mandible, and teeth, from the background. Techniques such as thresholding, region-growing, and active contour models are employed to achieve accurate segmentation.

- Feature Extraction: Once the image has been preprocessed and segmented, the next step is feature extraction, where key characteristics of the image, such as edges, corners, and textures, are identified. Feature extraction is critical for identifying anatomical landmarks, as it provides the data needed for subsequent analysis.

Automated landmark detection is at the core of cephalometric analysis. Several algorithms have been developed to automate this process, ranging from traditional machine learning approaches to more advanced deep learning models.

One of the earliest methods used for automated landmark detection is template matching.⁶⁷ In this approach, predefined templates of anatomical landmarks are created based on a set of reference images. These templates are then matched to the target image using techniques such as cross-correlation or normalized correlation coefficients. While template matching can be effective for well-defined landmarks, it is less robust in cases of anatomical variability or image distortion.

Active Shape Models (ASM) are statistical models that represent the shape of anatomical structures based on a set of training images.⁶⁸ ASM uses principal

component analysis (PCA) to capture the variability of shapes within the training set and to generate a model that can deform to fit new images. During landmark detection, the ASM iteratively adjusts its shape to match the target image, guided by local image features. ASM has been widely used in automated cephalometry due to its ability to adapt to variations in anatomy.

With the advent of deep learning, Convolutional Neural Networks (CNNs) have become the state-of-the-art approach for automated landmark detection.³⁷ CNNs are a class of deep learning models designed specifically for image analysis. They consist of multiple layers of neurons that learn hierarchical features from the input image, such as edges, textures, and complex patterns. In the context of cephalometry, CNNs can be trained on large datasets of annotated radiographs to automatically detect landmarks with high accuracy.

Multi-task learning is a deep learning approach where a single model is trained to perform multiple related tasks simultaneously.⁶⁹ In automated cephalometric analysis, multi-task learning can be used to detect multiple landmarks at once, with the model learning to identify relationships between landmarks to improve accuracy. This approach leverages the shared information between tasks, leading to better generalization and robustness.

Once the landmarks have been detected, the next step is to calculate the relevant cephalometric measurements. These measurements typically include linear distances, angles, and ratios that describe the relationships between various craniofacial structures. Automated systems use the detected landmarks to perform these calculations accurately and consistently.

Automated systems use predefined algorithms to construct reference lines and planes based on the detected landmarks. For example, the Frankfort Horizontal Plane is constructed using the landmarks Orbitale (Or) and Porion (Po), while the Occlusal Plane is defined by the position of the upper and lower molars.

Key cephalometric measurements, such as the SNA angle (Sella-Nasion-Point A), SNB angle (Sella-Nasion-Point B), and ANB angle (Point A-Nasion-Point B), are automatically calculated based on the positions of the landmarks. These

measurements are critical for diagnosing skeletal discrepancies and planning orthodontic treatment.

Beyond traditional measurements, automated systems can perform more advanced analyses, such as shape analysis and symmetry assessment. By comparing the shapes of different craniofacial structures or assessing the symmetry between the left and right sides of the face, these systems provide a more comprehensive evaluation of the patient's craniofacial morphology.

Several CNN architectures have been proposed for cephalometric landmark detection, including U-Net, VGGNet, and ResNet. These architectures differ in their depth, complexity, and approach to feature extraction, but all have been shown to perform well in detecting cephalometric landmarks. Recent research has also explored the use of attention mechanisms and multi-scale feature extraction to further improve accuracy.

Transfer learning is a technique where a pre-trained model (typically trained on a large dataset such as ImageNet) is fine-tuned on a specific task, such as cephalometric landmark detection. This approach allows models to leverage the knowledge learned from general image recognition tasks and apply it to cephalometry, often resulting in faster training and improved performance.

The performance of deep learning-based landmark detection models is typically evaluated using metrics such as mean squared error (MSE), mean radial error (MRE), and success detection rate (SDR). These metrics provide a quantitative assessment of the model's accuracy in detecting landmarks and its reliability in clinical settings.

Another key advancement in automated cephalometric analysis is the integration of 3D imaging modalities, such as Cone-Beam Computed Tomography (CBCT). While traditional cephalometry is based on 2D radiographs, 3D imaging provides a more comprehensive view of the craniofacial structures, allowing for more accurate analysis and treatment planning.

Ultra-reduced field of view CBCT in dentistry and orthodontics

CBCT has become a vital imaging modality in dentistry and orthodontics, offering a 3D visualization of craniofacial structures with high spatial resolution. Traditionally, CBCT systems have provided comprehensive imaging of large anatomical regions, which is essential for various diagnostic and treatment planning purposes. However, recent advancements have focused on developing ultra-reduced FOV CBCT systems, which capture highly localized regions with minimal radiation exposure. These ultra-reduced FOV systems are particularly useful in applications where detailed imaging of a specific area is required, and reducing patient radiation exposure is a priority.

This chapter explores the technical foundations of ultra-reduced FOV CBCT, its clinical applications in dentistry and orthodontics, and the benefits and challenges associated with this technology. We will delve into the principles of CBCT imaging, the advancements in FOV reduction, and the integration of ultra-reduced FOV CBCT with other technologies such as AI and automated cephalometry.

CBCT is a radiographic imaging method that produces 3D images of the craniofacial region using a cone-shaped X-ray beam and a flat-panel detector. Unlike conventional CT, which uses a fan-shaped beam and acquires images slice by slice, CBCT captures the entire volume in a single rotation around the patient. During a CBCT scan, the X-ray source and detector rotate around the patient's head, capturing multiple 2D projection images at different angles. These projections are then reconstructed into a 3D volumetric dataset using specialized algorithms such as filtered back-projection or iterative reconstruction.

Its resolution is determined by the size of the voxels in the reconstructed dataset. Smaller voxels result in higher spatial resolution, allowing for the visualization of fine anatomical details. CBCT systems typically offer voxel sizes ranging from 0.1mm to 0.4mm, depending on the scanning parameters and the FOV.

The FOV of a CBCT scan refers to the size of the anatomical region that is imaged. FOV can range from large (e.g., covering the entire craniofacial region) to ultra-reduced (e.g., focusing on a single tooth or a small anatomical structure such as the maxillary complex only). The choice of FOV depends on the clinical indication,

with larger FOVs used for comprehensive assessments and smaller FOVs for localized examinations.⁷⁰

One of the primary advantages of CBCT over conventional CT is the reduced radiation dose. However, the dose associated with CBCT can still vary significantly depending on the FOV, exposure settings, and the number of projections acquired. Radiation dose is a critical consideration in dental imaging, particularly in pediatric patients and situations where repeated imaging is necessary.⁷¹

The effective dose is a measure of the radiation risk associated with a scan, taking into account the type of radiation and the sensitivity of the tissues exposed.⁷² Effective dose is typically expressed in millisieverts (mSv) and is used to estimate the potential biological effects of radiation exposure.

To minimize the radiation dose, CBCT systems offer various dose reduction strategies, including the selection of ultra-reduced FOVs, adjustment of exposure parameters, and the use of optimized scanning protocols.⁷³ The goal is to achieve the necessary diagnostic information while keeping the radiation dose as low as reasonably achievable (ALARA principle).

Ultra-reduced FOV CBCT represents a significant advancement in dental imaging, enabling highly localized imaging with minimal radiation exposure. This section explores the technical innovations that have made ultra-reduced FOV CBCT possible, including improvements in detector technology, image reconstruction algorithms, and system design.

Smaller FOV CBCT has a wide range of clinical applications in dentistry and orthodontics, where detailed imaging of specific anatomical regions is essential for accurate diagnosis and treatment planning. This section explores some of the key applications of ultra-reduced FOV CBCT, including endodontics, implantology, periodontics, and, of course, orthodontics.

In orthodontics, the precise assessment of craniofacial structures is essential for diagnosing malocclusions, planning treatment, and monitoring progress. Ultra-reduced FOV CBCT offers a valuable tool for obtaining detailed images of specific anatomical regions, such as the dental arches.

Ultra-reduced FOV CBCT can be used to perform localized cephalometric analysis, focusing on specific regions of interest, such as the maxilla, mandible, or dental arch. This approach is particularly useful in cases where detailed analysis of a specific area is needed, such as in the assessment of asymmetry, the evaluation of surgical outcomes, or the planning of segmental osteotomies.

While ultra-reduced FOV CBCT systems are designed to minimize radiation exposure, the cumulative dose from repeated scans can still be a concern, particularly in pediatric patients or cases requiring multiple follow-up scans.

In cases where multiple ultra-reduced FOV CBCT scans are needed over the course of treatment, it is also essential to consider the cumulative radiation dose and weigh it against the diagnostic benefits. Clinicians must carefully evaluate the necessity of each scan and explore alternative imaging modalities, such as intraoral radiographs or low-dose CBCT protocols, when appropriate.

The decision to use ultra-reduced FOV CBCT should be based on a thorough assessment of the patient's specific needs, including their age, health status, and the clinical indication for the scan. For example, pediatric patients are more sensitive to radiation, so the use of ultra-reduced FOV CBCT should be justified by the clinical benefits and performed with the lowest possible radiation dose.

Therefore, exploring alternative data to ensure a proper analysis was the aim of the present project. The integration of ultra-reduce FOVs with facial and intraoral scans represents the potential solution to offer a radioprotection-driven cephalometric analysis available to orthodontists and maxillofacial surgery for conventional craniometry.

Project development

In this dissertation, we meticulously describe each component involved in the development of the software, encompassing the integration of artificial intelligence for automated cephalometric analysis, the implementation of virtual reality for enhanced user interaction, and the application of ultra-reduced CBCT FOV for precise imaging. Each section delves into the specific methodologies, algorithms, and technologies utilized, providing a comprehensive understanding of how these elements coalesce to form a cohesive and innovative solution within the field of orthodontics. Each task will be discussed in greater detail in subsequent sections of the dissertation.

1. Automated landmarking of CBCT data

Automated landmarking involves the use of AI to precisely identify and mark anatomical landmarks on cephalometric radiographs or CBCT scans. This task is critical for accurate cephalometric analysis, as it provides the foundational reference points necessary for subsequent measurements and assessments. The automation of this process significantly reduces the time and potential for human error associated with manual landmark identification. Automated landmarking included not only the recognizing of osseous and dental reference points, but also facial landmarks representing the soft tissue features of the face.

2. Tooth segmentation from CBCT data

Tooth segmentation from CBCT data focuses on isolating individual teeth from 3D CBCT scans. This task leverages advanced image processing and machine learning techniques to accurately delineate tooth boundaries, even in cases of overlapping structures or complex anatomy. The segmented teeth are essential for detailed analysis and further processing, such as alignment or fusion with other datasets.

3. Tooth segmentation from intraoral scanning

Like CBCT segmentation, this task involves the extraction of individual teeth from intraoral scans, which are typically high-resolution, three-dimensional surface scans of the dental arches. The segmentation process in this context is geared

towards capturing the fine details of the tooth surfaces, which are crucial for applications such as restorative dentistry, orthodontic planning, and digital impressions.

4. Matching between intraoral scanning and CBCT data

Matching between intraoral scanning and CBCT data is the process of aligning the surface details obtained from intraoral scans with the volumetric data from CBCT scans. This task ensures that the high-resolution surface details captured in intraoral scans are accurately integrated with the three-dimensional structural information from CBCT, providing a comprehensive representation of the dental anatomy.

5. Fusion and labelling between teeth obtained from CBCT and IOS segmentations

This task involves the integration of segmented teeth from both CBCT and intraoral scanning (IOS) datasets. The fusion process combines the volumetric information from CBCT with the detailed surface information from intraoral scans, while the labelling step ensures that each tooth is accurately identified and labeled across both datasets. This process is critical for creating a unified model that can be used for diagnostics, treatment planning, and simulation.

6. Maxillary bone segmentation

Maxillary bone segmentation focuses on isolating the maxillary bone from CBCT data. This task is essential for orthodontic and surgical planning, as it provides a clear view of the bone structure, enabling precise assessments of bone volume, quality, and the relationship between the maxilla and surrounding anatomical structures. Accurate segmentation of the maxillary bone is crucial for interventions such as implant placement and orthognathic surgery.

7. Face scan matching

Face scan (FS) matching involves the alignment and integration of facial surface scans with the underlying skeletal and dental structures obtained from CBCT or other imaging modalities. This task is particularly important for planning orthodontic and orthognathic treatments, as it allows for a holistic view of the

patient's facial aesthetics in relation to their craniofacial anatomy. The matching process ensures that the external facial features are accurately correlated with the internal bone and dental structures.

8. Automated landmarking of FS data

As previously mentioned, automated landmarking included not only the recognizing of osseous and dental reference points, but also facial landmarks representing the soft tissue features of the face. The automation of this process significantly reduces the time and potential for human error associated with manual landmark identification.

Each of these tasks represents a critical component of the software development process, contributing to the overall goal of creating a comprehensive, AI-driven virtual reality platform for automated cephalometric analysis and orthodontic treatment planning. These tasks will be explored in greater detail in the following chapters, where we will delve into the specific methodologies, algorithms, and technologies employed.

Automated landmark detection

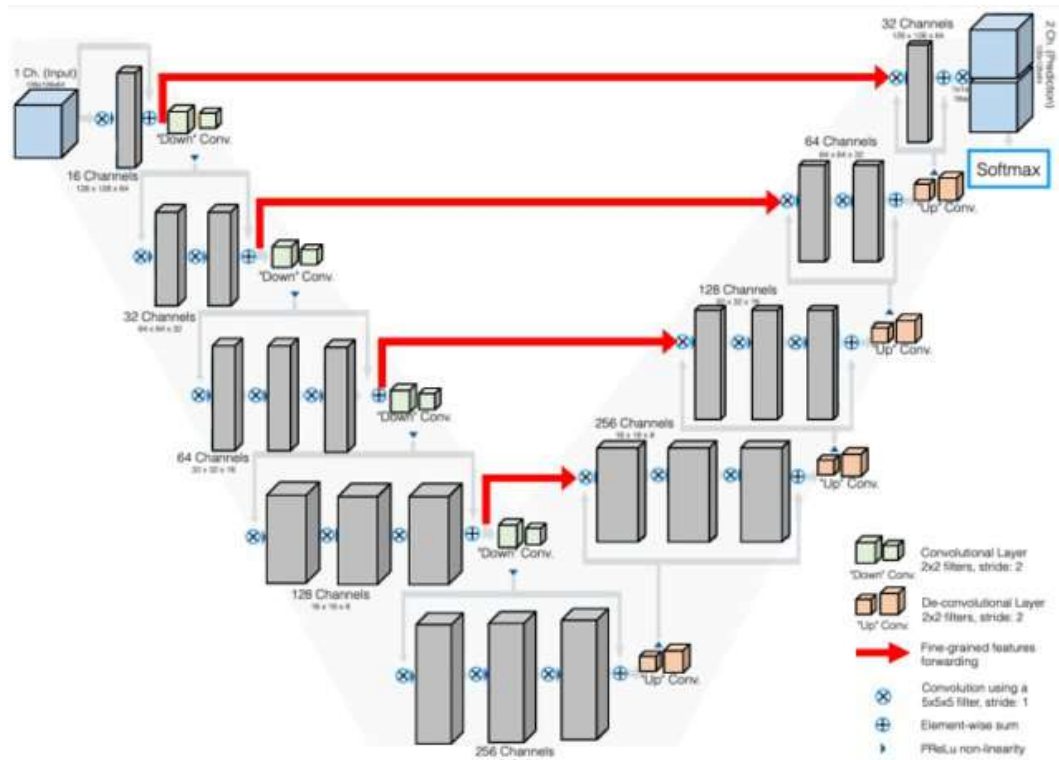
Automated landmark detection is a crucial process in the advancement of medical diagnostics, particularly when integrated with imaging modalities such as the CT used for the 3D cephalometric analysis. By leveraging DL algorithms, the accuracy, speed, and reproducibility of identifying critical anatomical landmarks can be significantly enhanced. This chapter would provide a comprehensive overview of the automated landmark detection process developed and trained in the present PhD project, detailing the underlying methodologies, training procedures, and the performance metrics used to evaluate the system, also included into the beta software developed by our research group.

The automated landmark detection system employed in this project utilizes a DL approach tailored for the segmentation and identification of cephalometric landmarks within CBCT scans. The system is based on the V-Net architecture, a DL CNN specifically designed for volumetric medical image segmentation.⁷⁴ The primary objective is to transform the task of landmark detection into a segmentation problem, where the model predicts the locations of landmarks by identifying regions of interest (ROI) inside the volumetric data provided by CBCT scans.

Among the various architectures developed for analysis of imaging, the V-Net excelled for its effectiveness in volumetric image segmentation. Originally designed for 3D medical imaging, V-Net has become a cornerstone in applications where detailed anatomical segmentation is required, such the ones elaborated by our beta software.

V-Net was introduced for the first time by Milletari et al. in 2016, specifically for volumetric medical image segmentation of human tissue or organs.⁷⁴ It built upon the previous U-Net architecture by incorporating 3D convolutions and a unique dice loss function, optimized for handling the class imbalance often found in medical datasets. V-Net's architecture is designed to effectively process volumetric data, making it particularly suitable for tasks such as bone structure analysis.

As mentioned, the architecture of V-Net is inspired by U-Net but with significant modifications to enhance its performance on 3D data.⁷⁵ U-Networks as the following image.



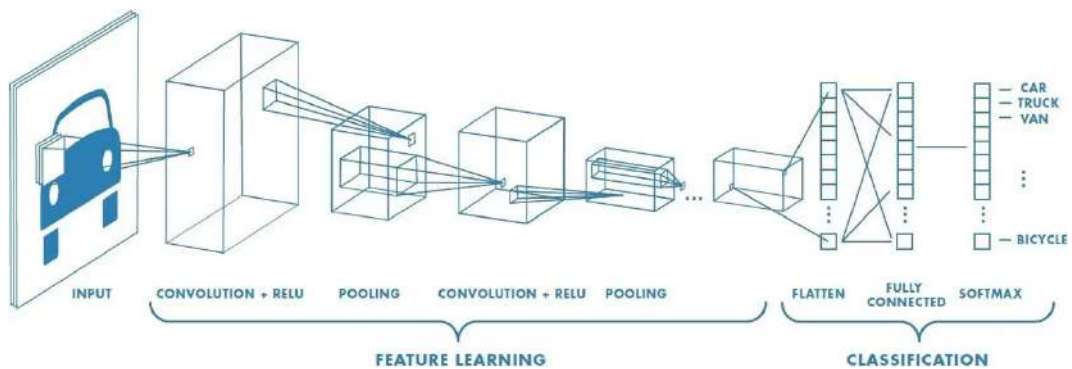
U-net architecture

This network follows an encoder-decoder structure, where the input image volume is progressively downsampled to capture high-level features and then upsampled to reconstruct the segmentation map. This structure is crucial for capturing both local and global context in the image.

Downsampling and upsampling steps

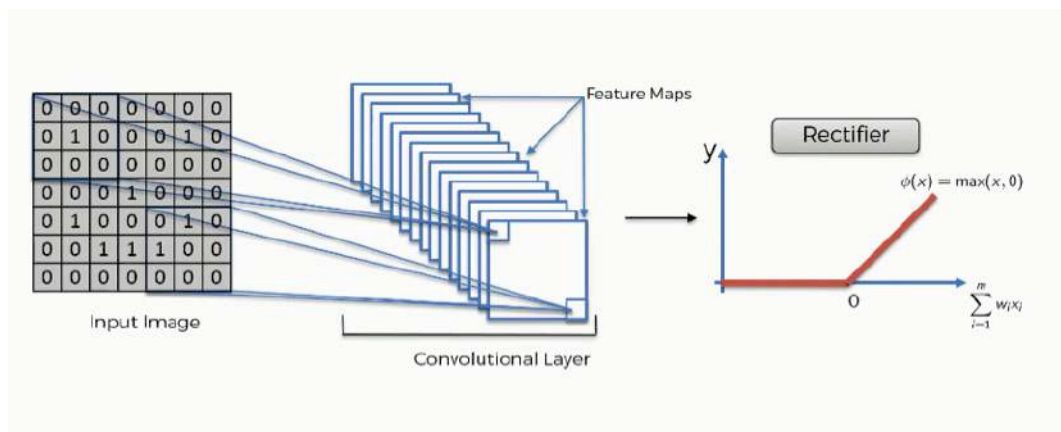
The encoder path consists of multiple convolutional layers that reduce the spatial dimensions of the input volume while increasing the depth of the feature maps. Each layer applies a convolution, followed by a rectified linear unit (ReLU) activation and a downsampling operation (typically max pooling).^{76,77} This pathway captures the hierarchical features of the image, essential for distinguishing between different anatomical structures.

Convolution is a mathematical operation used in signal processing and deep learning to combine two functions, typically an input signal and a filter or kernel, to produce a modified output that highlights specific features of the input.



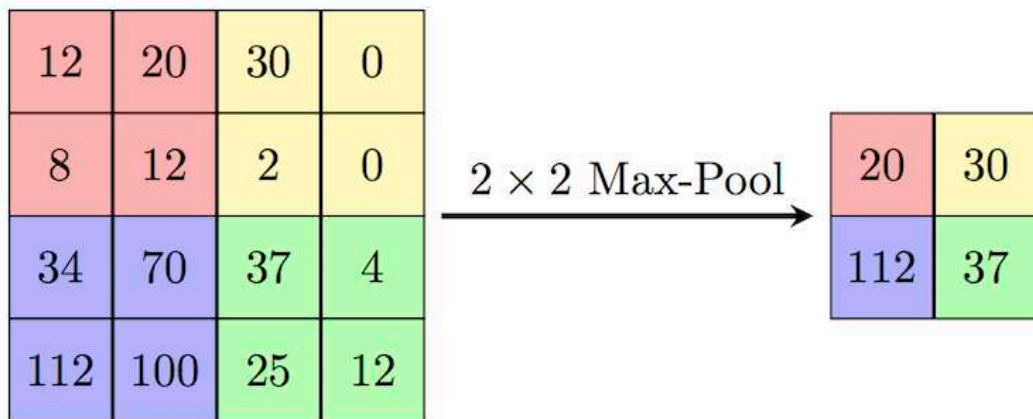
Typical convolutional pipeline

A Rectified Linear Unit (ReLU) is an activation function in neural networks that outputs the input directly if it is positive, or zero if it is negative, effectively introducing non-linearity into the model while avoiding the vanishing gradient problem.



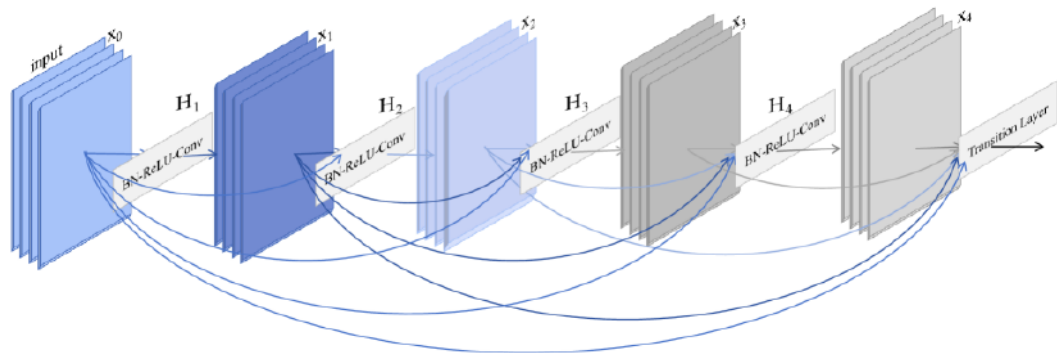
ReLU steps

Finally, the max pooling is a downsampling technique used in convolutional neural networks that reduces the spatial dimensions of the input by selecting the maximum value from a defined region, thereby retaining the most important features while reducing computational complexity.



Max pooling downsampling

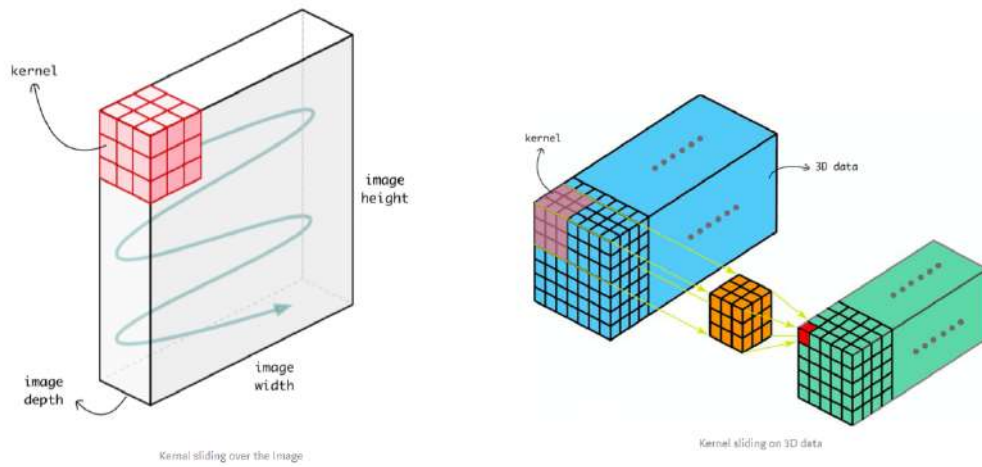
The decoder path mirrors the encoder but with upsampling layers that gradually restore the original spatial dimensions of the input volume. Skip connections between the encoder and decoder layers ensure that spatial information is preserved and combined with high-level features, improving the precision of the segmentation.



Skip connection representation

As previously mentioned, V-Net uses 3D convolutions, which are the core operations that process the volumetric data. Unlike 2D convolutions, which operate on image slices, 3D convolutions consider the entire volume, enabling the network to learn spatial dependencies across all three dimensions (x, y, and z axes).

The use of 3D kernels allows the network to convolve over volumes, capturing spatial relationships within the data.⁷⁸ This is particularly important in medical imaging, where anatomical structures extend across multiple slices.

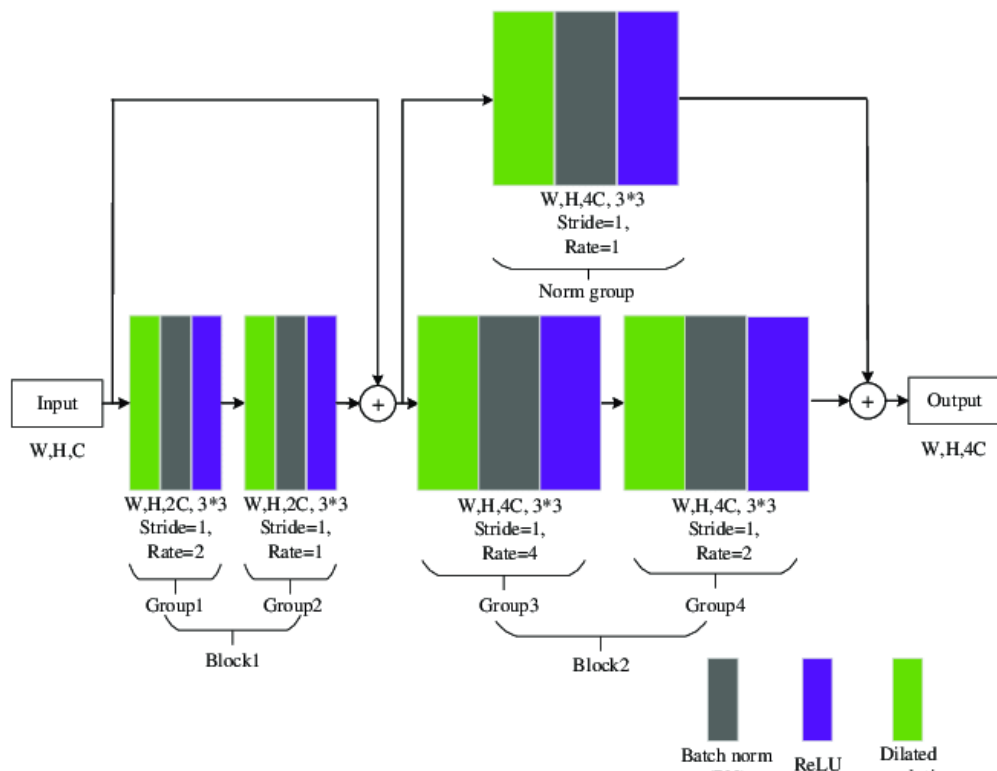


3D kernels feature

To capture larger context without increasing the number of parameters, dilated convolutions can be employed in V-Net.⁷⁹ These allow the network to have a larger receptive field, enabling it to incorporate broader contextual information into the segmentation process.

One of the key innovations in V-Net is the use of residual connections within the convolutional layers.⁸⁰ These connections help mitigate the vanishing gradient problem, which can occur in deep networks, by allowing the gradient to flow more easily through the network during backpropagation.

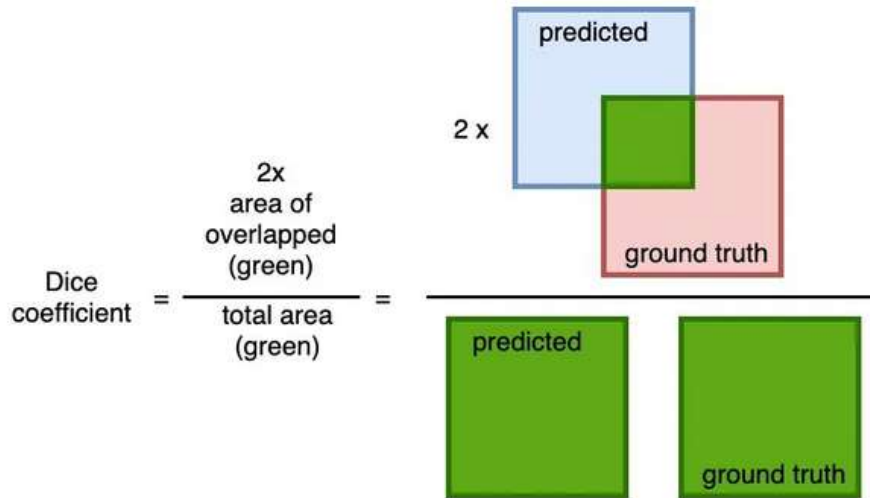
In V-Net, residual blocks are composed of two 3D convolutional layers with a skip connection that adds the input of the block directly to its output. This not only improves the learning process but also stabilizes training, particularly in deeper networks.



V-net residual blocks

The dice loss function is integral to the success of V-Net in medical imaging.⁸¹ Unlike traditional loss functions, which might be ill-suited for dealing with the high-class imbalance typical of medical images (where the foreground objects occupy a much smaller volume compared to the background), the dice loss directly optimizes for segmentation accuracy.

The dice coefficient is a measure of overlap between the predicted segmentation and the ground truth. It ranges from 0 (no overlap) to 1 (perfect overlap). The dice loss function is derived from the dice coefficient and is particularly effective in training models where the goal is to maximize the overlap between the predicted and true segmentations.



Dice coefficient graphical representation

By focusing on maximizing the dice coefficient, V-Net is particularly adept at handling cases where the foreground is sparse.

V-Net's performance in medical imaging tasks is typically evaluated using metrics that measure the accuracy and reliability of the segmentation results.

As mentioned, the dice score is the most commonly used metric for evaluating V-Net's performance. It provides a direct measure of the overlap between the predicted segmentation and the ground truth, making it a valuable indicator of model accuracy.

Beyond the dice score, sensitivity (true positive rate) and specificity (true negative rate) are also important metrics for evaluating V-Net's performance. These metrics provide insights into the model's ability to correctly identify the presence (sensitivity) or absence (specificity) of the target structures, such as reference points too.

The V-Net model used in this project is an adaptation of the standard U-Net architecture, optimized for 3D medical image segmentation and customized for the orthodontic purpose. After the encoder and decoder paths, the final layer of the V-Net applies a softmax activation function to generate a probability map for each voxel, indicating the likelihood of it being part of a specific landmark.⁸² The highest

probability voxels are then selected to determine the coordinates of the predicted landmarks.

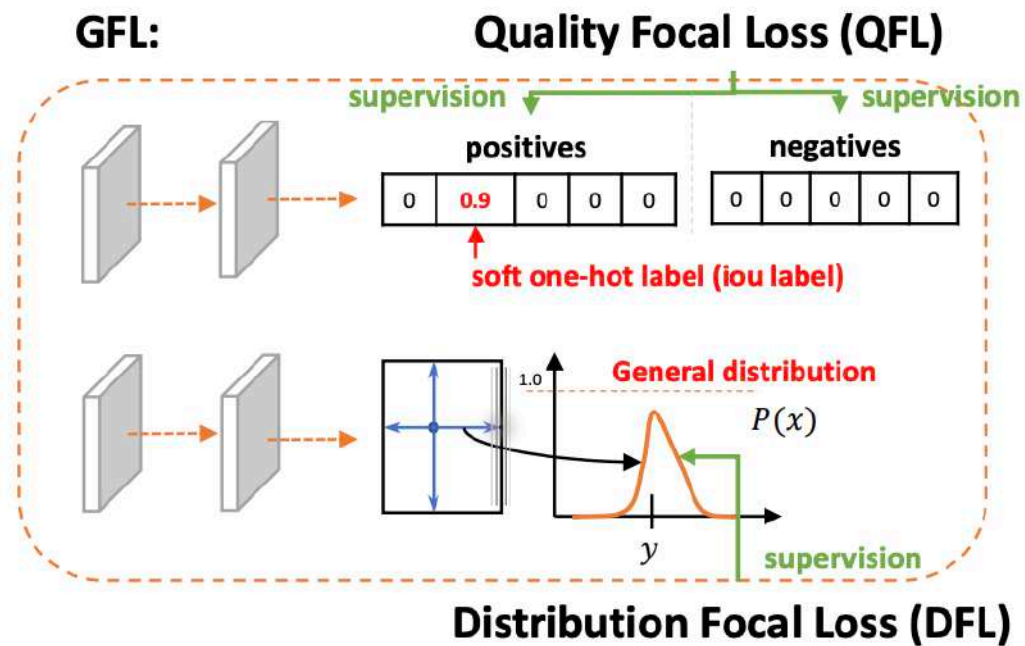
The quality and consistency of the input data are critical to the success of the automated landmark detection system. To ensure optimal performance, several preprocessing steps were employed priorly to training phase:

- Intensity Thresholding. Given that landmarks are located on cranial bones, intensity thresholding was applied to the CBCT volumes to isolate bones and teeth from soft tissues. Based on the Hounsfield unit (HU) values, a specific threshold range was defined, excluding voxels outside this range (e.g., lower than 226 HU and higher than 3071 HU) to focus the model on the relevant anatomical structures.⁸³

- Mask Creation. Ground truth masks were generated by creating spherical regions of ROIs centered on the coordinates of the landmarks as annotated by an expert clinician (Dr Marco Serafin). These masks served as the target labels for the segmentation network during training.

- Data Augmentation. To enhance the robustness of the model and prevent overfitting, data augmentation techniques were employed. These included random transformations such as rotations, translations, and the introduction of artifacts typical of medical imaging (e.g., random ghosting, bias fields, and blurring).⁸⁴ Augmentation expanded the diversity of the training dataset, allowing the model to generalize better to new, unseen data.

Training the V-Net model involved optimizing several key parameters to achieve the best possible performance. The Focal Loss (FL) function was employed to handle the class imbalance inherent in the landmark detection task. FL modifies the standard cross-entropy loss by adding a modulating factor that reduces the relative loss for well-classified examples, thereby focusing the model's learning on harder-to-classify landmarks.⁸⁵



Focal loss function

The model was trained over 250 epochs with a batch size of 8. The initial learning rate was set to $1e-4$, with a momentum of 0.99, and was gradually reduced over time to ensure convergence. The training process involved continuous validation using a separate validation set, allowing for the monitoring of model performance and the prevention of overfitting.

The best-performing model was selected based on the lowest validation loss achieved during training. This model was then used to make predictions on the test dataset. To evaluate the performance of the automated landmark detection system, the following metrics were computed:

- True Positives (TP): The number of correctly identified landmarks that matched the ground truth annotations within a predefined tolerance.
- False Positives (FP): Instances where the model incorrectly identified a landmark that did not correspond to any ground truth annotation.
- False Negatives (FN): Ground truth landmarks that the model failed to detect.
- Euclidean Distance: For each true positive, the 3D Euclidean distance between the predicted and ground truth landmark coordinates was calculated. This distance

serves as a direct measure of the model's accuracy in detecting the exact location of landmarks.

The results of the automated landmark detection system were evaluated on a test set comprising CBCT volumes not seen during training. Two models were tested according to the number of included landmarks.

The first included 16 landmarks: Nasion (N), Sella (Se), Basion (Ba), Menton (Me), Orbitale right (Or dx), Orbitale left (Or sx), Porion right (Po dx), Porion left (Po sx), Anterior Nasal Spine (ANS), Posterior Nasal Spine (PNS), Point A (A), Point B (B), Gonion right (Go dx), Gonion left (Go sx), Pogonion (Pg), and Gnation (Gn). A brief description of each cephalometric landmark is reports as follow:

N: The intersection point of the frontal bone and the nasal bones, located at the deepest point of the nasofrontal suture.

Se: The midpoint of the sella turcica, a saddle-shaped depression in the sphenoid bone where the pituitary gland is located.

Ba: The anterior inferior point of the occipital bone, located at the front of the foramen magnum.

Me: The most inferior point on the mandibular symphysis, marking the lowest point of the chin.

Or dx: The geometrical center of the right infraorbital foramen.

Or sx: The geometrical center of the right infraorbital foramen.

Po dx: The uppermost point on the right external auditory meatus, often used as a reference for the horizontal plane.

Po sx: The uppermost point on the left external auditory meatus, also used for horizontal plane reference.

ANS: The tip of the bony anterior nasal spine, located at the base of the nose where the maxilla meets the nasal septum.

PNS: The posterior end of the nasal spine of the palatine bone, marking the back part of the nasal cavity.

A: The deepest concavity on the anterior maxilla, between the anterior nasal spine and the maxillary alveolar process, often used to assess maxillary position.

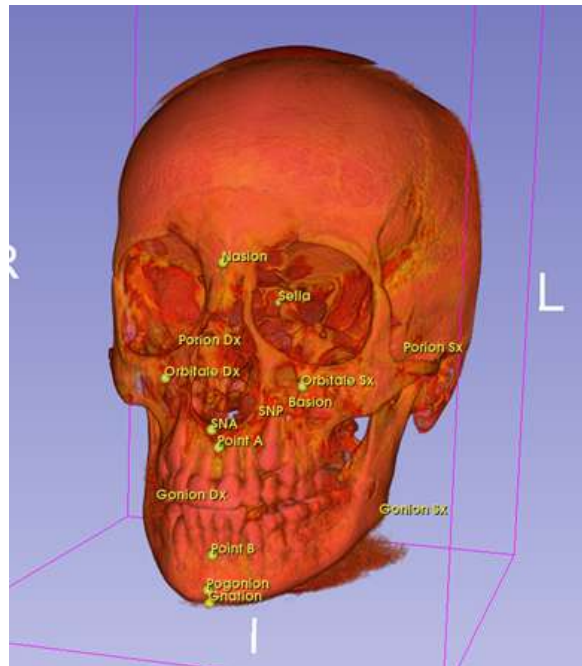
B: The deepest point on the anterior surface of the mandibular symphysis, between the chin and the mandibular alveolar process, often used to assess mandibular position.

Go dx: The most posterior-inferior point on the angle of the right mandible, marking the junction of the posterior and inferior borders of the mandible.

Go sx: The most posterior-inferior point on the angle of the left mandible, marking the junction of the posterior and inferior borders of the mandible.

Pg: The most anterior point on the chin, located at the front of the mandibular symphysis.

Gn: The midpoint between the Menton and Pogonion, representing the most anterior and inferior point on the osseous chin.



Skeletal landmarks

These landmarks are essential in cephalometric analysis for assessing craniofacial relationships and planning orthodontic treatment. The following table resumes the cases used and divided among the training, validation, and test sets.

	Number of cases
Training dataset (262)	204 (Policlinico)

	36 (Planmeca) 32 (SST)
Validation dataset (83)	72 (Policlinico) 11 (Planmeca)
Test dataset (15)	9 (Policlinico) 6 (Planmeca)

The validation test results are reported, spitted between the two datasets.

Policlinico dataset included 72 CBCT volumes. The mean distance between the predicted and the annotated 16 landmarks reached a value of 1.74mm. Accuracy in terms of mean distance, FN, FP, and TN are reported in the following table.

	Mean distance (mm)	FN	FP	TN
N	1.521709	3	0	0
Se	1.720998	3	0	0
Ba	1.662651	1	0	0
Me	2.240312	0	1	0
Or dx	1.782782	2	0	0
Or sx	1.847896	2	0	0
Po dx	1.543059	2	0	0
Po sx	1.334558	2	0	0
ANS	2.054705	1	0	0
PNS	1.655363	1	0	0
A	1.578688	1	0	0
B	1.540498	0	0	0
Go dx	1.981623	0	0	0
Go sx	2.125325	1	0	0
Pg	1.952085	0	1	0
Gn	1.301584	0	1	0

Planmeca dataset included 11 CBCT scans. The mean distance between the predicted and the annotated 16 landmarks reached a value of 2.18mm, without any

discrepancies between the capability of recognize each landmark. Accuracy in terms of mean distance, FN, FP, and TN are reported in the next table.

	Mean distance (mm)	FN	FP	TN
N	1.979558	0	0	0
Se	2.741616	0	0	0
Ba	2.404037	0	0	0
Me	2.003762	0	0	0
Or dx	2.365238	0	0	0
Or sx	2.557417	0	0	0
Po dx	1.455947	0	0	0
Po sx	1.672358	0	0	0
ANS	2.851577	0	0	0
PNS	1.987344	0	0	0
A	2.841577	0	0	0
B	1.763840	0	0	0
Go dx	2.392290	0	0	0
Go sx	2.072433	0	0	0
Pg	2.065839	0	0	0
Gn	1.697791	0	0	0

The model trained to detect 16 landmarks achieved a mean Euclidean distance error of 2.07 mm on the test set, indicating high accuracy. However, the validation set showed lower mean distance errors (1.79mm) and false negative rates, suggesting room for improvement in model robustness. The results of the test set were collected and shown in the following table.

	Mean distance (mm)	FN	FP	TN
N	1.684281	0	0	0
Se	2.014502	0	0	0
Ba	2.229155	1	0	0

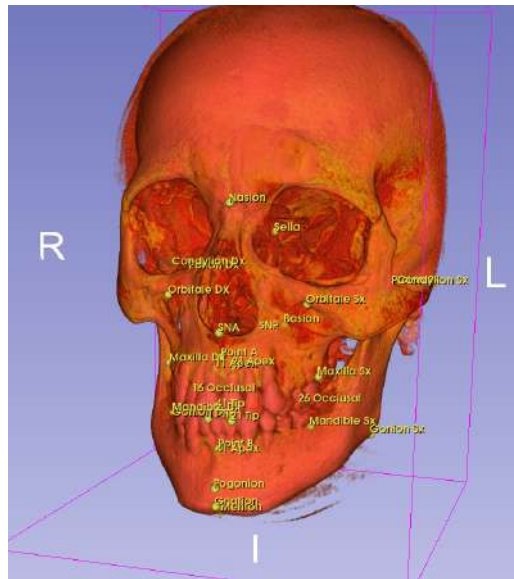
Me	2.726500	0	0	0
Or dx	1.856173	0	0	0
Or sx	1.965882	0	0	0
Po dx	1.409303	0	0	0
Po sx	1.338962	0	0	0
ANS	2.799469	0	0	0
PNS	1.981430	0	0	0
A	1.789457	0	0	0
B	2.074526	0	0	0
Go dx	2.476066	0	1	0
Go sx	2.593827	0	1	0
Pg	2.211089	0	0	0
Gn	1.996566	0	0	0

The performance of the V-Net trained with the 16 landmarks are reported in the next table.

Dataset	Mean distance (mm)	FP (%)	FN (%)	TN (%)
Validation	1.79	0.3	2.04	0
Test	2.07	0.8	0.4	0

Expanding the model to detect 32 landmarks increased the complexity of the task, resulting in a higher mean distance error of 2.468 mm on the test set. This increase in error highlights the challenges of scaling the model to detect a larger number of landmarks without sacrificing accuracy.

Beyond the previously mentioned landmarks, the present model included also: Condylion right (Co dx), Condylion left (Co sx), Maxilla right (Mx dx), Maxilla left (Mx sx), Mandible right (Md dx), Mandible left (Md sx), 1.1 Tip (1.1Tip), 2.1 Tip (2.1Tip), 1.1 Apex (1.1Apex), 2.1 Apex (2.1Apex), 3.1 Tip (3.1Tip), 4.1 Tip (4.1Tip), 3.1 Apex (3.1Apex), 4.1 Apex (4.1Apex), 1.6 Occlusal (1.6Occ), and 2.6 Occlusal (2.6Occ).



Skeletal landmarks

The next text describes the definition of these added 16 landmarks.

Co dx: The most superior and posterior point on the head of the right mandibular condyle.

Co sx: The most superior and posterior point on the head of the left mandibular condyle.

Mx right: The most outer point of the maxillary alveolar bone, located at the level of the furca of the upper first right molar.

Mx left: The most outer point of the maxillary alveolar bone, located at the level of the furca of the upper first left molar.

Md right: The most outer point of the mandibular alveolar bone, located at the level of the furca of the lower first right molar.

Md left: The most outer point of the mandibular alveolar bone, located at the level of the furca of the lower first left molar.

1.1Tip: The center of the incisal tip of the upper right central incisor.

2.1Tip: The center of the incisal tip of the upper left central incisor.

3.1Tip: The center of the incisal tip of the lower left central incisor.

4.1Tip: The center of the incisal tip of the lower right central incisor.

1.1Apex: The apical tip of the upper right central incisor.

2.1Apex: The apical tip of the upper left central incisor.

3.1 Apex: The apical tip of the lower left central incisor.

4.1 Apex: The apical tip of the lower right central incisor.

For this model, training, validation, and test sets were divided as follow.

	Number of cases
Training dataset (274)	212 (Policlinico) 39 (Planmeca) 23 (SST)
Validation dataset (81)	68 (Policlinico) 9 (Planmeca) 4 (SST)
Test dataset (15)	5 (Policlinico) 5 (Planmeca) 5 (SST)

The validation set reached a mean valued of 2.482mm. The metrics are presented in the following table.

	Mean distance (mm)	FN	FP	TN
N	4.201559	2	0	0
Se	1.681608	3	0	0
Ba	1.760954	1	0	0
Me	2.527083	0	1	0
Or dx	2.056792	2	0	0
Or sx	2.029754	2	0	0
Po dx	1.490377	2	0	0
Po sx	1.585711	2	0	0
ANS	2.046069	1	0	0
PNS	1.698621	1	0	0
A	1.943029	1	0	0
B	1.941689	0	0	0

Go dx	2.192001	0	0	0
Go sx	3.053299	0	0	0
Pg	1.855668	0	1	0
Gn	1.259544	0	1	0
Co dx	1.805638	2	0	0
Co sx	2.008200	2	0	0
Mx dx	1.124984	0	2	0
Mx sx	2.375395	0	1	0
Md dx	1.966811	0	2	0
Md sx	1.942213	0	3	0
1.1Tip	2.091015	0	1	0
2.1Tip	1.989130	0	1	0
3.1Tip	2.262023	0	2	0
4.1Tip	2.433938	0	1	0
1.1Apex	1.907486	1	1	0
2.1Apex	2.214910	1	1	0
3.1Apex	2.188358	0	2	0
4.1Apex	2.832937	0	1	0
1.6Occ	2-703726	0	1	0
2.6Occ	2.636193	0	1	0

The model trained to detect 32 landmarks achieved a mean Euclidean distance error of 2.468 mm on the test set, indicating high accuracy.

	Mean distance (mm)	FN	FP	TN
N	1.918497	0	0	0
Se	2.316805	0	0	0
Ba	2.432547	1	0	0
Me	3.037990	0	0	0
Or dx	1.828625	0	0	0
Or sx	1.792806	0	0	0

Po dx	1.677157	0	0	0
Po sx	1.952830	0	0	0
ANS	2.494862	0	0	0
PNS	2.014457	0	0	0
A	1.801464	0	0	0
B	2.059851	0	0	0
Go dx	2.663918	0	1	0
Go sx	2.861533	0	1	0
Pg	2.443046	0	0	0
Gn	2.064560	0	0	0
Co dx	2.488819	0	0	0
Co sx	2.976564	0	0	0
Mx dx	2.531436	0	0	0
Mx sx	2.274078	0	1	0
Md dx	2.655335	0	1	0
Md sx	2.466444	0	0	0
1.1Tip	2.790658	0	0	0
2.1Tip	2.518835	0	0	0
3.1Tip	2.109427	0	0	0
4.1Tip	2.906139	0	0	0
1.1Apex	2.306677	0	0	0
2.1Apex	2.049681	0	0	0
3.1Apex	2.389217	0	0	0
4.1Apex	3.010763	0	0	0
1.6Occ	5.443119	0	0	0
2.6Occ	2.692797	0	3	0

The result was superimposable of the validation set. The validation and test sets produced similar results, indicating that the model generalizes well across different datasets and performs consistently in both seen and unseen data.

Finally, the next table resumes the performance of the model trained on the 32 landmarks.

Dataset	Mean distance (mm)	FP (%)	FN (%)	TN (%)
Validation	2.48	1.45	1.34	0.48
Test	2.47	1	0	0

The results of this task, trained on only hard-tissue reference point, shown very good and promising results, especially when the model works on the detection of skeletal points only. Since our systematic revision and meta-analysis measured a mean distance of 2.44mm on the DL-based networks, we can conclude that our result are consistent, and the training of the V-Net is solid and in the right direction. Despite that, when dental point are included, the CBCT data might suffer distortion at the level of the dental crown, limiting the accuracy of the model. To solve this issue, we are just ending with the training of a similar V-Net based on the recognizing of dental reference points (incisal tips and mesiovestibular cusps). By the integration of digital model casts, this problem should be solved and thanks to this the mean accuracy should decrease more that the values reached by the 32 landmarks model.

The implementation of automated landmark detection presents several challenges, including:

- Anatomical Variability. The differences in craniofacial anatomy among patients can affect the model's performance. A more diverse training dataset could help improve the model's generalization capabilities.
- Class Imbalance. Certain landmarks may be underrepresented in the training data, leading to biased predictions. Techniques such as oversampling and targeted augmentation could address this issue and trained to extended datasets.
- Interpretability and Clinical Integration. Ensuring that the model's predictions are interpretable by clinicians and easily integrated into existing workflows is critical for its adoption in practice.

Our future work will focus on refining the V-Net architecture, exploring alternative deep learning models such as attention-based networks, and expanding the training dataset to improve the model's accuracy and robustness. Additionally, real-time

landmark detection capabilities and enhanced integration with clinical tools will be explored to further streamline orthodontic workflows.

Finally, the automated landmark detection system described in this chapter represents a significant advancement in orthodontic diagnostics, offering a reliable and efficient alternative to manual landmark identification. While challenges remain, the results demonstrate the potential of DL-based approaches to improve the accuracy and efficiency of cephalometric analysis. Further research and development will continue to push the boundaries of what is possible in this rapidly evolving field. Future research should increase the number of landmarks, including skeletal, dental, and soft-tissue reference points too. Therefore, the development of our beta-software is focused on the re-training of cephalometric cases that clinician can share with us; the feedback and the calculation between the predicted and the manually annotated landmarks could help in this issue, ensuring the training on several anatomic variabilities.

Automated tooth segmentation from intraoral scans

Automated tooth segmentation from intraoral scans (IOS) represents a significant technological advancement in modern dentistry, facilitating the accurate and efficient extraction of dental anatomy from 3D surface models. This chapter details the technical methodology behind the development and implementation of a deep learning-based tooth segmentation tool designed to handle complex intraoral data. The chapter discusses the data sources, model architecture, training process, and performance metrics used to evaluate the effectiveness of the segmentation tool.

IOSs have become a standard device in dental diagnostics, capturing highly detailed 3D images of clinical crowns and their surrounding mucosa. This technology is widely adopted in several branches of dentistry due to its accuracy, patient comfort, and efficiency. However, accurately segmenting and identifying individual teeth from IOS data remains challenging, especially in a fully automated manner such as the one purpose in the present project. Developing a robust and reliable AI-driven segmentation tool is critical for advancing clinical workflows by reducing the time and operator dependency associated with manual segmentation.

The development of a robust tooth segmentation model relies heavily on the quality and diversity of the training data. In this study, data were sourced from three primary datasets:

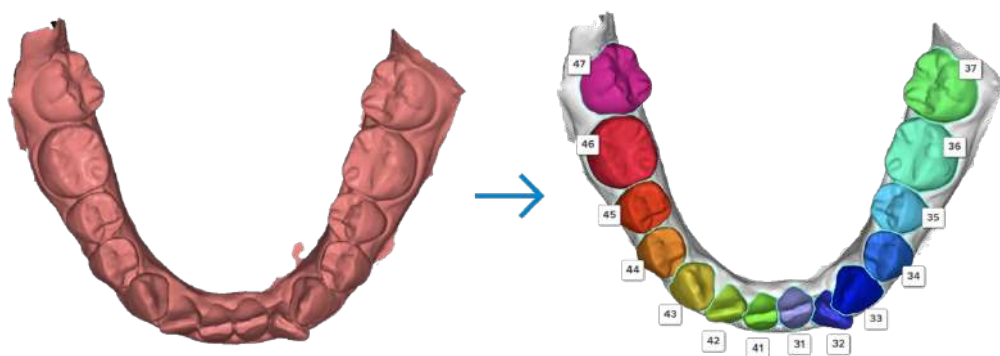
1. SST Dataset: this dataset was obtained from SST Clinica Odontoiatrica in Milan and includes IOS of the upper and lower dental arches from 104 patients. Annotations were performed semi-automatically using the RealGuide software, which allowed for unique identification and exportation of each tooth in STL file format.
2. Planmeca Dataset: similar to the SST dataset, the Planmeca dataset also originates from SST Clinica Odontoiatrica and comprises IOS data from 50 patients. The annotation process was consistent with that of the SST dataset, ensuring uniformity across the datasets.
3. 3DTeethSeg22 MICCAI Challenge Dataset: this dataset was sourced from the 3DTeethSeg22 MICCAI Challenge and includes IOS data from 900 patients. Each patient's upper and lower arches were scanned and validated by experienced

orthodontists and dental surgeons. The dataset provided labeled instances of each tooth, stored in JSON format.

For the purpose of training, validation, and testing, these datasets were combined and preprocessed to create a comprehensive dataset that included a wide range of dental anatomies and conditions.

Effective preprocessing and data augmentation are essential to enhance the model's robustness and generalization capability across different patient data. The following steps were undertaken:

1. Mesh Preprocessing: each mesh was downsampled to 16,000 faces and converted into the PLY format. This standardization ensures that the input data is consistent in terms of size and format, making it suitable for the deep learning model.
2. Label Assignment: unique labels were assigned to each tooth crown within the mesh, with specific color coding for each face of the mesh to differentiate between teeth.
3. Data Augmentation: to further diversify the training set, several augmentation techniques were applied, including rotation (rotating the mesh around its center of mass by a specified angle along the three axes), translation (shifting the mesh by a specific displacement along the three axes), and scaling (uniformly scaling the mesh while maintaining its proportions). These transformations were applied to generate five distinct samples for each training example, significantly increasing the dataset size.



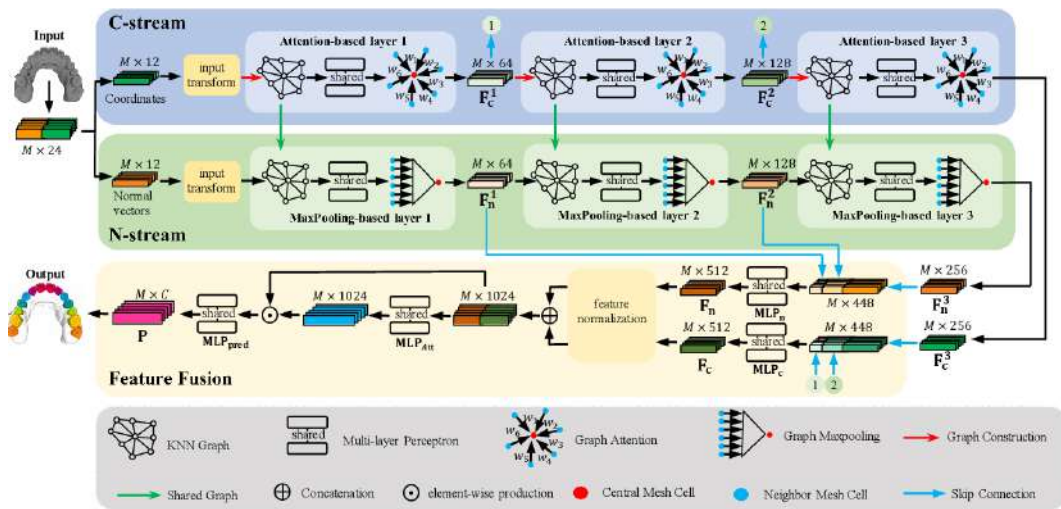
Automated tooth labelling

The core of the segmentation process is the Two-Stream Graph Convolutional Network (TSGCN), a deep learning model designed specifically for 3D surface

segmentation tasks. The TSGCN model is characterized by its dual learning streams, which process geometric data from the intraoral scans:

- **Input Structure.** The input to the TSGCN is a matrix of size $M \times 24$, where M represents the number of cells (triangular faces) in the mesh. Each cell is described by a 24-dimensional vector comprising 3D coordinates (12 elements) and normal vectors (12 elements). The firsts represent the spatial positions of the three vertices of the triangular cell and its centroid while vectors represent the surface normals at the vertices and centroid, capturing the orientation of the cell.

- **Dual Learning Streams.** It is composed by the Coordinate Stream (C), the stream processes the 3D coordinate information, capturing the spatial relationships and positional features of the cells, and the normal stream (N) that handles the normal vectors, which provide information about the orientation and curvature of the mesh surfaces.



TSGCN architecture

By separating these two streams, the model effectively handles the different types of geometric information, reducing the risk of confusion and improving the overall discrimination capability.

After processing through their respective streams, the features are combined using a self-attention mechanism. This allows the model to adaptively weigh the

importance of each stream's output, enhancing the discriminative power of the final representation.

The final output of the TSGCN is a matrix of size $M \times C$, where C is the number of predefined classes (17 in this case, one for each tooth and the gingiva). Each row of the matrix represents the probability distribution over the classes for a given cell, allowing for precise classification of each mesh cell.

The training of the TSGCN model involved careful management of the data and hyperparameters to ensure optimal performance. The data were split into training and internal validation sets:

- Training Set: 772 meshes (80% of the dataset)
- Validation Set: 194 meshes (20% of the dataset)

Then, the Adam optimizer was used with a learning rate schedule implemented through StepLR, which reduces the learning rate by a factor of 0.1 every 20 epochs, starting from an initial rate of 10^{-3} .

The Cross-Entropy Segmentation Loss was selected as the objective function, given its effectiveness in handling multi-class classification tasks.

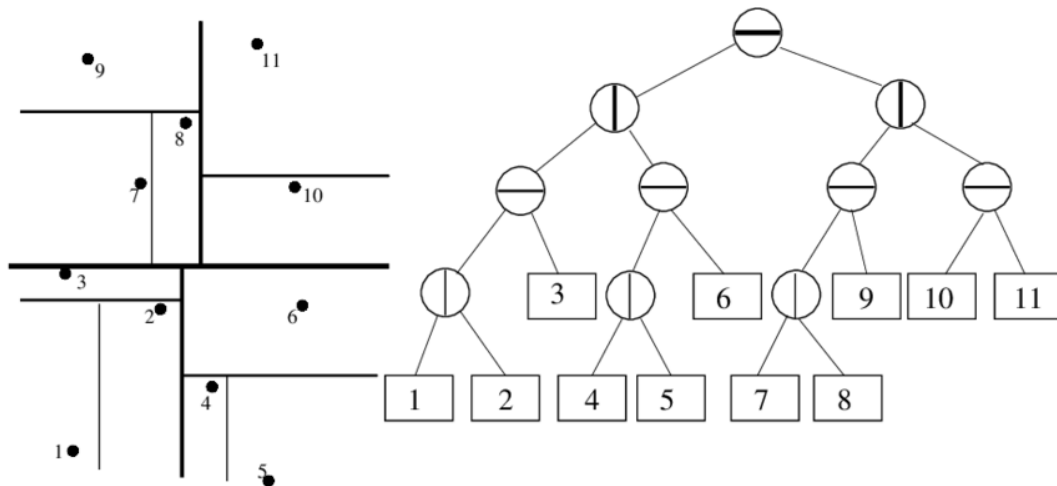
The training configuration was set as follow:

- Batch Size. Set to 1, reflecting the complexity and size of the input data.
- Maximum Epochs. 100 epochs were set as the limit, balancing the need for thorough training with the risk of overfitting.

The same rotation, translation, and scaling techniques used during data augmentation were applied during training to further enhance the model's robustness. The model achieving the highest accuracy on the validation set was selected as the final model.

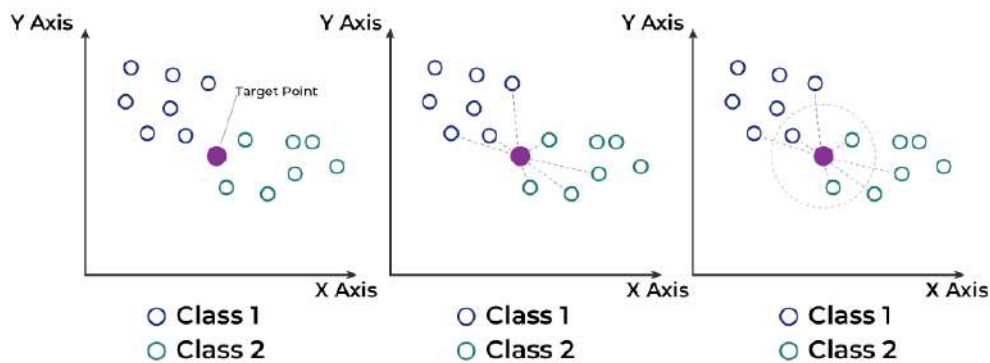
Following the initial segmentation, a postprocessing step was applied to refine the results:

1. Label Reassignment. Cells with areas below a certain threshold were re-evaluated using a KD-Tree to explore the neighborhood. The labels of these small objects were adjusted based on the surrounding larger regions to correct potential misclassifications.



KD-Tree algorithm

2. k-Nearest Neighbors (kNN) Upsampling. During upsampling, the original number of mesh faces was restored, and the kNN classifier was used to assign labels to each face based on the majority label among the three closest neighbors ($k=3$). This process helped maintain the consistency of the segmentation across the entire mesh.

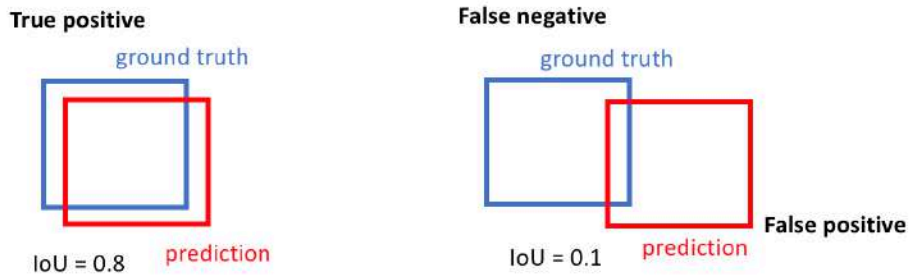


k-Nearest neighbors architecture

The performance of the segmentation models was validated using a test set comprising 64 patients' IOS data, which included both mandibular and maxillary scans. The following metrics were used to evaluate model performance:

1. Overall Accuracy. Defined as the ratio of correctly labeled faces to the total number of faces in the mesh, this metric provides a direct measure of the model's segmentation accuracy.

- Upper Arch: The average accuracy was 0.948
- Lower Arch: The average accuracy was 0.941



Comparison between true positive and false negative

2. Mean Intersection over Union (mIoU). The mIoU measures the overlap between the predicted and ground truth segmentations, averaged over all classes.

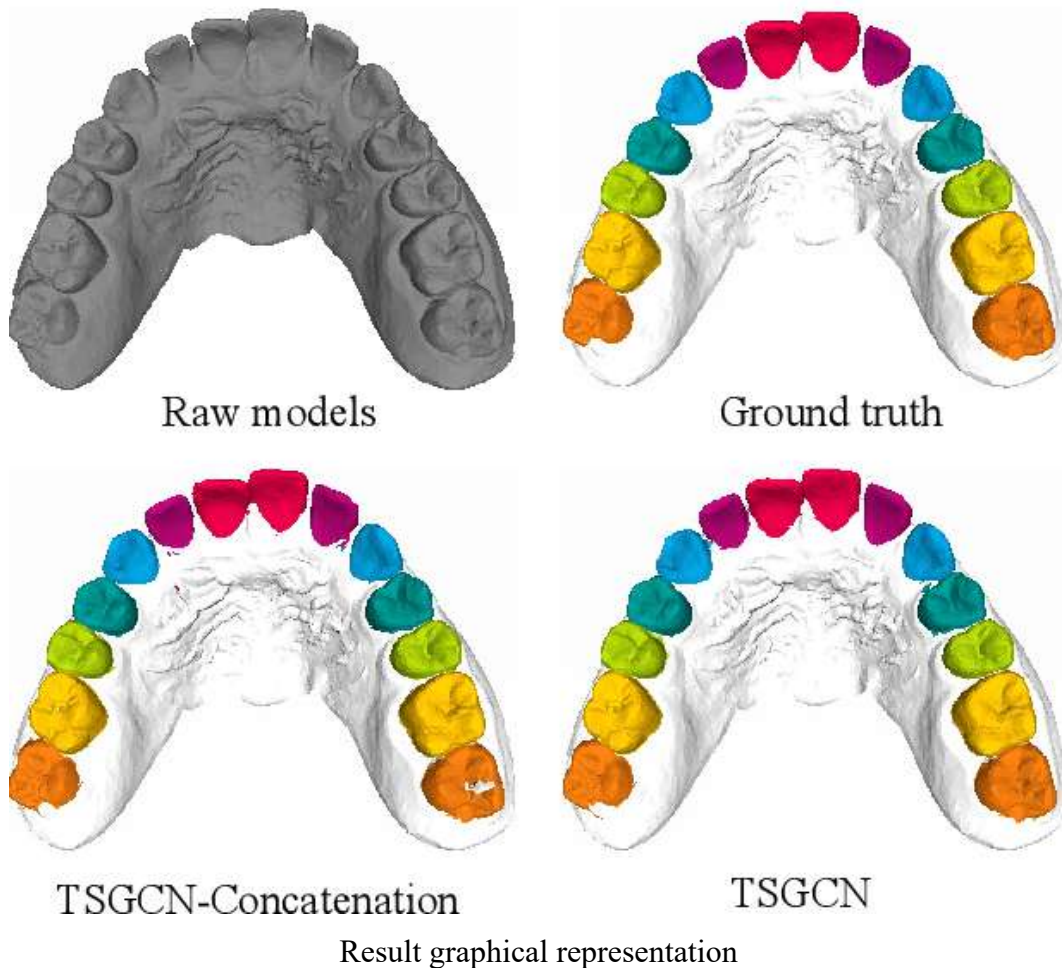
- Upper Arch mIoU: 0.801
- Lower Arch mIoU: 0.795

$$\text{IoU} = \frac{\text{Area of Overlap}}{\text{Area of Union}}$$

The diagram shows two overlapping blue rectangles. The top rectangle is slightly offset to the right and up from the bottom rectangle. The intersection of the two rectangles is shaded a darker blue. Below the rectangles, a solid blue shape represents the union of the two rectangles.

Intersection over union ratio

3. Prediction Time. The average time required for the entire pipeline (including loading, preprocessing, prediction, postprocessing, and saving) was approximately 10 seconds on a GPU and 70 seconds on a CPU per mesh.



The development of automated tooth segmentation from intraoral scans presents several challenges. The first one might be represented by the variability in scan quality. IOSs can vary significantly in quality due to differences in scanner technology, operator technique, and patient cooperation. These variations can introduce noise and artifacts, which may affect segmentation accuracy.

Also, certain teeth, particularly molars and premolars, may be underrepresented in the training data due to their less frequent or less complete appearance in intraoral scans. Addressing this imbalance through data augmentation or selective oversampling is crucial for improving model performance. The complex shapes and

close proximity of teeth, particularly in crowded dentitions, pose a challenge for accurate segmentation. Advanced modeling techniques, such as the use of multi-scale features or more sophisticated attention mechanisms, may help mitigate these challenges.

To further enhance the capabilities of the tooth segmentation model, several areas for future research and development are proposed and anticipated.

Combining IOS with CBCT data could provide a more comprehensive understanding of both the soft and hard tissues, improving the accuracy of segmentation, especially in cases involving complex dental restorations or orthodontic appliances. Moreover, refining the postprocessing steps, particularly the use of more advanced neighborhood exploration algorithms, could reduce the occurrence of minor misclassifications, further improving segmentation accuracy.

Automated tooth segmentation from IOSs is a critical advancement in digital dentistry, offering the potential for highly accurate and efficient extraction of dental crowns from 3D surface models. The use of advanced DL architectures, such as the TSGCN, has demonstrated strong performance in handling the complexities of intraoral data. While challenges remain, the continued refinement of these models and the integration with CBCT and other imaging modalities promise to further elevate the standard of care in dental diagnostics and treatment planning.

Automated tooth segmentation from cbct data: monolabel and multilabel approaches

Automated tooth segmentation from CBCT data is a critical task in orthodontics and various other dental specialties.⁸⁶ The segmentation process can be approached in two primary ways: monolabel segmentation, where teeth are segmented as a single class, and multilabel segmentation, where each tooth is identified as a distinct class. This chapter provides a detailed technical exploration of both approaches, examining the datasets, model architectures, training procedures, and performance metrics involved.

The segmentation models were developed using datasets from both online sources and clinical settings. These datasets were prepared with specific focus on ensuring consistent annotation, preprocessing, and augmentation techniques.

The online dataset was sourced from an open repository, consisting of 148 CBCT scans with corresponding segmentation masks. These masks were initially created with individual segmentation for each tooth, but the labels varied across the dataset, necessitating standardization. This dataset included CBCT scans captured with closed mouths.

Acquired from the SST orthodontic clinic, this dataset comprised 104 CBCT scans from different patients, some of which were also accompanied by Intraoral Scans (IOS). The segmentation masks were manually annotated for individual tooth segmentation, providing a comprehensive set for training. This annotation task The scans in this dataset were captured with open mouths, which introduced additional variability.

For the monolabel segmentation approach, the CBCT data were simplified into binary masks (tooth and background) where all teeth were labeled as a single class. In contrast, for the multilabel segmentation approach, each tooth was assigned a unique label. The final datasets were as follows:

- Training Dataset: 95 scans from the online dataset.
- Validation Dataset: 24 scans from the online dataset.
- Test Dataset: 29 scans from the online dataset and 28 scans from the SST dataset.

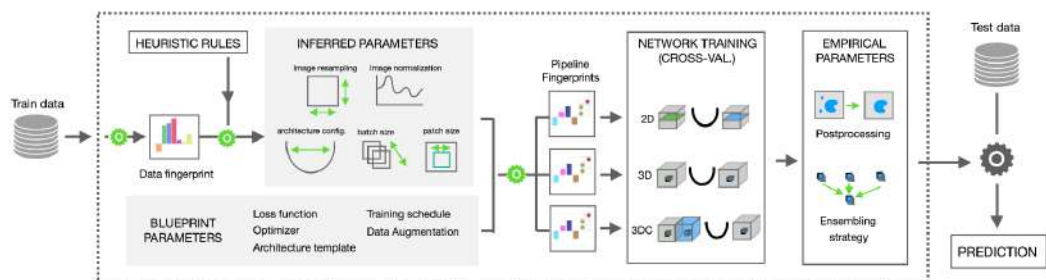
In the monolabel segmentation approach, the objective is to segment all teeth from the background (i.e., non-teeth regions). This approach simplifies the segmentation task by treating all teeth as a single class or mask.

The monolabel segmentation was implemented using the nnU-Net framework, a robust and highly adaptable deep learning model for semantic segmentation.⁸⁷ nnU-Net is known for its automatic configuration capabilities, which optimize model parameters based on the dataset characteristics.

nnU-Net is a semantic segmentation method that automatically adapts to a given dataset. It will analyze the provided training cases and automatically configure a matching U-Net-based segmentation pipeline. Given a new dataset, nnU-Net will systematically analyze the provided training cases and create a 'dataset fingerprint'. nnU-Net then creates several U-Net configurations for each dataset.

nnU-Net then configures these segmentation pipelines based on a three-step recipe:

- Fixed parameters are not adapted. During development of nnU-Net a robust configuration is identified (that is, certain architecture and training properties) that can simply be used all the time. This includes, for example, nnU-Net's loss function, (most of the) data augmentation strategy and learning rate.
- Rule-based parameters use the dataset fingerprint to adapt certain segmentation pipeline properties by following hard-coded heuristic rules. For example, the network topology (pooling behavior and depth of the network architecture) is adapted to the patch size; the patch size, network topology, and batch size are optimized jointly given some GPU memory constraint.
- Empirical parameters are essentially trial-and-error. For example, the selection of the best U-net configuration for the given dataset (2D, 3D full resolution, 3D low resolution, 3D cascade) and the optimization of the postprocessing strategy.



nnU-Net architecture

nnU-Net leverages a U-Net-based architecture, designed to capture both low-level and high-level features through its encoder-decoder structure. The network is configured to handle 3D medical image data, making it well-suited for CBCT scans.

Given the high resolution of CBCT scans, the model was trained on patches of size [320, 448], ensuring that the computational load remained manageable while allowing the network to focus on localized features.

Extensive data augmentation was applied, including rotations, scaling, Gaussian noise, and other transformations. These augmentations helped the model generalize better to unseen data, particularly when dealing with the anatomical variability present in the CBCT scans.

The model was trained for 1000 epochs, ensuring that the network had sufficient time to learn from the data. A batch size of 21 was used, optimized for the available GPU memory. The Dice Loss function was employed to handle the class imbalance between the teeth and background regions. In this situation, the Dice coefficient is particularly effective in medical image segmentation, where the target class (teeth) often occupies a small portion of the image.⁸¹

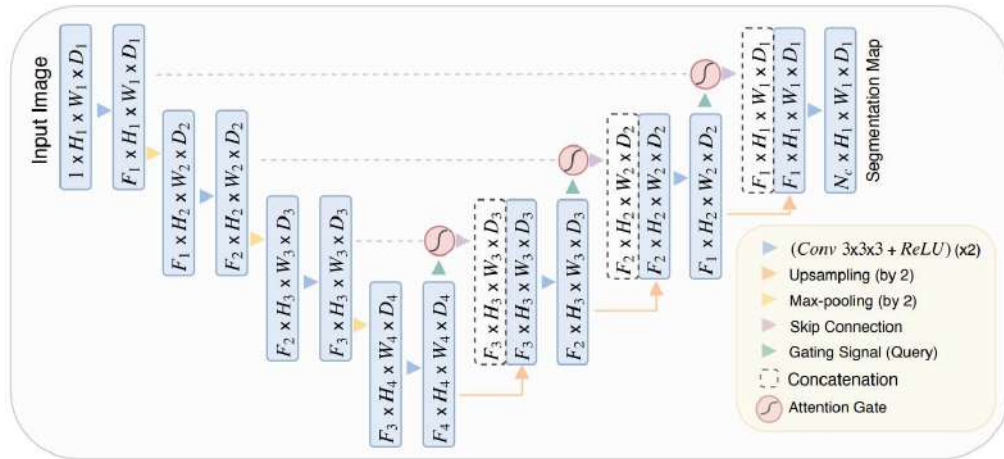
The performance of the monolabel segmentation model was evaluated using the Dice score, to measure the overlap between the predicted segmentation and the ground truth. Mean Dice Scores (0-1) obtained were:

- Online Dataset: 0.95
- SST Dataset: 0.92

The Dice scores indicate a high level of accuracy in segmenting teeth from the CBCT scans. The model performed slightly better on the online dataset, which had more consistent annotations, compared to the SST dataset.

Multilabel segmentation involves classifying each tooth as a separate entity, which is more complex than the monolabel approach. This approach is crucial for applications requiring detailed analysis of individual teeth, such as orthodontic treatment planning and implant placement.

For the multilabel segmentation task, an Attention U-Net architecture was used.⁸⁸ This model enhances the standard U-Net by incorporating attention mechanisms that focus the model's processing on relevant regions, effectively ignoring irrelevant background information.



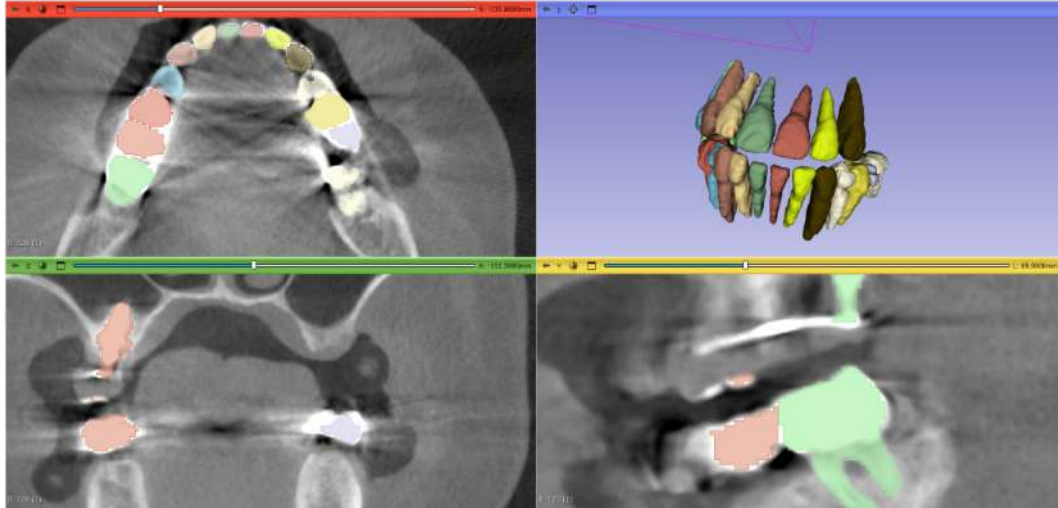
Attention U-Net architecture

The Attention U-Net maintains the encoder-decoder structure but adds attention gates that allow the model to prioritize features associated with specific teeth. This is particularly beneficial in multilabel segmentation, where the model must distinguish between closely situated teeth.

Similar to the monolabel approach, the model was trained on patches of size [64, 64, 64]. This smaller patch size was selected to ensure that the model could effectively focus on the intricate details necessary for distinguishing individual teeth. No data augmentation was applied in this case, as the model's attention mechanisms were designed to inherently manage variations within the data.

The Attention U-Net was trained for 100 epochs, balancing the need for thorough training with the risk of overfitting. A batch size of 32 was used, which allowed for efficient training without overwhelming the computational resources. The Dice Loss function was again employed, tailored to handle the multilabel nature of the task, where the objective is to maximize the overlap for each tooth class.

The multilabel segmentation model was evaluated using the mean Dice score across all tooth classes, providing a comprehensive measure of the model's performance.



Automated tooth segmentation

Mean Dice score over 16 Labels was 0.62. The multilabel segmentation model achieved a lower Dice score compared to the monolabel approach, reflecting the increased complexity of the task. Therefore, the attention mechanisms, while effective, highlighted the need for further refinement to improve accuracy in distinguishing between individual teeth.

Both monolabel and multilabel segmentation approaches present unique challenges that must be addressed to improve performance and clinical applicability.

The variability in craniofacial anatomy across patients, particularly in complex cases such as those involving orthodontic appliances or severe dental crowding, can significantly affect the segmentation accuracy. Incorporating more diverse datasets and enhancing model robustness through advanced data augmentation techniques could mitigate these challenges.

In the multilabel approach, certain teeth may be underrepresented in the training data, leading to biased predictions. Addressing this imbalance through oversampling, synthetic data generation, or loss function adjustment could improve model performance.

The increased complexity of the multilabel segmentation task requires more sophisticated models, which in turn demand greater computational resources. Optimizing model architecture and training strategies to balance accuracy with efficiency will be crucial for practical deployment in clinical settings.

Future research will focus on refining the model architectures, particularly the attention mechanisms in the multilabel approach, to improve their ability to accurately segment individual teeth. Additionally, integrating these segmentation models with other diagnostic tools, such as automated landmark detection or IOS data, could provide a more comprehensive solution for dental professionals.

In conclusion, automated tooth segmentation from CBCT data, whether through monolabel or multilabel approaches, is a critical task in modern orthodontics. While the monolabel segmentation model demonstrated high accuracy, the multilabel approach highlighted the challenges associated with distinguishing individual teeth. Continued refinement of these models, alongside the integration of additional data sources and advanced techniques, will be essential for advancing the field and improving patient outcomes.

Automated cranial bone segmentation from CBCT data

Automated cranial bone segmentation from CBCT data is a useful task in the field of orthodontics and maxillofacial surgery. Accurate segmentation of cranial structures, such as the maxilla, mandible, and cranial base, is essential for diagnostic purposes, treatment planning, and surgical navigation.⁸⁹ This chapter provides a detailed technical analysis of the automated segmentation process, focusing on the datasets used, the architecture of the deep learning models implemented, and the performance evaluation of these models.

The success of any segmentation model is highly dependent on the quality and diversity of the training data. In this project, datasets were compiled from multiple sources, annotated, and processed to create a robust training environment for the deep learning models.

The datasets used for training, validation, and testing were compiled from the following sources:

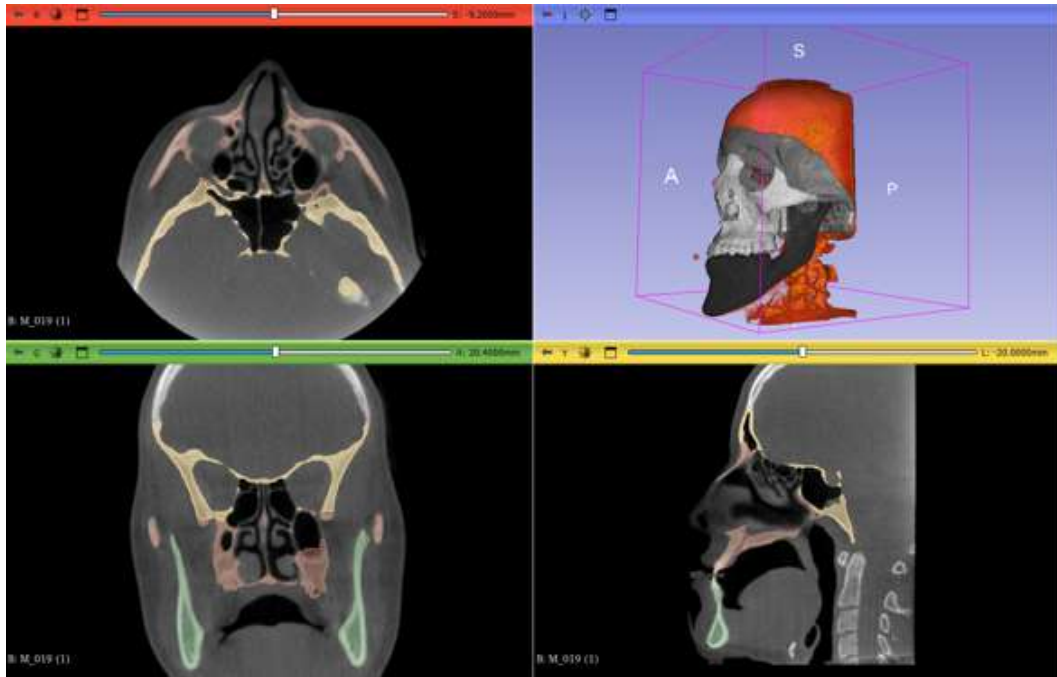
- Planmeca Dataset: This dataset comprises 30 CBCT scans, with 24 used for training and 6 for validation. These scans were provided by a clinical partner, and the segmentation of cranial bones was performed manually by a team of orthodontic experts.
- Policlinico Dataset: Sourced from a major hospital, this dataset includes 64 CBCT scans, with 49 used for training and 15 for validation. Like the Planmeca dataset, the segmentation annotations were manually generated by experienced clinicians.

The segmentation masks for both the Planmeca and Policlinico datasets were created using the AMASS model.⁹⁰ This tool provided the initial segmentation, which was then refined and validated by human experts to ensure accuracy.

For the purpose of this study, only three key cranial structures were segmented: the maxilla, mandible, and cranial base. Each structure was assigned a unique label:

- 0: Background (non-bone regions)
- 1: Maxilla
- 2: Mandible
- 3: Cranial base

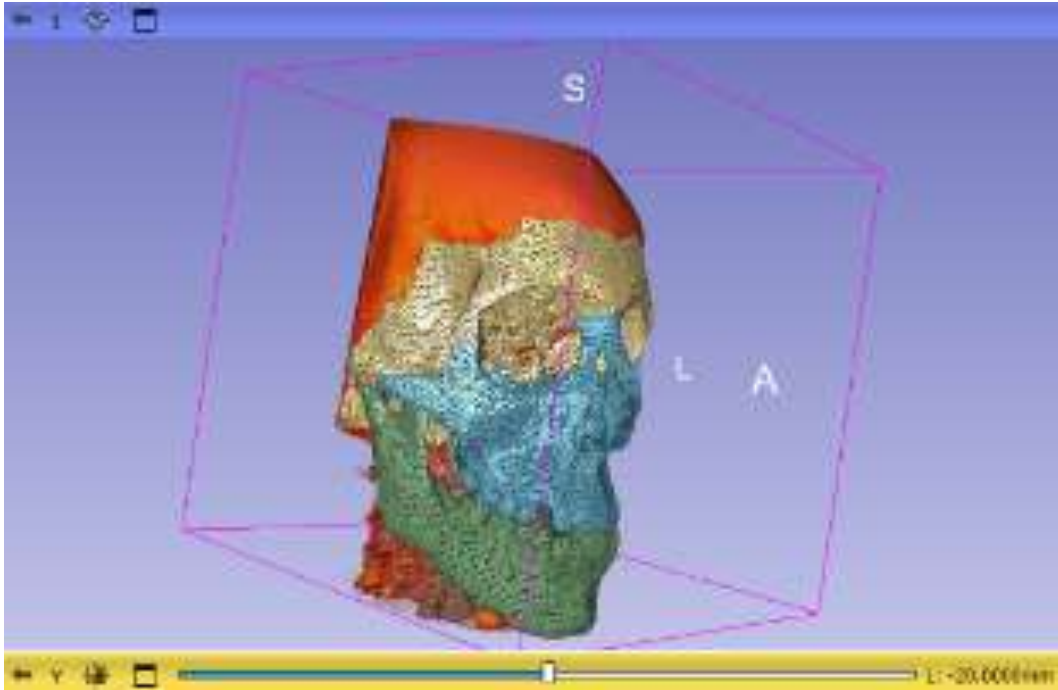
The ground truth labels from the original datasets were multiclass and had to be converted into binary masks for each structure. This was done to streamline the segmentation process and reduce the computational complexity. The conversion process involved isolating each structure and generating a separate binary mask that the model could use during training.



Automated skull bone segmentation

To ensure the model's robustness and generalization capability, the data underwent several preprocessing steps:

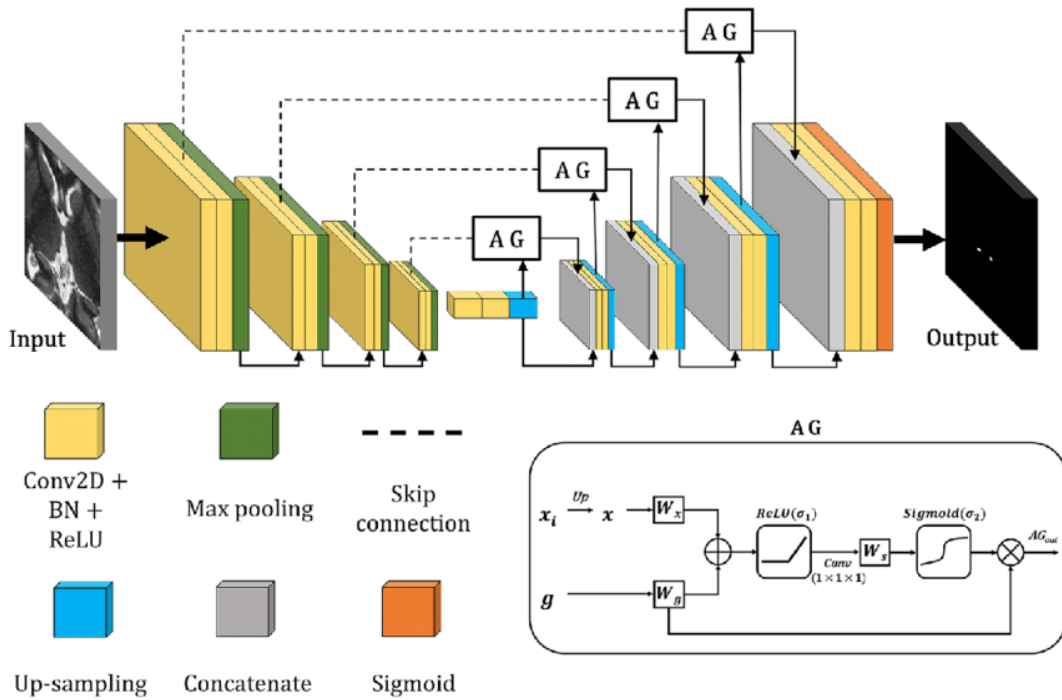
- Resampling: The CBCT scans were resliced to a uniform spacing of [0.6, 0.6, 0.6] mm to standardize the input resolution across different datasets.
- Normalization: The voxel intensities of the CBCT scans were normalized to ensure that the input data had a consistent range of values, which is crucial for effective model training.
- Data Augmentation: Although the final model did not use data augmentation, initial experiments included rotation, translation, and scaling to assess their impact on model performance. Ultimately, augmentation was excluded to maintain the fidelity of the original data.



Segmented volume of skeletal cranium, labelled according to positioned bones

For the segmentation task, the Attention U-Net architecture was selected due to its ability to focus on relevant features while ignoring irrelevant background information.⁸⁸ This characteristic is particularly important in medical imaging, where the distinction between structures can be subtle and prone to noise.

The Attention U-Net enhances the traditional U-Net architecture by incorporating attention gates that allow the model to dynamically prioritize important regions of the image. This results in more precise segmentation, particularly in complex regions such as the cranial base, where different bone structures may be closely aligned.



Attention U-Net architecture

The model consists of an encoder that progressively reduces the spatial dimensions of the input while increasing the depth of feature maps, capturing both low- and high-level features. The decoder then reconstructs the spatial dimensions, combining the extracted features to produce the final segmentation map.

The attention mechanism is integrated into the skip connections between the encoder and decoder. These gates evaluate the relevance of the features from the encoder before passing them to the decoder, allowing the network to focus on critical regions such as the boundaries between the maxilla, mandible, and cranial base.

The model was trained for 100 epochs, balancing the need for thorough training with the risk of overfitting. A batch size of 32 was used, optimized for the available GPU memory. Given the large size of CBCT scans, the model was trained on patches of size [64, 64, 64]. This patch-based approach ensures that the model can focus on local features while maintaining computational efficiency. The Dice Loss function was used due to its effectiveness in handling class imbalance in medical

image segmentation.⁸¹ This loss function maximizes the overlap between the predicted segmentation and the ground truth.

The performance of the Attention U-Net model was evaluated using the Dice score. The model's performance was assessed across the three cranial structures of interest:

- Maxilla: The model achieved a Dice score of 0.96, indicating near-perfect segmentation accuracy. The attention mechanism was particularly effective in distinguishing the maxilla from adjacent structures, such as the nasal cavity and zygomatic bones.
- Mandible: The segmentation of the mandible yielded a Dice score of 0.90. Although slightly lower than the maxilla, this score still reflects a high level of accuracy, with most errors occurring at the boundaries where the mandible interfaces with the cranial base (temporomandibular joint fossa).
- Cranial Base: The cranial base segmentation achieved a Dice score of 0.88. The lower score can be attributed to the complex anatomy of the cranial base, where numerous foramina and sutures present challenges for accurate segmentation.

Automated segmentation of cranial bones from CBCT data presents several challenges, which must be addressed to further improve model performance.

The cranial base, in particular, poses significant challenges due to its complex anatomy, which includes multiple foramina, fissures, and sutures. The presence of dense bone and closely packed structures can lead to segmentation errors, particularly at the boundaries between different bones.

Differences in CBCT scan quality, patient positioning, and scanner calibration can introduce variability that affects segmentation accuracy. Ensuring consistency in scan acquisition and preprocessing is crucial for reliable segmentation.

The relative size of the structures being segmented (e.g., the cranial base versus the maxilla) can lead to class imbalance issues, where the model may be biased towards the more prominent structures. Techniques such as weighted loss functions or oversampling of underrepresented classes could help mitigate this issue.

To further enhance the accuracy and applicability of the segmentation model, several areas for future research are proposed, as follow.

Combining CBCT data with other imaging modalities, such as MRI or intraoral scans, could provide a more comprehensive understanding of craniofacial anatomy. This multimodal approach could improve segmentation accuracy, particularly in regions where CBCT alone is insufficient.

Developing a model capable of real-time segmentation would greatly enhance clinical workflows, allowing for immediate feedback during patient consultations and surgical planning in maxillofacial surgery.

Refining postprocessing steps, such as morphological operations or the use of advanced machine learning techniques for error correction, could further improve the quality of the segmentation results.

Finally, automated cranial bone segmentation from CBCT data is a critical component of modern dental and maxillofacial imaging, providing the foundation for accurate diagnosis and treatment planning. The Attention U-Net model demonstrated strong performance in segmenting key cranial structures, particularly the maxilla and mandible, with some challenges remaining in the segmentation of the cranial base. Continued refinement of the model, alongside the integration of additional data sources and advanced techniques, will be essential for further advancing the field and improving patient outcomes.

Automated registration and fusion of IOS and CBCT segmented teeth

In the field of digital dentistry, integrating data from different imaging modalities is crucial for creating a comprehensive and accurate representation of a patient's oral anatomy. IOS provide high-resolution surface data of dental crowns, while CBCT offers detailed volumetric data, including the internal structure of teeth and surrounding bones. This chapter focuses on the automated registration and fusion process between IOS and CBCT segmented teeth, enabling the creation of a unified model that combines the strengths of both modalities.

Combining IOS and CBCT data has significant clinical implications. IOS provides detailed surface information, essential for restorative dentistry and orthodontic treatment planning, while CBCT offers insights into the bone structure and root anatomy, critical for implantology and surgical interventions, but also all the procedures that moves teeth and roots as orthodontics.⁹¹ The fusion of these datasets facilitates the virtual extraction of complete teeth, including both crowns and roots, providing a more comprehensive tool for diagnosis and treatment planning.⁹²

For this task, a dataset was compiled from patients who had both IOS and CBCT scans taken within a two-week timeframe to minimize discrepancies due to temporal changes in dental anatomy. The dataset included 12 patient cases, resulting in a total of 24 jaws (12 upper and 12 lower). The IOS data consisted of segmented dental crowns, while the CBCT data provided segmented teeth, including roots and surrounding bone structures.

The IOS data were acquired using advanced intraoral scanning devices, which captured detailed 3D models of the dental arches. Each tooth was individually segmented and labeled by expert clinicians, providing high-quality surface data for each crown.

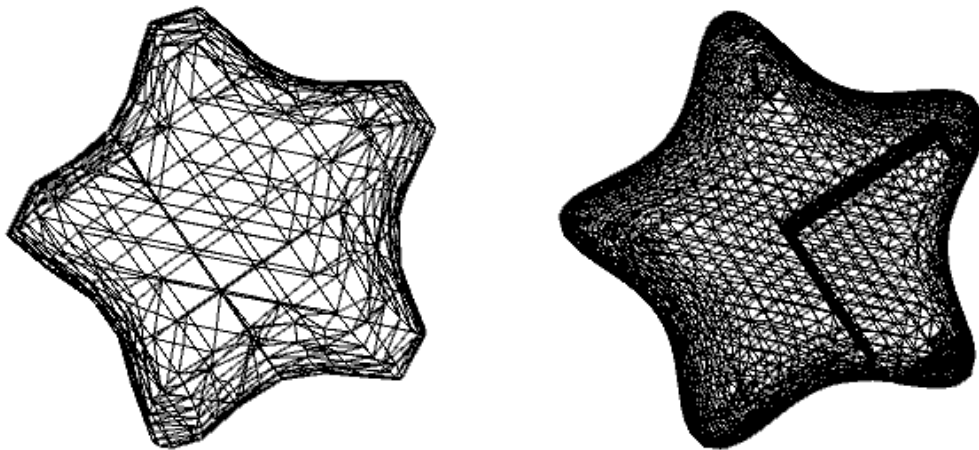
The CBCT scans were processed to segment teeth, including their roots, as previously explained. The segmentation was performed manually by experienced operators using specialized software (Realguide, 3Demme, Italy), resulting in

accurate 3D models of each tooth, which were then used as the volumetric counterpart to the IOS surface data.

The registration and fusion of IOS and CBCT data involved several critical steps, including initial preprocessing, coarse registration, fine registration, and the final fusion process. The following sections detail each step.

Before the registration process, both IOS and CBCT datasets were preprocessed to ensure compatibility and enhance the accuracy of the subsequent steps.

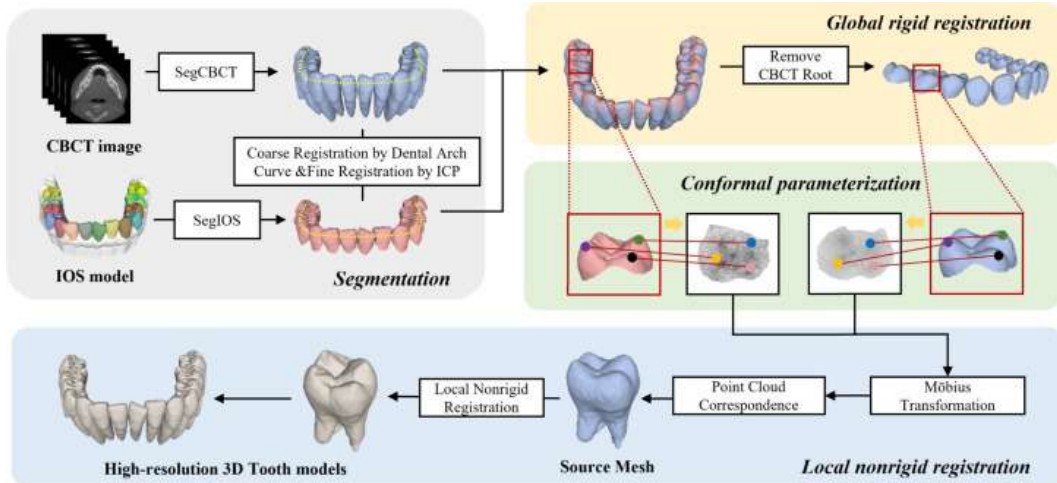
Both point clouds from the IOS and CBCT data were downsampled to reduce computational complexity while retaining key features necessary for accurate registration.



Downsampling of a STL file

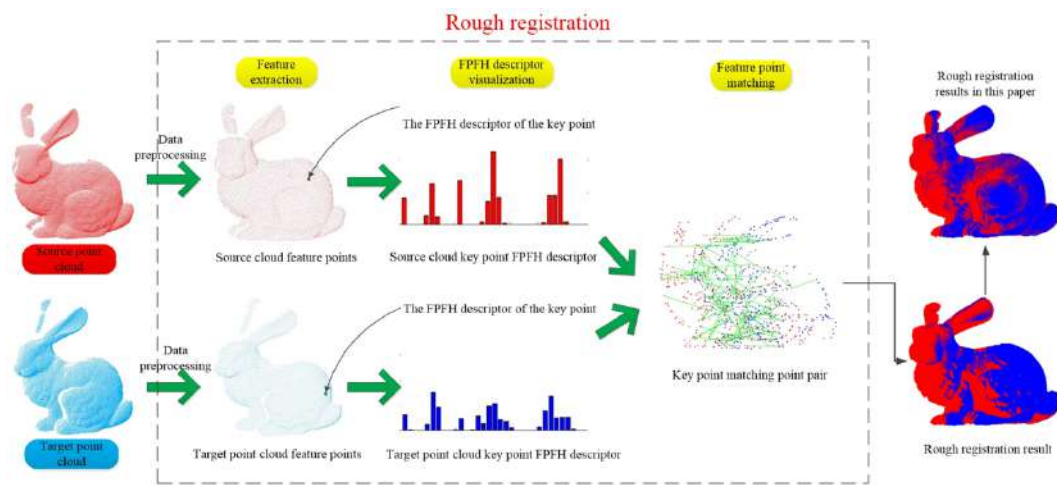
The point clouds were therefore normalized to ensure that both datasets were scaled similarly, facilitating the alignment process.

The first step in the registration process was to achieve a rough alignment between the IOS and CBCT datasets. This was accomplished using the Global Coarse Rigid Registration algorithm available in the Open3D Python library.⁹³



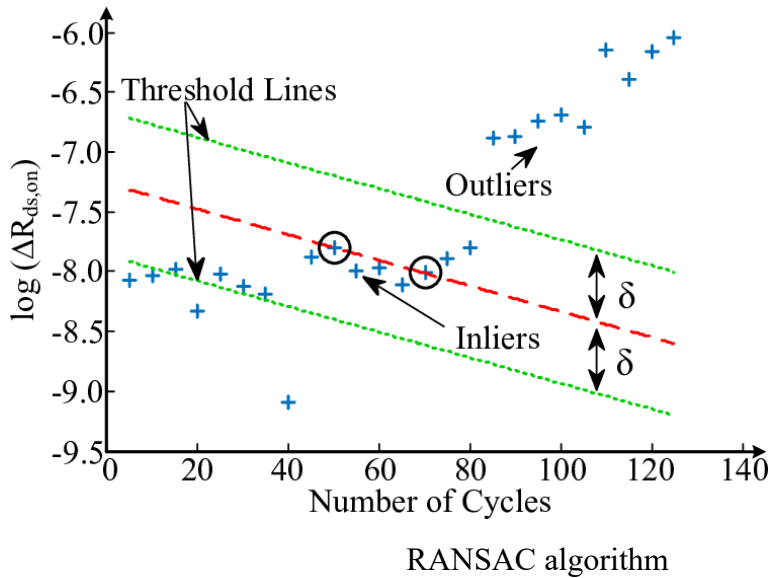
Global rigid registration

The Fast Point Feature Histograms (FPFH) were computed for each point in both the IOS and CBCT point clouds.⁹⁴ These histograms encode the geometric properties of the points and serve as descriptors for the alignment process.

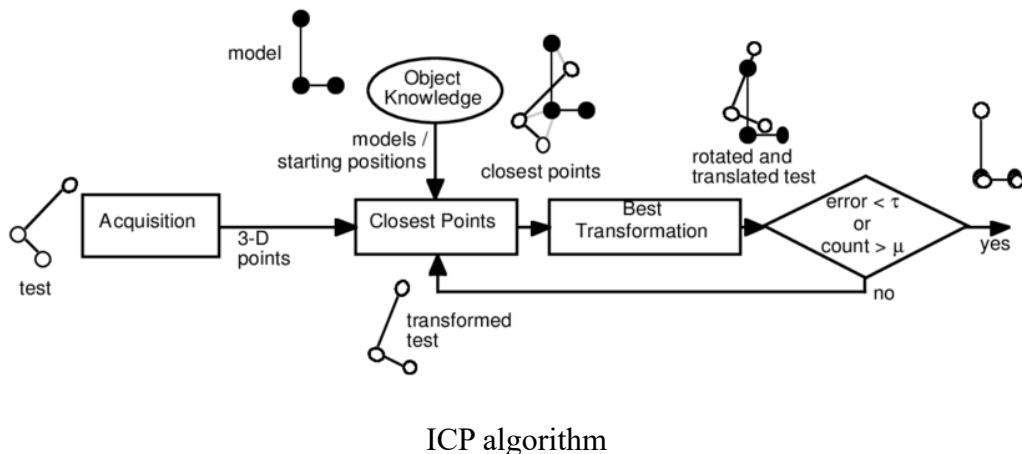


FPFH architecture

The Random Sample Consensus (RANSAC) algorithm was applied to the FPFH features to perform an initial alignment. RANSAC is an iterative method used to estimate parameters of a mathematical model while handling outliers, which, in this context, are primarily related to differences in tooth roots present in CBCT but absent in IOS.⁹⁵

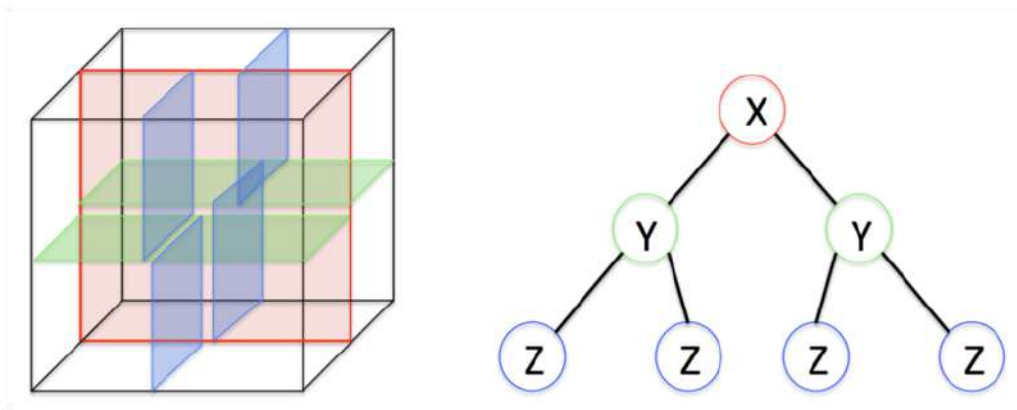


After the initial coarse alignment, the Iterative Closest Point (ICP) algorithm was used to refine the registration.⁹⁶ The ICP algorithm iteratively adjusts the position of the IOS point cloud to minimize the distance between corresponding points in the CBCT data. This fine-tuning process ensures a more accurate alignment, particularly in the regions where the IOS and CBCT data overlap. The ICP process continued until the change in alignment error fell below a predefined threshold, indicating that further iterations would not significantly improve the alignment.



Once the IOS and CBCT data were accurately aligned, the fusion process was carried out to create a unified model that incorporates both the detailed crown surfaces from IOS and the root structures from CBCT.

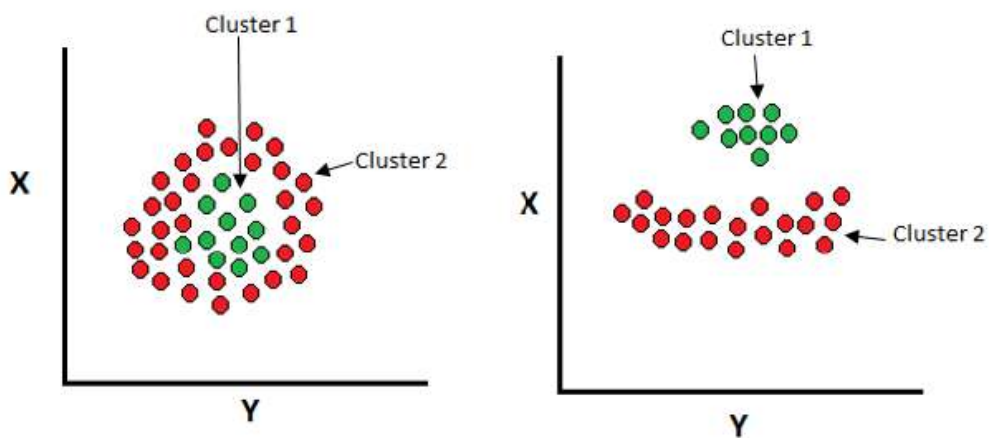
A KD-Tree structure was used to efficiently compute the distances between points in the CBCT dataset and their nearest neighbors in the IOS dataset.⁹⁷ This allowed for the precise identification of overlapping regions and the removal of redundant data.



KD-Tree architecture

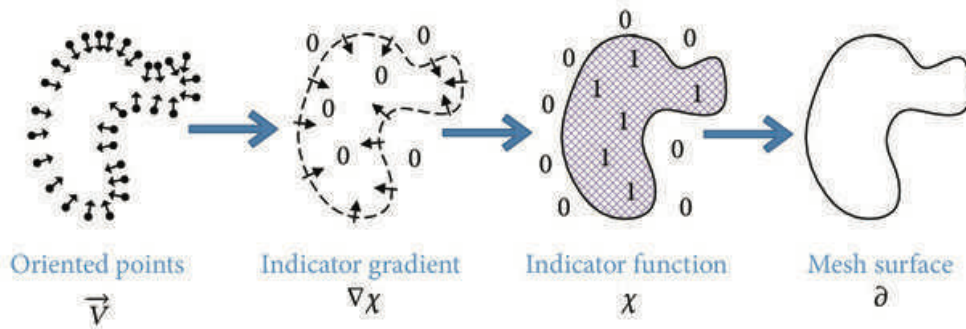
Points in the CBCT dataset corresponding to dental crowns (based on proximity to IOS points) were removed. This step eliminated the less accurate crown data from CBCT, retaining only the root structures, which are not captured in IOS.

Then, the DBSCAN (Density-Based Spatial Clustering of Applications with Noise) algorithm was employed to remove isolated clusters of points that did not belong to the main tooth structures, further refining the data.⁹⁸



DBSCAN algorithm functioning

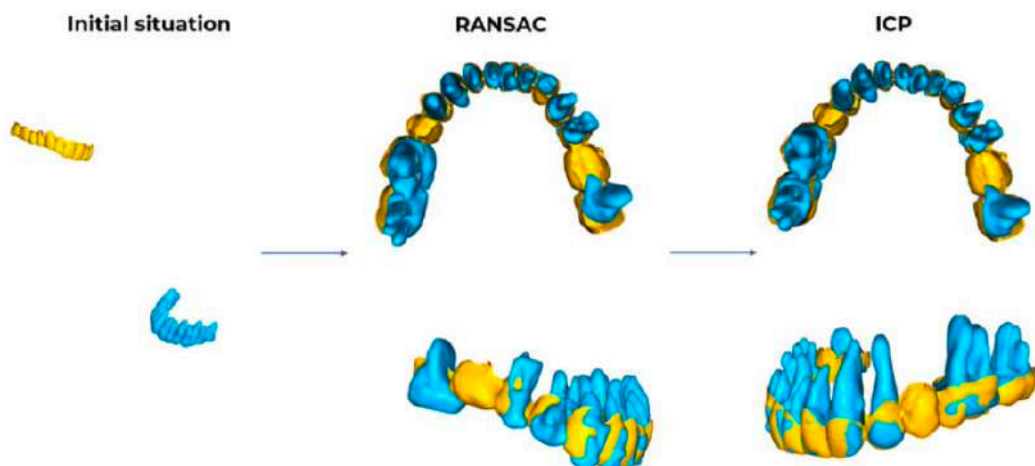
The remaining points from the CBCT roots and IOS crowns were merged, and a Poisson surface reconstruction algorithm was used to generate a continuous mesh.⁹⁹ This final model accurately represents the full anatomy of the teeth, including both the crowns and roots.



Creation of the final mesh

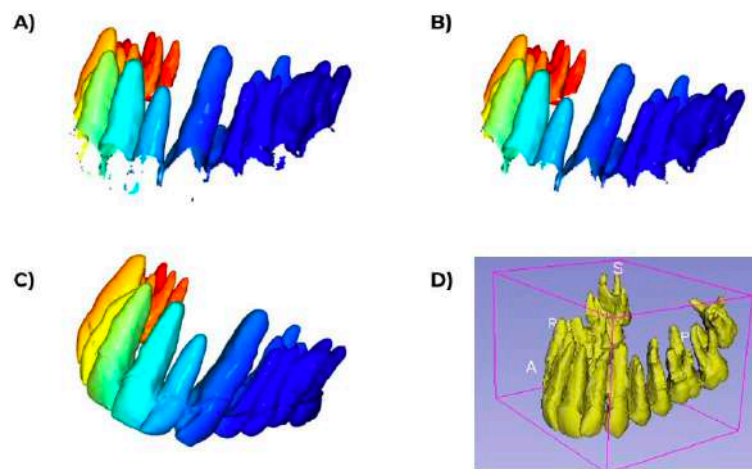
The quality of the registration and fusion process was primarily assessed through visual inspection, with the fused models demonstrating a high degree of alignment and continuity between the crowns and roots.

The fused models were examined for alignment accuracy, particularly focusing on the interface between the IOS-derived crowns and the CBCT-derived roots. The results showed that the fusion process successfully combined the detailed crown surfaces from IOS with the root structures from CBCT, creating a seamless model that accurately represents the full dental anatomy.



Graphic pipeline of registration and fusion of CBCT and IOS data

While the primary evaluation was qualitative, future work will involve quantitative assessments, such as comparing the fused models to manually segmented teeth and evaluating the accuracy of the crown-root interface. Among the quantitative methods, actually, we are measuring the discrepancies between the model and the manual ground truth by metrics such as the Root Mean Square Error (RMSE) between the fused model and manual segmentations will be used to quantify the accuracy of the fusion process.



Graphic pipeline of registration and fusion of CBCT and IOS data

The automated registration and fusion of IOS and CBCT data pose several challenges that must be addressed to improve the robustness and accuracy of the process. One of the primary challenges is the inherent differences between IOS and CBCT data, including variations in resolution, occlusion, and imaging artifacts. These discrepancies can lead to misalignments, particularly in areas with significant occlusions or where metallic artifacts are present in CBCT scans.

Moreover, the registration and fusion processes are computationally intensive, particularly when dealing with high-resolution point clouds. Optimizing the algorithms for efficiency, without sacrificing accuracy, is crucial for practical clinical implementation.

Ensuring that the fused models are both accurate and reliable across different patient datasets requires extensive validation. Additionally, developing standardized

protocols for the registration and fusion process will be essential for widespread clinical adoption.

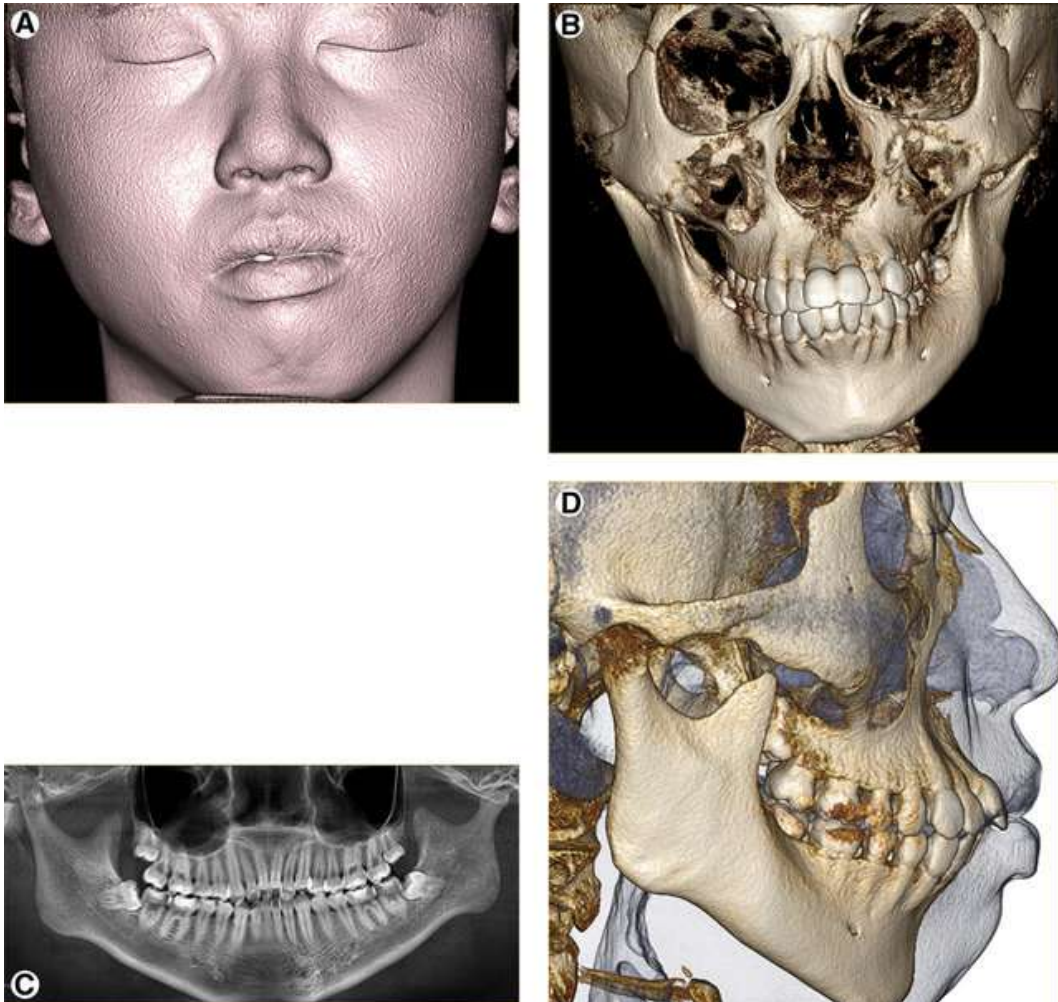
Future work will focus on refining the registration and fusion algorithms, improving the efficiency of the process, and conducting extensive validation studies to ensure the clinical reliability of the fused models. Developing real-time fusion capabilities would greatly enhance clinical workflows, allowing for immediate feedback during patient consultations and surgical planning.

Furthermore, expanding the fusion process to include other imaging modalities, such as MRI or stereophotogrammetry, could provide even more comprehensive models that incorporate soft tissue information alongside the dental and bony structures.

In conclusion, the automated registration and fusion of IOS and CBCT segmented teeth represent a significant advancement in evaluating the virtual patient, enabling the creation of comprehensive dental models that combine the detailed surface data from IOS with the volumetric information from CBCT. While challenges remain, particularly in addressing discrepancies between the modalities and optimizing computational efficiency, the results demonstrate the potential of this approach to enhance diagnosis, treatment planning, and surgical outcomes in dental practice. Further research and development will continue to refine these processes, moving towards fully integrated, real-time solutions for clinical use.

Automated face scan matching with CBCT data

Face scan (FS) matching with CBCT data is a pivotal development in orthodontics, maxillofacial surgery, and craniofacial research. By integrating the high-resolution surface details of facial scans with the volumetric anatomical information provided by CBCT, this technique enables clinicians to evaluate both the external and internal structures of the craniofacial region. Such integration offers a detailed understanding of aesthetic and functional relationships, fostering enhanced diagnosis and treatment planning. Moreover, the use of facial reference points is an innovative method for cephalometric analysis.



Registration result between FS and CBCT data

The process of FS matching begins with the acquisition of two distinct datasets. Facial scans are obtained using 3D optical scanners, which provide a detailed representation of the soft tissue surface. Meanwhile, CBCT captures volumetric data of the craniofacial skeleton, including bones, airways, and some soft tissues. These datasets often differ in resolution and modality, necessitating careful preprocessing to prepare them for integration. Preprocessing involves noise reduction to eliminate artifacts, segmentation to isolate relevant structures, and normalization to ensure that both datasets share a consistent coordinate system, scale, and orientation.

The registration process begins with the extraction of 3D representations from both CBCT data and facial scans. In CBCT imaging, a thresholding technique (-200 HU) isolates the scalp and facial structures, generating a binary mask that is converted into a 3D mesh using the Visualization Toolkit (VTK). This mesh provides a surface representation of the facial craniofacial structures.

Facial scans, obtained from high-resolution optical scanning devices, represent the external soft tissue (Planmeca Proface, Helsinki, Finland). These are converted into dense point clouds (STLs) that capture the intricate geometry of facial surfaces, which are then prepared for alignment with CBCT data.

For global rigid transformation, the Open3D library's global alignment method was used. First, the point clouds of the face and CBCT scalp were downsampled; a global transformation framework is established using Fast Point Feature Histograms (FPFH), which encode local geometric properties of each point. The FPFH is a 33-dimensional vector that describes the local geometric properties of a point. The RANSAC (Random Sample Consensus) algorithm then estimates an initial alignment by iteratively refining correspondences between facial and CBCT-derived meshes. RANSAC's robustness to outliers ensures that noisy data or missing regions do not significantly affect the global alignment. RANSAC algorithm was applied with a maximum of 100.000.000 iterations and a confidence probability of 0.7. A voxel size of 1mm was chosen. The RANSAC algorithm is an iterative method used to estimate the parameters of a mathematical model from observed data that contains outliers. During each iteration, RANSAC samples a set

of candidate correspondences, generates an alignment based on these correspondences, and evaluates the alignment. The algorithm repeats this process until a consensus set with sufficient inliers is obtained, providing a robust solution to align the data despite the presence of outliers.

To refine the alignment, the Iterative Closest Point (ICP) algorithm minimizes errors by iteratively optimizing correspondences. This fine-grained registration adjusts the transformation parameters to achieve a closer fit between the datasets, focusing on minimizing discrepancies between matched points in the two meshes. Global registration was performed on the down-sampled point cloud, so the result of registration was not optimal. To refine alignment, the ICP algorithm was applied, achieving higher accuracy by iteratively updating correspondences between face and CBCT data. A voxel size of 3 was chosen.

The accuracy of the registration process is validated through both qualitative visual assessments and quantitative metrics. Quantitative evaluation employs distance-based measures such as Median Distance (MD), Root Mean Squared Distance (RMSD), and Hausdorff Distance (HD). These metrics provide a detailed analysis of the alignment precision, ensuring that the results meet clinical requirements.

The registration process was applied to a dataset of 22 cases, with both CBCT and facial scan data. The results demonstrated the robustness and precision of the methodology:

- Median Distance: The median distance across all datasets was 0.369mm, indicating a high level of accuracy given the voxel sizes of 0.2–0.4 mm.
- Alignment Metrics: Other measures, such as RMSD and HD, supported the precision of the alignment, showing minimal variation across datasets.
- Processing Time: The average time required for registration was approximately 75 seconds per case, highlighting the computational efficiency of the pipeline.

Visual assessments also confirmed the successful alignment of facial scans with CBCT-derived scalp meshes. Key anatomical landmarks, such as the nasion and orbital points, were consistently aligned, ensuring the clinical usability of the integrated datasets.

The V-Net architecture played a pivotal role in refining landmark detection and segmentation accuracy. This deep learning model was trained on augmented datasets to enhance its robustness, achieving sub-millimeter precision in landmark identification. By combining 3D convolutional layers and residual connections, V-Net effectively captured spatial dependencies, enabling reliable segmentation of complex craniofacial structures.

Artifacts in CBCT imaging, such as scatter from metallic restorations, can complicate the alignment process. Moreover, the high resolution of facial scans often creates dense point clouds that require computationally intensive processing. This issue caused the increased values of the Hausdorff distances.

The methodology for face scan registration with CBCT data demonstrates remarkable accuracy, efficiency, and clinical applicability. The results validate the robustness of the alignment process, supported by advanced algorithms and deep learning networks. This integration of facial scans and CBCT imaging has the potential to transform craniofacial diagnostics and treatment planning, offering a radioprotection-based craniofacial analysis combining both skeletal and soft-tissues. Future developments in machine learning and imaging technologies will likely refine this process further, enhancing its precision and accessibility.

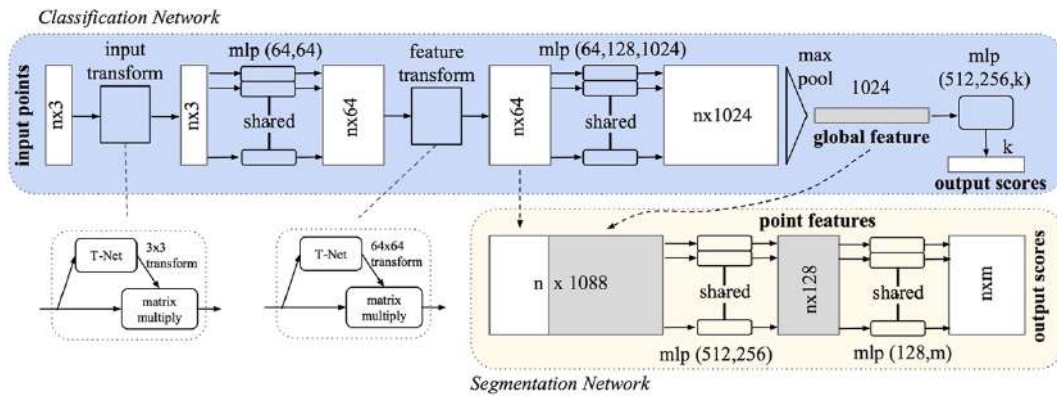
Automated landmarking of facial reference points on facial scan

Facial landmarking is integral to various medical and research applications, including orthodontics, maxillofacial surgery, and aesthetic medicine. While manual annotation of facial landmarks has historically been the standard, it is time-consuming, subjective, and prone to inconsistencies. The advent of automated systems, powered by advanced imaging modalities and deep learning algorithms, has significantly enhanced precision, efficiency, and reproducibility in landmark detection. This chapter provides a detailed exploration of the technical methodologies employed in automated facial landmarking, focusing on the integration of stereophotogrammetry, CBCT, and advanced computational models such as CNNs and PointNet.

Automated landmarking relies on a combination of advanced imaging techniques, data preprocessing, and ML algorithms. The process begins with data acquisition using high-resolution imaging modalities. Stereophotogrammetry, for instance, captures detailed 3D surface data of the face using a set of calibrated cameras. This technology leverages the principles of stereo vision to construct dense point clouds that accurately represent facial contours. Similarly, CBCT provides volumetric imaging of craniofacial structures, capturing both soft and hard tissues with high resolution. To optimize the clinical utility of CBCT, techniques such as ultra-reduced FOV imaging are employed, which minimize radiation exposure while maintaining diagnostic quality.

The core of the automated landmarking process lies in DL models specifically designed for 3D data processing. CNNs, particularly architectures like V-Net, are tailored for volumetric data segmentation. These models decompose the input data into multidimensional arrays, extracting hierarchical features that correspond to anatomical landmarks. The V-Net architecture, an extension of the widely used U-Net, incorporates 3D convolutions and residual connections to enhance its ability to learn spatial relationships within the data.

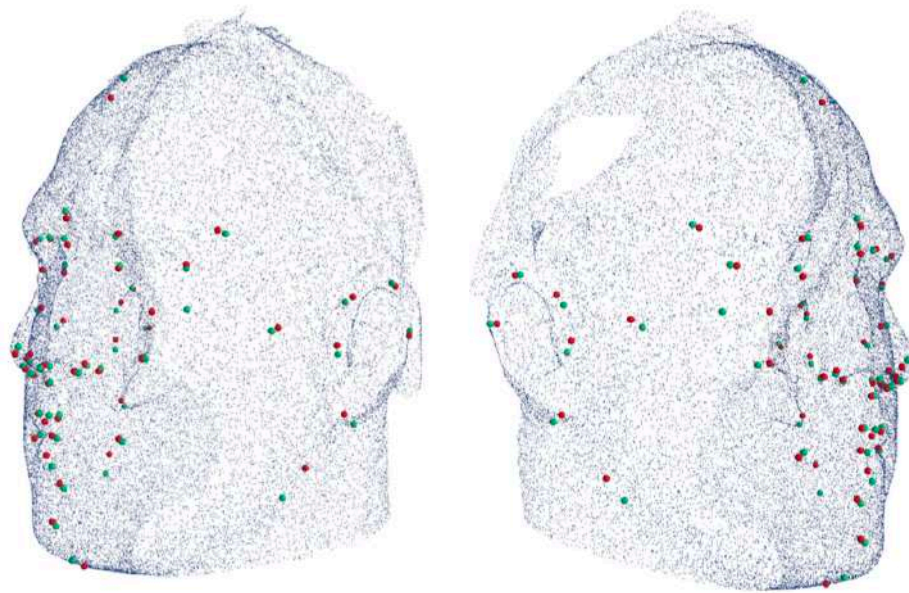
PointNet, another prominent model, processes unordered point cloud data, offering a flexible approach to handling the spatial complexity of 3D facial structures. ¹⁰⁰PointNet employs a transformation network, T-Net, to normalize the input data by addressing rotational and translational variations. This ensures that the downstream layers receive data in a canonical form, improving consistency and reducing variability in predictions.



PointNet architecture

To achieve high localization accuracy, a two-stage model is often implemented. In the first stage, termed the Estimation stage, pointwise CNNs extract features and predict approximate landmark locations. These predictions guide the second stage, known as the Refinement stage, which isolates regions around the predicted landmarks and performs a finer analysis. This iterative approach enhances the precision of landmark localization, achieving millimeter-level accuracy.

Post-processing techniques address residual inaccuracies. For instance, the predicted landmark coordinates, which may deviate from the true surface due to data sparsity or model complexity, are adjusted by selecting the closest point in the point cloud or computing the centroid of nearby points. These refinements ensure that the predicted landmarks align more closely with the anatomical features.



Automated landmarking of FS compared to manual annotation

The performance of automated landmarking systems is evaluated using quantitative metrics such as Mean Euclidean Distance (MED) between predicted and ground truth landmark coordinates. The following summarizes key results from recent studies:

1) Validation on CBCT data

- A model trained on 16 craniofacial landmarks achieved a mean Euclidean distance of 1.74 mm on validation data from a hospital database. Landmarks such as Nasion and Sella demonstrated minimal error (<1.8mm), while complex regions like Menton and Pogonion showed slightly higher deviations (~2.2mm).

2) Performance on point clouds

- Using point clouds derived from stereophotogrammetry, the Refined Estimation model achieved a MED of 3.0mm on training data and 4.1mm on test data. Incorporating T-Net further reduced localization errors, with the Refined EsTi model showing superior consistency and a narrower error distribution.

3) Data augmentation and sampling

- Models trained with non-rigid augmentation showed improved performance, achieving MED values of 2.8mm on augmented datasets. Variations in point cloud density (10,000–30,000 vertices) revealed that denser datasets slightly improved accuracy, though computational demands increased.

4. Comparison across landmark types

- In a broader model trained to detect 32 landmarks, the mean Euclidean distance rose to 2.47mm due to increased complexity. However, critical landmarks essential for cephalometric analysis (e.g., Nasion, Point A, and Point B) maintained high precision, supporting clinical applicability.

5. Robustness and error analysis

- Models demonstrated resilience against outliers and anatomical variability. Error patterns were consistent across datasets, with models leveraging augmentation strategies to minimize the impact of sparsity and noise.

The results of the study demonstrate the efficacy of the developed deep learning-based system for automated facial landmark localization. The refined two-step approach, utilizing CNNs and T-Net architecture, achieved a mean Euclidean distance error of approximately 3.9mm across diverse preprocessing scenarios, including data augmentation and point cloud resampling. Specifically, the model's ability to consistently identify 50 anatomical landmarks on 3D facial models, with accuracy comparable to manual annotations by experts, highlights its clinical relevance. Among the configurations tested, the Refined EsTi model exhibited superior robustness and precision, maintaining a more uniform error distribution and lower residual standard deviation compared to alternative models. The system's adaptability to various preprocessing pipelines and augmentation strategies underscores its potential for broader applications in clinical and research settings. These findings establish the proposed methodology as a significant advancement in automated 3D anthropometric analysis.

Despite its potential, automated landmarking of facial scans faces several challenges. Variability in facial anatomy across individuals poses a significant hurdle, as the network must generalize across diverse datasets while maintaining high accuracy. The presence of artifacts, such as occlusions caused by glasses or facial hair, can interfere with landmark detection, requiring robust preprocessing techniques.

Another challenge lies in the annotation of training datasets. Manual annotation of facial landmarks is time-consuming and subject to inter-observer variability, which can affect the consistency of the training data. Moreover, achieving real-time processing speeds remains an area of active research, particularly for applications requiring immediate feedback during clinical consultations.

Automated landmarking of facial reference points on 3D facial scans is revolutionizing the fields of orthodontics and maxillofacial surgery. By leveraging cutting-edge neural networks and computational techniques, this approach offers unparalleled precision and efficiency in identifying critical landmarks. While challenges remain, ongoing advancements in AI and imaging technologies continue to push the boundaries of what is possible, making automated landmarking an indispensable tool in modern clinical practice and research.

Scientific papers related to the purpose of new cephalometric measurements obtained by ultra-reduced FOV CBCT scans

As mentioned, the advent CBCT has revolutionized dental imaging, offering high-resolution, three-dimensional visualization of craniofacial structures essential for accurate diagnosis and treatment planning in orthodontics, implantology, and maxillofacial surgery. However, the widespread use of CBCT has raised significant concerns regarding patient radiation exposure, particularly in routine procedures such as cephalometric analysis.

In response to these concerns, the ultra-reduced FOV CBCT could emerge as a promising solution, aligning with radioprotection principles by minimizing radiation dose while maintaining diagnostic efficacy. The ultra-reduced FOV CBCT focuses the imaging field on specific anatomical regions of interest, reducing unnecessary exposure to surrounding tissues. This technique is particularly advantageous in cephalometric analysis, where precise measurements of craniofacial landmarks are critical, but a full cranial view may not be required.

Over the years of the PhD, I have conducted extensive research to explore and validate various techniques that leverage ultra-reduced FOV CBCT for cephalometric analysis. These studies collectively demonstrate that, by optimizing the FOV and employing advanced imaging protocols, it is possible to achieve high-quality cephalometric assessments while adhering to the stringent radioprotection guidelines. Each paper contributes to a growing body of evidence that supports the use of ultra-reduced FOV CBCT as a safe, effective, and patient-friendly approach in dental imaging.

The research presented in these cited papers underscores the critical importance of balancing diagnostic accuracy with patient safety in dental imaging. Through the application of ultra-reduced FOV CBCT, these studies have demonstrated that it is possible to perform precise cephalometric analyses while significantly reducing radiation exposure, thus aligning with radioprotection principles. The findings offer compelling evidence that ultra-reduced FOV CBCT not only meets the clinical

demands for high-quality imaging but also adheres to the ethical imperative of minimizing harm to patients. As these techniques gain acceptance and integration into routine practice, they have the potential to set new standards for safe, effective, and patient-centered dental care. The drafts submitted for publication will hopefully contribute to the broader adoption of these practices, influencing both current and future generations of clinicians.

Manuscripts related:

Serafin et al. (2024) Radioprotection-based cephalometric analysis: validation of AB-ratio for sagittal assessment of malocclusion. Journal of Orthodontics (Under review)

Serafin et al. (2024) Can maxillomandibular assessment be calculated despite the skeletal bite interference? The ABwise appraisal and its correlation with ANB angle. Journal of Clinical Medicine

Serafin et al. (2024) From Nasion to Sellion: repositioning landmarks for radioprotection-tailored 3D cephalometric analysis. Clinical and investigative orthodontics.

Serafin et al. (2024) Accuracy of facial scanning registration: comparison between full-cranium and ultra-reduced FOV CBCT. Imaging Science in Dentistry (under review)

Serafin et al. (2024) Camper-Wits appraisal as method for maxillomandibular sagittal assessment: validation study based on CBCT dataset.

Serafin et al. (2024) A novel approach to three-dimensional intramaxillary skeletal assessment: correlation between ANB angle and bisector-wits appraisal. Journal of Orofacial Orthopedics

AIOral – A Beta Software for Advanced Diagnostics and Radioprotection

The development and implementation of AIOral mark a significant milestone in the integration of AI within orthodontics and radioprotection. This beta software emerges as a groundbreaking platform capable of automating complex diagnostic tasks, reducing human error, and advancing the principles of radioprotection through intelligent image processing. While still in its beta stage, AIOral already demonstrates remarkable capabilities in automated cephalometric landmark detection, IOS and CBCT segmentation, and data alignment. Its primary output—a virtual patient—is a leap forward in diagnostic precision, offering a cohesive representation of craniofacial anatomy. Currently limited to diagnostics, AIOral’s potential for future expansion into treatment planning and simulation heralds a transformative era in orthodontic practice.

Automated Landmark Detection: The Cornerstone of AIOral

The core of AIOral lies in its ability to perform automated landmark detection with remarkable precision. This feature addresses one of the most labor-intensive aspects of orthodontic diagnostics: the identification of cephalometric landmarks. Traditionally, this process requires trained clinicians to manually annotate radiographic images, a task prone to variability and error due to operator fatigue and subjectivity. AIOral employs advanced deep learning algorithms, such as V-Net and CNNs, to automate this process. These algorithms analyze CBCT data, isolate anatomical regions of interest, and accurately locate landmarks critical for cephalometric analysis.

The landmark detection process within AIOral begins with preprocessing the CBCT scans to enhance image clarity. Techniques such as intensity thresholding isolate bone and dental structures from soft tissues, while noise reduction filters ensure high-fidelity data input for the algorithm. Following preprocessing, AIOral’s deep learning models segment the volumetric data, identifying regions that correspond to craniofacial landmarks. Each landmark is detected based on its unique

anatomical and spatial features, ensuring high accuracy even in complex cases involving anatomical asymmetries or distortions.

AIOral's automated landmarking is not only a time-saving tool but also a step towards standardizing orthodontic diagnostics. By eliminating human variability, the software ensures consistent and reproducible results, fostering confidence in the diagnostic process. Furthermore, its ability to process large datasets efficiently makes it suitable for integration into clinical workflows, where rapid and accurate diagnostics are essential.

Automated Segmentation: Unlocking the Potential of CBCT and IOS Data

Beyond landmark detection, AIOral excels in the automated segmentation of teeth and bones from both CBCT and IOS. Segmentation—the process of delineating anatomical structures from surrounding tissues—is a critical step in creating detailed 3D models of the craniofacial complex. In orthodontics, accurate segmentation is indispensable for understanding dental occlusion, jaw alignment, and other structural relationships that inform diagnosis and treatment planning.

AIOral's segmentation capabilities extend to CBCT scans, where it isolates teeth, maxillary and mandibular bones, and other skeletal components with precision. Using volumetric data, the software applies segmentation algorithms to identify and extract individual structures. Advanced image processing techniques ensure that even in cases of overlapping or crowded teeth, the segmentation remains accurate. This is particularly important in complex cases where traditional methods might fail to provide clear delineation due to low image quality or structural anomalies.

IOS present a different challenge, as they are surface-based representations of dental arches. AIOral leverages high-resolution data from IOS to perform segmentation with fine detail, capturing the unique morphology of each tooth. This level of precision is crucial for applications such as restorative dentistry and the design of orthodontic appliances. By combining IOS and CBCT data, AIOral creates comprehensive 3D models that incorporate both surface and volumetric information.

Data Alignment and the Creation of the Virtual Patient

One of AIOra's most innovative features is its ability to align data from multiple imaging modalities to create a virtual patient. This process involves the fusion of segmented CBCT data with IOS and facial scans, resulting in a cohesive representation of the patient's craniofacial anatomy. The virtual patient is not merely a collection of static images but an interactive model that integrates skeletal, dental, and soft tissue data.

The alignment process is a technical achievement that underscores AIOra's sophistication. CBCT provides volumetric data with high spatial resolution, while IOS offers detailed surface morphology of the dental arches. AIOra's algorithms use advanced matching techniques to ensure that the two datasets align seamlessly. The integration of facial scans adds an additional layer of complexity, as the software must correlate external features with internal structures. This holistic approach enables clinicians to visualize the interplay between form and function, bridging the gap between aesthetics and biomechanics.

The creation of the virtual patient has profound implications for orthodontic diagnostics. It allows clinicians to explore craniofacial structures in three dimensions, offering insights that are unattainable through traditional two-dimensional radiographs. The virtual patient can be manipulated in real-time, enabling dynamic assessments of jaw movements, occlusal relationships, and asymmetries. This interactive capability enhances diagnostic precision and provides a valuable tool for patient education, as complex anatomical concepts can be visualized and explained with clarity.

Radioprotection: A Guiding Principle in AIOra's Development

Radioprotection is a fundamental concern in the use of imaging technologies, particularly in orthodontics, where repeated imaging is often required. AIOra addresses this concern by integrating features that align with the principles of justification, optimization, and dose limitation. By utilizing ultra-reduced CBCT

FOV, AIOral minimizes radiation exposure without compromising diagnostic quality.

The use of ultra-reduced FOV is particularly significant in pediatric patients, who are more sensitive to radiation. AIOral's segmentation and landmarking algorithms are optimized for these smaller datasets, ensuring accurate diagnostics even with limited imaging. Additionally, the software's ability to combine CBCT with IOS and facial scans further reduces the need for additional radiographic imaging, adhering to the ALARA principle.

AIOral's commitment to radioprotection extends beyond dose reduction. The software provides real-time feedback on radiation exposure, enabling clinicians to make informed decisions about imaging protocols. This feature not only enhances patient safety but also ensures compliance with regulatory guidelines, fostering a culture of responsibility in the use of radiographic technologies.

Applications and Future Prospects

Currently, AIOral's functionalities are limited to diagnostic applications, but its potential for future expansion is vast. The virtual patient model created by AIOral could serve as a foundation for treatment planning and simulation. By integrating predictive algorithms, the software could simulate orthodontic treatment outcomes, providing clinicians with valuable insights into the long-term implications of their decisions. This capability would be particularly beneficial in complex cases involving orthognathic surgery or interdisciplinary care.

AIOral's development roadmap also includes the integration of VR for enhanced visualization and interaction. VR technology could allow clinicians to immerse themselves in the virtual patient environment, exploring craniofacial structures with unprecedented detail. This immersive capability would not only improve diagnostic accuracy but also enhance patient communication by providing a tangible representation of treatment goals.

In the context of radioprotection, AIOral's future iterations could incorporate dose optimization algorithms that adapt imaging parameters based on patient-specific factors. These advancements would further reduce radiation exposure while maintaining high diagnostic standards.

Conclusion

AIOral represents a pioneering effort to integrate AI, advanced imaging, and radioprotection into orthodontic diagnostics. Its current capabilities—automated landmark detection, segmentation, data alignment, and virtual patient creation—demonstrate the transformative potential of technology in improving diagnostic precision and patient safety. While still in its beta stage, AIOral lays the groundwork for future innovations that could revolutionize orthodontic practice. By addressing the challenges of radioprotection and harnessing the power of AI, AIOral exemplifies the convergence of technology and medicine, paving the way for a safer, more efficient, and patient-centered approach to orthodontic care.



Actual aspect of AI Oral beta software

Conclusions

This PhD project represents a significant advancement at the confluence of radioprotection, advanced imaging technologies, and artificial intelligence, with a specific focus on enhancing orthodontic diagnostics and treatment planning. The research successfully addresses critical challenges associated with balancing diagnostic efficacy and patient safety by integrating ultra-reduced CBCT FOV, AI-driven automation, and virtual reality applications.

A central theme of this study is the commitment to radioprotection principles, including justification, optimization, and dose limitation. The work demonstrates how ultra-reduced CBCT FOVs can achieve significant reductions in radiation exposure while maintaining the precision necessary for effective diagnosis. This development is particularly relevant in pediatric orthodontics, where minimizing radiation risks is paramount. By introducing innovative methodologies and technologies, the study not only improves diagnostic protocols but also aligns them with contemporary demands for environmental sustainability and patient safety.

The integration of AI into cephalometric analysis represents a groundbreaking step forward in orthodontic care. Through the development of advanced deep learning models, the research achieves high levels of accuracy in detecting and analyzing craniofacial landmarks, automating a process that has traditionally relied on manual expertise. This innovation reduces the potential for human error, enhances reproducibility, and significantly streamlines clinical workflows. Moreover, the fusion of intraoral scans with CBCT data creates a unified and highly detailed representation of craniofacial structures, providing an unparalleled level of diagnostic precision.

Equally transformative is the application of VR, which offers clinicians an immersive, dynamic platform for analyzing and interpreting complex craniofacial data. The ability to visualize 3D anatomical structures interactively fosters improved communication between practitioners and patients, while also aiding in more precise treatment planning. This novel use of VR, creating a virtual patient,

underscores the project's commitment to leveraging cutting-edge technologies to advance orthodontic care.

The contributions of this research extend beyond the technical achievements. It underscores the potential for interdisciplinary approaches to redefine diagnostic practices in orthodontics and maxillofacial surgery, emphasizing patient-specific, eco-conscious methodologies that prioritize safety and precision. By demonstrating the feasibility of these advancements, the study sets the stage for future innovations aimed at minimizing the environmental and biological impacts of diagnostic imaging.

In conclusion, the present PhD project not only addresses pressing challenges in orthodontic radiology but also paves the way for a future where patient safety, environmental sustainability, and diagnostic excellence coexist seamlessly. It represents a crucial step toward a new paradigm in orthodontic care, where cutting-edge technologies are harnessed responsibly to deliver optimal outcomes for patients and practitioners alike.

References

1. Copeland ES. MECHANISMS OF RADIOPROTECTION—A REVIEW. *Photochem Photobiol* 1978;28(4–5).
2. Do KH. General principles of radiation protection in fields of diagnostic medical exposure. *J Korean Med Sci* 2016;31.
3. Michael Moores B. A review of the fundamental principles of radiation protection when applied to the patient in diagnostic radiology. *Radiat Prot Dosimetry* 2017;175(1).
4. González AJ. Radiation safety standards and their application: International policies and current issues. In: *Health Physics* Vol 87.; 2004.
5. Fiebich M. Praktischer Strahlenschutz am Patienten in der radiologischen Diagnostik. *Radiologe* 2017;57:534–40.
6. Johnke RM, Sattler JA, Allison RR. Radioprotective agents for radiation therapy: Future trends. *Future Oncology* 2014;10(15).
7. Jones CG. A review of the history of U.S. radiation protection regulations, recommendations, and standards. *Health Phys* 2005;88(6).
8. Clarke R, Valentin J. A history of the international commission on radiological protection. *Health Phys* 2005;88(5).
9. Wojcik A, Harms-Ringdahl M. Radiation protection biology then and now. *Int J Radiat Biol* 2019;95(7).
10. Prasad KN, Cole WC, Haase GM. Radiation protection in humans: Extending the concept of as low as reasonably achievable (ALARA) from dose to biological damage. *British Journal of Radiology* 2004;77(914).
11. Malone J. X-rays for medical imaging: Radiation protection, governance and ethics over 125 years. *Physica Medica* 2020;79.
12. Moores BM, Regulla D. A review of the scientific basis for radiation protection of the patient. *Radiat Prot Dosimetry* 2011;147(1–2).
13. Joseph BB, George S. The road to radiation safety and ALARA: A review. *IP International Journal of Maxillofacial Imaging* 2021;6(4).
14. Fisher DR, Fahey FH, Phys Author manuscript H. APPROPRIATE USE OF EFFECTIVE DOSE IN RADIATION PROTECTION AND RISK ASSESSMENT HHS Public Access Author manuscript. *Health Phys* 2017;113(2):102–9.

15. Dainiak N. Radiation dose and stochastic risk from exposure to medical imaging. *Chest* 2013;144(5):1431–3. Available at: <http://journal.chestnet.org/article/S0012369213607096/fulltext>. Accessed July 20, 2024.
16. Hendee WR, O'Connor MK. Radiation Risks of Medical Imaging: Separating Fact from Fantasy. <https://doi.org/10.1148/radiol.12112678> 2012;264(2):312–21. Available at: <https://pubs.rsna.org/doi/10.1148/radiol.12112678>. Accessed July 20, 2024.
17. Rosenblatt E, Zubizarreta E, Wondergem J, Fidarova E, Izewska J. The International Atomic Energy Agency (IAEA): An active role in the global fight against cancer. *Radiotherapy and Oncology* 2012;104(3):269–71. Available at: <http://www.thegreenjournal.com/article/S0167814011006049/fulltext>. Accessed July 20, 2024.
18. Konijnenberg M, Herrmann K, Kobe C, et al. EANM position paper on article 56 of the Council Directive 2013/59/Euratom (basic safety standards) for nuclear medicine therapy. *Eur J Nucl Med Mol Imaging* 2021;48(1):67–72. Available at: <https://link.springer.com/article/10.1007/s00259-020-05038-9>. Accessed July 20, 2024.
19. Raghavan UN, Hall CS, Tellis R, Mabotuwana T, Wald C. Probabilistic Modeling of Exam Durations in Radiology Procedures. *J Digit Imaging* 2019;32(3):386–95. Available at: <https://link.springer.com/article/10.1007/s10278-018-00175-y>. Accessed July 20, 2024.
20. Nikzad S, Pourkaveh M, Vesal NJ, Gharekhanloo F. Cumulative Radiation Dose and Cancer Risk Estimation in Common Diagnostic Radiology Procedures. *Iranian Journal of Radiology* 2018 15:3 2018;15(3):60955. Available at: <https://brieflands.com/articles/ijradiology-60955>. Accessed July 20, 2024.
21. European Society of Radiology (ESR), Akata D, Adam EJ, et al. Summary of the European Directive 2013/59/Euratom: essentials for health professionals in radiology. *Insights Imaging* 2015;6(4):411–7. Available at: <https://link.springer.com/articles/10.1007/s13244-015-0410-4>. Accessed July 20, 2024.

22. Giusti M, Nardi C, Bonaccorsi G, Lorini C, Persiani N. Key words • 2013/50/EURATOM • radioprotection • training • health literacy • health organizational Organizational Health Literacy as a supportive tool for the effective implementation of the 2013/59/ EURATOM Directive in Italy. *Ann Ist Super Sanità* 2024;60(2):145–53.
23. Hans MG, Martin Palomo J, Valiathan M. History of imaging in orthodontics from Broadbent to cone-beam computed tomography. *American Journal of Orthodontics and Dentofacial Orthopedics* 2015;148(6):914–21.
24. Alam MK, Abutayyem H, Kanwal B, A. L. Shayeb M. Future of Orthodontics— A Systematic Review and Meta-Analysis on the Emerging Trends in This Field. *Journal of Clinical Medicine* 2023, Vol. 12, Page 532 2023;12(2):532. Available at: <https://www.mdpi.com/2077-0383/12/2/532/htm>. Accessed July 20, 2024.
25. Durão AR, Pittayapat P, Rockenbach IB, et al. Validity of 2D lateral cephalometry in orthodontics: a systematic review. *Prog Orthod* 2013;14(1):31. Available at: </pmc/articles/PMC3882109/>. Accessed July 20, 2024.
26. Kapila SD, Nervina JM. CBCT in orthodontics: Assessment of treatment outcomes and indications for its use. *Dentomaxillofacial Radiology* 2015;44(1). Available at: <https://dx.doi.org/10.1259/dmfr.20140282>. Accessed July 20, 2024.
27. Dipalma G, Inchingolo AD, Inchingolo AM, et al. Artificial Intelligence and Its Clinical Applications in Orthodontics: A Systematic Review. *Diagnostics* 2023, Vol. 13, Page 3677 2023;13(24):3677. Available at: <https://www.mdpi.com/2075-4418/13/24/3677/htm>. Accessed July 20, 2024.
28. Kiełczykowski M, Kamiński K, Perkowski K, Zadurska M, Czochrowska E. Application of Artificial Intelligence (AI) in a Cephalometric Analysis: A Narrative Review. *Diagnostics (Basel)* 2023;13(16). Available at: <https://pubmed.ncbi.nlm.nih.gov/37627899/>. Accessed August 12, 2024.
29. Pittayapat P, Limchaichana-Bolstad N, Willems G, Jacobs R. Three-dimensional cephalometric analysis in orthodontics: a systematic review. *Orthod Craniofac Res* 2014;17(2):69–91. Available at: <https://onlinelibrary.wiley.com/doi/full/10.1111/ocr.12034>. Accessed August 12, 2024.

30. Nasseh I, Al-Rawi W. Cone Beam Computed Tomography. *Dent Clin North Am* 2018;62(3):361–91. Available at: <http://www.dental.theclinics.com/article/S001185321830017X/fulltext>. Accessed August 12, 2024.
31. Işınlı K, Tomografinin B, Kavramları T, Kullanım D, Venkatesh AE, Elluru SV. CONE BEAM COMPUTED TOMOGRAPHY: BASICS AND APPLICATIONS IN DENTISTRY. *J Istanb Univ Fac Dent* 2017;51(3 Suppl 1):102–21. Available at: <https://dergipark.org.tr/en/pub/jiufd/issue/37941/438255>. Accessed August 12, 2024.
32. Schulze D, Heiland M, Thurmann H, Adam G. Radiation exposure during midfacial imaging using 4- and 16-slice computed tomography, cone beam computed tomography systems and conventional radiography. *Dentomaxillofacial Radiology* 2004;33(2):83–6. Available at: <https://dx.doi.org/10.1259/dmfr/28403350>. Accessed August 12, 2024.
33. Olch AJ, Alaei P. How low can you go? A CBCT dose reduction study. *J Appl Clin Med Phys* 2021;22(2):85–9. Available at: <https://onlinelibrary.wiley.com/doi/full/10.1002/acm2.13164>. Accessed August 12, 2024.
34. Kaur H, Kaur N. Historical Review of CBCT Orthodontics. *Journal of Orofacial & Health Sciences* 2015;6(3):113.
35. Mureşanu S, Almăşan O, Hedeşiu M, Dioşan L, Dinu C, Jacobs R. Artificial intelligence models for clinical usage in dentistry with a focus on dentomaxillofacial CBCT: a systematic review. *Oral Radiol* 2023;39(1):18–40. Available at: <https://link.springer.com/article/10.1007/s11282-022-00660-9>. Accessed August 12, 2024.
36. Loubele M, Bogaerts R, Van Dijck E, et al. Comparison between effective radiation dose of CBCT and MSCT scanners for dentomaxillofacial applications. *Eur J Radiol* 2009;71(3):461–8.
37. Serafin M, Baldini B, Cabitza F, et al. Accuracy of automated 3D cephalometric landmarks by deep learning algorithms: systematic review and meta-analysis. *Radiologia Medica* 2023;128(5):544–55. Available at:

<https://link.springer.com/article/10.1007/s11547-023-01629-2>. Accessed August 12, 2024.

38. Li C, Teixeira H, Tanna N, et al. The reliability of two- and three-dimensional cephalometric measurements: A CBCT study. *Diagnostics* 2021;11(12):2292. Available at: <https://www.mdpi.com/2075-4418/11/12/2292/htm>. Accessed August 12, 2024.

39. Stucki J, Dastgir R, Baur DA, Quereshy FA. Iatrogenic rerouting of the lateral antebrachial cutaneous nerve during distal biceps tendon repair: a case report. *JSES Open Access* 2017;1:139–40. Available at: <https://doi.org/10.1016/j.oopen.2023.07.001>. Accessed August 12, 2024.

40. Marradi F, Staderini E, Zimbalatti MA, Rossi A, Grippaudo C, Gallenzi P. How to Obtain an Orthodontic Virtual Patient through Superimposition of Three-Dimensional Data: A Systematic Review. *Applied Sciences* 2020, Vol. 10, Page 5354 2020;10(15):5354. Available at: <https://www.mdpi.com/2076-3417/10/15/5354/htm>. Accessed August 12, 2024.

41. Zhou M;, Antonelli Y;, Becker A;, et al. The Application of Artificial Intelligence for Tooth Segmentation in CBCT Images: A Systematic Review. *Applied Sciences* 2024, Vol. 14, Page 6298 2024;14(14):6298. Available at: <https://www.mdpi.com/2076-3417/14/14/6298/htm>. Accessed August 12, 2024.

42. Xiang B, Lu J, Yu J. Evaluating tooth segmentation accuracy and time efficiency in CBCT images using artificial intelligence: A systematic review and Meta-analysis. *J Dent* 2024;146:105064.

43. Polizzi A, Quinzi V, Ronsivalle V, et al. Tooth automatic segmentation from CBCT images: a systematic review. *Clin Oral Investig* 2023;27(7):3363–78. Available at: <https://link.springer.com/article/10.1007/s00784-023-05048-5>. Accessed August 12, 2024.

44. Kaul V, Enslin S, Gross SA. History of artificial intelligence in medicine. *Gastrointest Endosc* 2020;92(4):807–12.

45. Neapolitan RE. A Comparison Of The Mycin Model For Reasoning Under Uncertainty To A Probability Based Model. <https://doi.org/10.1117/12.964152> 1986;0635:375–83. Available at: <https://www.spiedigitallibrary.org/conference->

- proceedings-of-spie/0635/0000/A-Comparison-Of-The-Mycin-Model-For-Reasoning-Under-Uncertainty/10.1117/12.964152.full. Accessed August 12, 2024.
46. Haug CJ, Drazen JM. Artificial Intelligence and Machine Learning in Clinical Medicine, 2023. *New England Journal of Medicine* 2023;388(13):1201–8. Available at: <https://www.nejm.org/doi/full/10.1056/NEJMra2302038>. Accessed August 12, 2024.
47. Maceachern SJ, Forkert ND. Machine learning for precision medicine. *Genome* 2021;64(4):416–25. Available at: <https://cdnsiencepub.com/doi/10.1139/gen-2020-0131>. Accessed August 12, 2024.
48. Caruana R, Niculescu-Mizil A. An empirical comparison of supervised learning algorithms. *ACM International Conference Proceeding Series* 2006;148:161–8. Available at: <https://dl.acm.org/doi/10.1145/1143844.1143865>. Accessed August 12, 2024.
49. Dike HU, Zhou Y, Deveerasetty KK, Wu Q. Unsupervised Learning Based On Artificial Neural Network: A Review. *2018 IEEE International Conference on Cyborg and Bionic Systems, CBS 2018* 2018:322–7.
50. Xu X, Zuo L, Huang Z. Reinforcement learning algorithms with function approximation: Recent advances and applications. *Inf Sci (N Y)* 2014;261:1–31.
51. Lecun Y, Bengio Y, Hinton G. Deep learning. *Nature* 2015 521:7553 2015;521(7553):436–44. Available at: <https://www.nature.com/articles/nature14539>. Accessed August 12, 2024.
52. Yamashita R, Nishio M, Do RKG, Togashi K. Convolutional neural networks: an overview and application in radiology. *Insights Imaging* 2018;9(4):611–29. Available at: <https://link.springer.com/articles/10.1007/s13244-018-0639-9>. Accessed August 12, 2024.
53. Salehinejad H, Sankar S, Barfett J, Colak E, Valaee S. Recent Advances in Recurrent Neural Networks. 2017. Available at: <https://arxiv.org/abs/1801.01078v3>. Accessed August 12, 2024.
54. Aggarwal A, Mittal M, Battineni G. Generative adversarial network: An overview of theory and applications. *International Journal of Information Management Data Insights* 2021;1(1):100004.

55. Baris, kayalibay BB, Jensen G, Van Der Smagt P. CNN-based Segmentation of Medical Imaging Data. 2017. Available at: <https://arxiv.org/abs/1701.03056v2>. Accessed August 13, 2024.
56. Zou Z, Chen K, Shi Z, Guo Y, Ye J. Object Detection in 20 Years: A Survey. *Proceedings of the IEEE* 2023;111(3):257–76.
57. Cai L, Gao J, Zhao D. A review of the application of deep learning in medical image classification and segmentation. *Ann Transl Med* 2020;8(11):713–713. Available at: </pmc/articles/PMC7327346/>. Accessed August 13, 2024.
58. Schwendicke F, Samek W, Krois J. Artificial Intelligence in Dentistry: Chances and Challenges. *J Dent Res* 2020;99(7):769–74. Available at: <https://journals.sagepub.com/doi/full/10.1177/0022034520915714>. Accessed August 13, 2024.
59. Subramanian AK, Chen Y, Almalki A, Sivamurthy G, Kafle D. Cephalometric Analysis in Orthodontics Using Artificial Intelligence—A Comprehensive Review. *Biomed Res Int* 2022;2022(1):1880113. Available at: <https://onlinelibrary.wiley.com/doi/full/10.1155/2022/1880113>. Accessed August 13, 2024.
60. Yoh MS. The reality of virtual reality. *Proceedings - 7th International Conference on Virtual Systems and Multimedia, VSMM 2001* 2001:666–74.
61. Li L, Yu F, Shi D, et al. Application of virtual reality technology in clinical medicine. *Am J Transl Res* 2017;9(9):3867. Available at: </pmc/articles/PMC5622235/>. Accessed August 13, 2024.
62. Huang TK, Yang CH, Hsieh YH, Wang JC, Hung CC. Augmented reality (AR) and virtual reality (VR) applied in dentistry. *Kaohsiung J Med Sci* 2018;34(4):243–8.
63. Joda T, Gallucci GO. The virtual patient in dental medicine. *Clin Oral Implants Res* 2015;26(6):725–6. Available at: <https://onlinelibrary.wiley.com/doi/full/10.1111/clr.12379>. Accessed August 13, 2024.
64. Xia J, Ip HHS, Samman N, et al. Three-dimensional virtual-reality surgical planning and soft-tissue prediction for orthognathic surgery. *IEEE Transactions on Information Technology in Biomedicine* 2001;5(2):97–107.

65. van der Kruk SR, Zielinski R, MacDougall H, Hughes-Barton D, Gunn KM. Virtual reality as a patient education tool in healthcare: A scoping review. *Patient Educ Couns* 2022;105(7):1928–42.
66. Junaid N, Khan N, Ahmed N, et al. Development, Application, and Performance of Artificial Intelligence in Cephalometric Landmark Identification and Diagnosis: A Systematic Review. *Healthcare (Switzerland)* 2022;10(12):2454. Available at: <https://www.mdpi.com/2227-9032/10/12/2454/htm>. Accessed August 13, 2024.
67. Kaur A, Singh C. Automatic cephalometric landmark detection using Zernike moments and template matching. *Signal Image Video Process* 2015;9(1):117–32. Available at: <https://link.springer.com/article/10.1007/s11760-013-0432-7>. Accessed August 13, 2024.
68. Hutton TJ, Cunningham S, Hammond P. An evaluation of active shape models for the automatic identification of cephalometric landmarks. *Eur J Orthod* 2000;22(5):499–508. Available at: <https://dx.doi.org/10.1093/ejo/22.5.499>. Accessed August 13, 2024.
69. Lian C, Wang F, Deng HH, et al. Multi-task Dynamic Transformer Network for Concurrent Bone Segmentation and Large-Scale Landmark Localization with Dental CBCT. *Lecture Notes in Computer Science (including subseries Lecture Notes in Artificial Intelligence and Lecture Notes in Bioinformatics)* 2020;12264 LNCS:807–16. Available at: https://link.springer.com/chapter/10.1007/978-3-030-59719-1_78. Accessed August 13, 2024.
70. Dillenseger JP, Gros CI, Sayeh A, et al. Image quality evaluation of small FOV and large FOV CBCT devices for oral and maxillofacial radiology. *Dentomaxillofacial Radiology* 2016;46(1). Available at: <https://dx.doi.org/10.1259/dmfr.20160285>. Accessed August 13, 2024.
71. Vogiatzi T, Menz R, Verna C, Bornstein MM, Dagassan-Berndt D. Effect of field of view (FOV) positioning and shielding on radiation dose in paediatric CBCT. *Dentomaxillofacial Radiology* 2022;51(6):51. Available at: <https://pubmed.ncbi.nlm.nih.gov/35043625/>. Accessed August 13, 2024.
72. Lorenzoni DC, Bolognese AM, Garib DG, Guedes FR, Sant’Anna EF. Cone-Beam Computed Tomography and Radiographs in Dentistry: Aspects Related to Radiation Dose. *Int J Dent* 2012;2012(1):813768. Available at: <https://pubmed.ncbi.nlm.nih.gov/22413768/>.

<https://onlinelibrary.wiley.com/doi/full/10.1155/2012/813768>. Accessed August 13, 2024.

73. Ding GX, Munro P, Pawlowski J, Malcolm A, Coffey CW. Reducing radiation exposure to patients from kV-CBCT imaging. *Radiotherapy and Oncology* 2010;97(3):585–92.

74. Milletari F, Navab N, Ahmadi SA. V-Net: Fully convolutional neural networks for volumetric medical image segmentation. *Proceedings - 2016 4th International Conference on 3D Vision, 3DV 2016* 2016:565–71.

75. Siddique N, Paheding S, Elkin CP, Devabhaktuni V. U-Net and Its Variants for Medical Image Segmentation: A Review of Theory and Applications. *IEEE Access* 2021;9:82031–57.

76. Christlein V, Spranger L, Seuret M, Nicolaou A, Kral P, Maier A. Deep generalized max pooling. *Proceedings of the International Conference on Document Analysis and Recognition, ICDAR 2019*:1090–6.

77. Fred Agarap AM. Deep Learning using Rectified Linear Units (ReLU). 2018. Available at: <https://arxiv.org/abs/1803.08375v2>. Accessed August 15, 2024.

78. Lei H, Akhtar N, Mian A. Spherical Kernel for Efficient Graph Convolution on 3D Point Clouds. *IEEE Trans Pattern Anal Mach Intell* 2021;43(10):3664–80.

79. Giddwani B, Tekchandani H, Verma S. Deep dilated V-Net for 3D volume segmentation of pancreas in CT images. *2020 7th International Conference on Signal Processing and Integrated Networks, SPIN 2020* 2020:591–6.

80. Zhang L, Zhang J, Shen P, et al. Block Level Skip Connections across Cascaded V-Net for Multi-Organ Segmentation. *IEEE Trans Med Imaging* 2020;39(9):2782–93.

81. Zhao R, Qian B, Zhang X, et al. Rethinking dice loss for medical image segmentation. *Proceedings - IEEE International Conference on Data Mining, ICDM 2020*;2020-November:851–60.

82. Wang M, Lu S, Zhu D, Lin J, Wang Z. A High-Speed and Low-Complexity Architecture for Softmax Function in Deep Learning. *2018 IEEE Asia Pacific Conference on Circuits and Systems, APCCAS 2018* 2018:223–6.

83. Pauwels R, Jacobs R, Singer SR, Mupparapu M. CBCT-based bone quality assessment: Are Hounsfield units applicable? *Dentomaxillofacial Radiology*

- 2015;44(1). Available at: <https://dx.doi.org/10.1259/dmfr.20140238>. Accessed August 15, 2024.
84. Lo J, Cardinell J, Costanzo A, et al. Medical Augmentation (Med-Aug) for Optimal Data Augmentation in Medical Deep Learning Networks. *Sensors* 2021, Vol. 21, Page 7018 2021;21(21):7018. Available at: <https://www.mdpi.com/1424-8220/21/21/7018/htm>. Accessed August 15, 2024.
85. Hossain MS, Betts JM, Paplinski AP. Dual Focal Loss to address class imbalance in semantic segmentation. *Neurocomputing* 2021;462:69–87.
86. Polizzi A, Quinzi V, Ronsivalle V, et al. Tooth automatic segmentation from CBCT images: a systematic review. *Clin Oral Investig* 2023;27(7):3363–78. Available at: <https://link.springer.com/article/10.1007/s00784-023-05048-5>. Accessed August 26, 2024.
87. Dot G, Schouman T, Dubois G, Rouch P, Gajny L. Fully automatic segmentation of craniomaxillofacial CT scans for computer-assisted orthognathic surgery planning using the nnU-Net framework. *Eur Radiol* 2022;32(6):3639–48. Available at: <https://link.springer.com/article/10.1007/s00330-021-08455-y>. Accessed August 26, 2024.
88. Shen F. Improvement Methods for Medical Image Segmentation Based on Attention U-Net Networks. *2024 5th International Seminar on Artificial Intelligence, Networking and Information Technology, AINIT 2024* 2024:1231–4.
89. Vaitiekunas M, Jegelevicius D, Sakalauskas A, Grybauskas S. Automatic Method for Bone Segmentation in Cone Beam Computed Tomography Data Set. *Applied Sciences* 2020, Vol. 10, Page 236 2019;10(1):236. Available at: <https://www.mdpi.com/2076-3417/10/1/236/htm>. Accessed August 26, 2024.
90. Mahmood N, Ghorbani N, Troje NF, Pons-Moll G, Black MJ. AMASS: Archive of Motion Capture As Surface Shapes. 2019:5442–51. Available at: <https://amass.is.tue.mpg.de/>. Accessed August 26, 2024.
91. Mangano F, Gandolfi A, Luongo G, LogoZZo S. Intraoral scanners in dentistry: a review of the current literature. *BMC Oral Health* 2017 17:1 2017;17(1):1–11. Available at: <https://link.springer.com/articles/10.1186/s12903-017-0442-x>. Accessed August 23, 2024.

92. Joda T, Wolfart S, Reich S, Zitzmann NU. Virtual Dental Patient: How Long Until It's Here? *Curr Oral Health Rep* 2018;5(2):116–20. Available at: <https://link.springer.com/article/10.1007/s40496-018-0178-y>. Accessed August 23, 2024.
93. Sloan JM, Goatman KA, Siebert JP. Learning rigid image registration utilizing convolutional neural networks for medical image registration. *BIOIMAGING 2018 - 5th International Conference on Bioimaging, Proceedings; Part of 11th International Joint Conference on Biomedical Engineering Systems and Technologies, BIOSTEC 2018* 2018;2:89–99.
94. Rusu RB, Blodow N, Beetz M. Fast Point Feature Histograms (FPFH) for 3D Registration. *Proc IEEE Int Conf Robot Autom* 2009:3212–7.
95. Chum O, Matas J. Optimal randomized RANSAC. *IEEE Trans Pattern Anal Mach Intell* 2008;30(8):1472–82.
96. Zhang J, Yao Y, Deng B. Fast and Robust Iterative Closest Point. *IEEE Trans Pattern Anal Mach Intell* 2022;44(7):3450–66.
97. Nüchter A, Lingemann K, Hertzberg J. Cached k-d tree search for ICP algorithms. *3DIM 2007 - Proceedings 6th International Conference on 3-D Digital Imaging and Modeling* 2007:419–26.
98. Schubert E, Sander J, Ester M, Kriegel HP, Xu X. DBSCAN Revisited, Revisited. *ACM Transactions on Database Systems (TODS)* 2017;42(3). Available at: <https://dl.acm.org/doi/10.1145/3068335>. Accessed August 23, 2024.
99. Kazhdan M, Bolitho M, Hoppe H. Poisson Surface Reconstruction. *Eurographics Symposium on Geometry Processing* 2006.
100. Qi CR, Su H, Mo K, Guibas LJ. PointNet: Deep Learning on Point Sets for 3D Classification and Segmentation. *Proceedings - 30th IEEE Conference on Computer Vision and Pattern Recognition, CVPR 2017* 2016;2017-January:77–85. Available at: <https://arxiv.org/abs/1612.00593v2>. Accessed December 11, 2024.